

# Foot and Ankle Motion Analysis Using Dynamic Radiographic Imaging

Benjamin Donald McHenry  
*Marquette University*

---

## Recommended Citation

McHenry, Benjamin Donald, "Foot and Ankle Motion Analysis Using Dynamic Radiographic Imaging" (2013). *Dissertations (2009 -)*. Paper 276.  
[http://epublications.marquette.edu/dissertations\\_mu/276](http://epublications.marquette.edu/dissertations_mu/276)

FOOT AND ANKLE MOTION ANALYSIS USING DYNAMIC  
RADIOGRAPHIC IMAGING

by

Benjamin D. McHenry, B.S.

A Dissertation submitted to the Faculty of the Graduate School,  
Marquette University,  
in Partial Fulfillment of the Requirements for  
the Degree of Doctor of Philosophy

Milwaukee, Wisconsin

May 2013

ABSTRACT  
FOOT AND ANKLE MOTION ANALYSIS USING DYNAMIC  
RADIOGRAPHIC IMAGING

Benjamin D. McHenry, B.S.

Marquette University, 2013

Lower extremity motion analysis has become a powerful tool used to assess the dynamics of both normal and pathologic gait in a variety of clinical and research settings. Early rigid representations of the foot have recently been replaced with multi-segmental models capable of estimating intra-foot motion. Current models using externally placed markers on the surface of the skin are easily implemented, but suffer from errors associated with soft tissue artifact, marker placement repeatability, and rigid segment assumptions. Models using intra-cortical bone pins circumvent these errors, but their invasive nature has limited their application to research only. Radiographic models reporting gait kinematics currently analyze progressive static foot positions and do not include dynamics.

The goal of this study was to determine the feasibility of using fluoroscopy to measure *in vivo* intra-foot dynamics of the hindfoot during the stance phase of gait. The developed fluoroscopic system was synchronized to a standard motion analysis system which included a multi-axis force platform. Custom algorithms were created to translate points of interest from 2D fluoroscopic image space to global tri-axial space. From these translated points of interest, a hindfoot specific model was developed to quantify sagittal plane talocrural and subtalar dynamics.

The new hindfoot model was evaluated and applied to a pilot population of thirteen healthy adults during barefoot and toe-only rocker walking conditions. The barefoot kinematic and kinetic results compared favorably with barefoot dynamics reported by other authors. As a result of the barefoot study, it was concluded that inter-subject variability in sagittal plane kinematics was higher for the talocrural joint than the subtalar joint. The toe-only rocker analysis was the first report of hindfoot kinematics within a rocker sole shoe modification. Hindfoot kinematic inter-subject variability was significantly lower in the toe-only rocker condition when compared to barefoot results.

This study represents the first use of fluoroscopy to quantify *in vivo* intra-foot dynamics during the stance phase of gait. Talocrural and subtalar dynamics of healthy adult subjects are reported. The technology developed for this study is capable of examining soft tissue and bony abnormalities associated with the pathologic foot. Based on the overall results of this study, it is recommended that development continue for further analysis within the clinical environment, and examination of complex *in vivo* foot and ankle dynamics.

## ACKNOWLEDGMENTS

Benjamin D. McHenry, B.S.

The list of people who have guided my journey towards the completion of this dissertation is far too long to be succinctly made. The experience has been a truly humbling one. While proud of the personal accomplishment, it is with regret that only my name adorns the cover of this text.

I would like to thank my dissertation director Dr. Gerald Harris, a teacher and mentor whose influence on my life has been far beyond academic. I am grateful for the ability to seek his council as I begin my career.

I would additionally like to thank the other members of my dissertation committee—Dr. Jason Long, Dr. Philip Voglewede, Dr. Taly Gilat-Schmidt, and Dr. Peter Smith. Your wide spectrum of expertise in the field illuminated my path, and your encouragement during the final few months was invaluable.

I would like to thank my best friend Edyta Brania, a woman who continues to show me the true meaning of strength. I would additionally like to thank Bill Powers, a teacher and friend whose fellowship has been cherished as I trudge the road of happy destiny.

Finally, I would like to thank my family for their unconditional love and encouragement—my father Richard, my brother Calen, and my sister Colleen. Above all, I would like to thank my mother Petronella, a woman whose support for me goes far beyond maternal.

## TABLE OF CONTENTS

ACKNOWLEDGMENTS .....	i
LIST OF TABLES .....	v
LIST OF FIGURES .....	vi
<b>1. Introduction</b> .....	1
1.1 Statement of Problem .....	3
1.2 External Marker Based Models .....	3
1.2.1 Skin Motion Artifact .....	4
1.2.2 Marker Placement Sensitivity .....	5
1.2.3 Rigid Segment Assumption.....	7
1.3 Bone Marker Based Models .....	8
1.3.1 Invasive Nature .....	9
1.3.2 Gait Pattern Alteration .....	9
1.4 Fluoroscopic Models .....	10
1.4.1 Anatomic Limitations.....	11
1.4.2 Fluoroscopic Technology.....	12
1.4.3 Foot and Ankle Fluoroscopy.....	13
1.5 Hindfoot Specific Modeling.....	14
1.5.1 Axes of Motion.....	14
1.5.2 Kinematic Methodologies .....	15
1.6 Kinetic Modeling.....	17
1.6.1 Force Measurement Technology.....	17
1.6.2 Body Segment Parameters .....	19
1.7 Hypotheses and Specific Aims.....	20
<b>2. A Model for Assessment of <i>In vivo</i> Hindfoot Motion During Gait</b> .....	22
2.1 Introduction .....	22
2.2 Materials and Methods .....	24
2.2.1 System Configuration.....	24
2.2.2 System Synchronization.....	26
2.2.3 Image Construction .....	26
2.2.4 Global Referencing .....	27

2.2.5	Kinematic Model.....	28
2.2.6	Kinematic Model Sensitivity.....	30
2.2.7	Kinetic Model.....	31
2.2.8	Body Segment Parameters .....	34
2.2.9	Subject Selection.....	35
2.3	Results .....	36
2.3.1	Global Referencing .....	36
2.3.2	Joint Kinematics.....	37
2.3.3	Kinematic Model Sensitivity.....	38
2.3.4	Joint Kinetics.....	39
2.3.5	Kinetic Body Segment Parameter Effects.....	40
2.4	Discussion.....	41
2.5	Conclusion.....	47
<b>3.</b>	<b>Pilot Investigation: <i>In Vivo</i> Hindfoot Kinematics During</b>	
	<b>Normal Barefoot Gait.....</b>	<b>49</b>
3.1	Introduction .....	49
3.2	Materials and Methods .....	51
3.2.1	Subject Selection.....	52
3.2.2	Testing Protocol .....	52
3.2.3	Statistical Methods .....	54
3.3	Results .....	56
3.3.1	Joint Kinematics.....	56
3.3.2	Statistics .....	58
3.4	Discussion.....	60
3.5	Conclusion.....	65
<b>4.</b>	<b>Pilot Investigation: Comparing Barefoot and Toe-Only</b>	
	<b>Rocker Soled Shoe Hindfoot Kinematics.....</b>	<b>67</b>
4.1	Introduction .....	67
4.2	Materials and Methods .....	70
4.2.1	Subject Selection.....	70
4.2.2	Testing Protocol .....	70

4.2.3	Statistical Methods .....	72
4.3	Results .....	74
4.3.1	Joint Kinematics .....	74
4.3.2	Statistics .....	77
4.4	Discussion.....	80
4.5	Conclusion.....	82
<b>5.</b>	<b>Conclusion</b> .....	<b>85</b>
5.1	Summary of Findings .....	86
5.2	Limitations and Future Directions .....	89
	<b>Bibliography</b> .....	<b>91</b>
	<b>Appendices</b> .....	<b>104</b>

## LIST OF TABLES

Table 2.1 Equations used for global referencing .....	28
Table 2.2 External marker locations .....	29
Table 2.3 Segment coordinate system axes definition.....	29
Table 2.4 Body segment parameters.....	34
Table 2.5 Fluoroscopic and bone pin kinematics.....	38
Table 2.6 Kinematic model sensitivity .....	39
Table 2.7 Kinetic body segment parameter effects.....	40
Table 3.1 Talocrural kinematic statistics .....	59
Table 3.2 Subtalar kinematic statistics.....	59
Table 3.3 Temporal spatial statistics.....	59
Table 3.4 Fluoroscopic and bone pin kinematics.....	62
Table 4.1 Kinematic statistics during LR .....	78
Table 4.2 Kinematic statistics during MSt.....	78
Table 4.3 Kinematic statistics during TSt.....	79
Table 4.4 Temporal spatial statistics.....	80

## LIST OF FIGURES

Figure 1-1 Hindfoot anatomy.....	2
Figure 2-1 System configuration .....	25
Figure 2-2 Typical fluoroscopic image.....	27
Figure 2-3 Virtual marker locations.....	28
Figure 2-4 Calcaneal segment centroid locus .....	33
Figure 2-5 Global referencing matrix .....	36
Figure 2-6 Global referencing error based on position in capture volume .....	37
Figure 2-7 Sagittal plane kinematic results.....	38
Figure 2-8 Sagittal plane kinetic results.....	40
Figure 3-1 Talocrural sagittal plane kinematics.....	57
Figure 3-2 Subtalar sagittal plane kinematics .....	57
Figure 3-3 Sagittal plane kinematic results.....	61
Figure 4-1 Toe-only rocker shoe.....	71
Figure 4-2 Sagittal plane kinematic results during LR .....	75
Figure 4-3 Sagittal plane kinematic results during MSt .....	75
Figure 4-4 Sagittal plane kinematic results during TSt .....	76
Figure A-1 Raw kinematics: Subject 1 .....	106
Figure A-2 Raw kinematics: Subject 2 .....	107
Figure A-3 Raw kinematics: Subject 3 .....	108
Figure A-4 Raw kinematics: Subject 4 .....	109
Figure A-5 Raw kinematics: Subject 5 .....	110
Figure B-1 Raw kinematics: Subject 1 .....	112
Figure B-2 Raw kinematics: Subject 2 .....	113
Figure B-3 Raw kinematics: Subject 3 .....	114
Figure B-4 Raw kinematics: Subject 4 .....	115
Figure B-5 Raw kinematics: Subject 5 .....	116
Figure B-6 Raw kinematics: Subject 6 .....	117
Figure B-7 Raw kinematics: Subject 7 .....	118
Figure B-8 Raw kinematics: Subject 8 .....	119
Figure B-9 Raw kinematics: Subject 9 .....	120

Figure B-10 Raw kinematics: Subject 10 .....	121
Figure B-11 Raw kinematics: Subject 11 .....	122
Figure B-12 Raw kinematics: Subject 12 .....	123
Figure B-13 Raw kinematics: Subject 13 .....	124

## 1. Introduction

Gait analysis has become a powerful tool used by clinicians to assess the kinematics and kinetics of patients, both pre- and post-operatively, for both rehabilitation and research purposes. Early lower extremity models used external markers to define a segmental chain that often defined the foot as a single rigid segment at the end of the leg<sup>[1-5]</sup>. These rigid segment representations of the foot failed to recognize the shank-foot complex as the intricate, multi-joint mechanism that it is<sup>[6]</sup>. As motion capture technology became commercially available and computer processing speeds increased, more advanced models were introduced that subdivided the foot into multiple segments<sup>[7-10]</sup>. Over the years, these customized models have been adapted for clinical use, and standards set for reporting their results<sup>[11]</sup>. Unfortunately, most of the segments defined by these models were derived not by clinical relevance, but by their ability to repeatedly locate anatomic features that define the segments. While these models are efficient in reliably and repeatedly tracking marker motion, the inter-segmental joint results they estimate may lack significant clinical meaning, depending on the model assumptions, joint anatomy, and pathology being analyzed.

The subtalar joint (Figure 1-1) is clinically significant in many pathologies including pes planovalgus and tarsal coalition, but because talar position cannot be tracked via externally mounted skin markers<sup>[9]</sup>, *in vivo* subtalar joint motion cannot be defined by their use. In fact, all clinically relevant multi-segmental foot models using skin mounted markers combine the talus with at least one additional bone (usually calcaneus) in a lumped “hindfoot” segment. Hindfoot intra-segmental motion is either not reported or is attributed to a neighboring inter-segmental joint. The only way to

quantify and describe true *in vivo* subtalar joint motion is to define the talus and calcaneus as individual segments within the model. This cannot be accurately accomplished with skin mounted external markers.

The use of intra-cortical bone mounted markers (markers affixed to the end of surgically implanted bone pins) is one way to distinguish the

bones of the foot. Multiple studies using this technique have described lower extremity bony motion in normal adult populations<sup>[12-17]</sup>. Of these studies, two report talocrural and subtalar joint motion normalized over stance phase<sup>[12, 14]</sup>, though neither include a kinetic analysis. While intra-cortical bone pin methodologies appear to circumvent many of the limitations associated with skin mounted external marker use, their invasive nature and gait altering potential prevents widespread application in pathology or pediatrics.

Radiography offers an alternative, non-invasive, method to determine the position of individual bones within the foot. Several examples of static foot position radiographs used for gait analysis appear in the literature. Hindfoot coronal alignment (calcaneus relative to tibia), is often determined via static x-ray in the evaluation and treatment of pathologic conditions<sup>[18]</sup>. The Milwaukee Foot Model (a clinically used multi-segmental foot model) requires static radiographic images to create correction matrices for aligning marker-based segment orientations to the underlying bony anatomy<sup>[8]</sup>. There have even

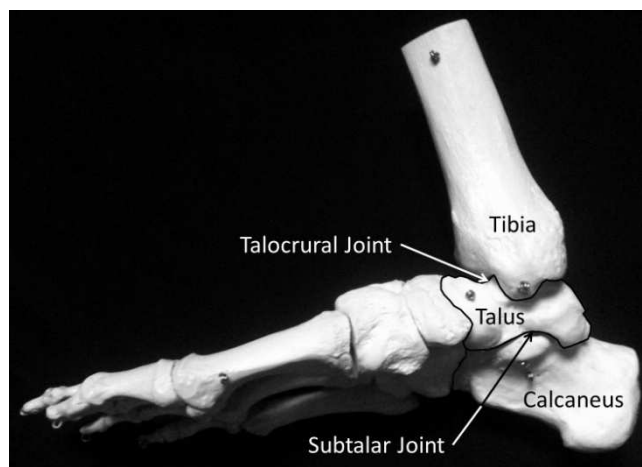


**Figure 1-1** Hindfoot anatomy. The hindfoot is comprised of two articulations. The talocrural joint defines the motion between the talus and tibia while the subtalar joint defines the motion between the calcaneus and talus.

been studies reporting hindfoot and/or ankle kinematics using static radiographic techniques (fluoroscopy, MRI, CT)<sup>[19-21]</sup>, but to date there have been no ankle and/or foot studies in which radiographs were used to quantify natural dynamic gait.

### 1.1 Statement of Problem

Current foot models, including multi-segmental models, that use externally mounted skin markers for lower extremity gait analysis, accept known limitations from skin motion artifact, misplacement errors, and rigid segment assumptions. Foot models that use bone mounted markers, meant to circumvent these errors, are invasive and have the potential to alter normal gait patterns. Current radiographic models reporting gait kinematics only analyze static foot positions and do not include dynamics. The purpose of this study was to determine the feasibility of using fluoroscopy to quantify *in vivo* intra-foot kinematics and kinetics of the hindfoot during stance phase.

### 1.2 External Marker Based Models

The most frequently used method for measuring human movement involves attaching markers (passive or active) to the surface of the skin<sup>[22]</sup>. Multiple markers (three or more) are positioned to define a body segment, and the collective movement of these markers is meant to infer a change in position and/or orientation of the body segment being analyzed. This requires the synchronized capture of each marker position, which is typically accomplished through stereophotogrammetry. Errors associated with reconstruction of marker position are known as instrumentation errors and, if not properly

accounted for, can have a significant impact on human movement analysis<sup>[23]</sup>.

Fortunately, these errors can be minimized through proper calibration, filtering, camera placement and use of redundant markers. The other errors associated with external marker use are not as easily accounted for.

### 1.2.1 Skin Motion Artifact

The shifting effect of externally placed markers in relation to the underlying anatomy has long been reported in lower extremity motion<sup>[24]</sup>. These artifacts are independently caused by inertial effects, skin deformation, and muscle contraction<sup>[25]</sup>. Multiple studies have attempted to verify and estimate this motion using a diverse spectrum of techniques including cadaveric, bone pin, external fixator, and radiographic methodologies<sup>[17, 26-31]</sup>. Cappozzo et al. reported greater trochanter, lateral epicondyle, fibula head, and lateral malleolus displacements between 10-30 mm using external fixators<sup>[26]</sup>. In a 2D roentgen study by Tranberg et al., the motion was quantified and found to be up to 4.3 mm when placed near the medial malleolus<sup>[28]</sup>. A recent hindfoot study used single-plane fluoroscopy and reported translational soft tissue artifact at the calcaneus ranging from  $5.9 \pm 7.3$  mm at heel strike to  $12.1 \pm 0.3$  mm at toe-off<sup>[27]</sup>. While the discrepancies between these studies can be attributed to their methodologies, it is generally concluded that soft tissue artifact errors introduced by skin mounted external marker use are larger than instrumentation error, task-dependent, and not repeatable among subjects<sup>[25]</sup>. Because of the high task variability in soft tissue artifacts among subjects, it is difficult to define an inter-subject correction algorithm that will also account for the variations associated with pathology.

In light of these difficulties, existing lower extremity models are unable to correct for soft tissue artifacts. Thus, the resulting biomechanical analysis reflects these artifact errors as they propagate through the kinematic analysis. For large segments like the thigh and shank, skin motion artifact error is minimized because the markers used to define the segment are placed at greater distances from each other, where the distance between them preserves their spatial relationships. In multi-segmental foot models, however, inter-marker distances are small, resulting in angle definition sensitivity<sup>[32]</sup>. Because this study's proposed foot model uses fluoroscopy to define talar and calcaneal position, skin motion artifacts have been eliminated as a source of error.

### 1.2.2 Marker Placement Sensitivity

Due to the cyclic nature of the gait cycle, trial to trial inter-segmental dynamics have fairly low variability once external markers are placed on a subject. This low intra-subject kinematic variability was first quantified and reported by Kadaba et al. as “within-day” repeatability<sup>[33]</sup>. Kadaba also reported intra-subject “between-day” repeatability that was always lower than “within-day” and attributed to “uncertainties in the reapplication of markers on successive days”<sup>[33]</sup>. Although great care is taken when placing markers on palpable anatomic landmarks, misplacements are inevitable. Della Croce et al. attributed these misplacements to three main factors: (1) anatomic landmarks are surfaces, not points, which can be large and irregular in shape; (2) landmarks are covered by a soft tissue layer of variable thickness and composition; and (3) anatomic location identification depends on palpation procedure<sup>[32]</sup>. Because the anatomic locations associated with foot models (e.g., malleoli, metatarsal heads) are generally

more superficial than other landmarks used in gait analysis (e.g., iliac spine, greater trochanter) the misplacement error is minimized. Despite this, foot intra and inter-examiner precision (RMS distance from the mean position) values as high as 10.3 and 21.5 mm respectively have been reported<sup>[34]</sup>.

Similar to the displacement errors associated with soft tissue artifact, misplacement errors influence the position of local coordinate frames which propagate through the kinematic model and are reflected in the reported analysis. Because of the non-linear dependency between reported kinematics and anatomic locations, the effects of misplacements are unpredictable<sup>[32]</sup>. Empirical quantifications of errors associated with marker misplacement are difficult to identify among other error sources (soft tissue artifact/instrumentation), though most multi-segmental foot models are vetted for repeatability where the only variation tested is marker placement (both intra and inter-examiner). In a four-segmental foot model developed by Carson et al., inter-segmental angles as high as  $6^\circ$  and  $6.5^\circ$  were reported for inter-day repeatability and inter-tester repeatability, respectively (using 95% confidence intervals)<sup>[7]</sup>. In a similar study applied to a five-segmental foot model Caravaggi et al. reports averaged variability as high as  $11.4^\circ$  and  $11.5^\circ$  for different day and examiner repeatability<sup>[35]</sup>. In general, joint angle sensitivity to variations in local coordinate system position (derived from marker placement) have been shown to be higher among angles that undergo small variations<sup>[32]</sup>. Because of this, foot models are especially susceptible to kinematic variations due to marker misplacement. The proposed foot model avoids these misplacement errors by not using external markers to define the calcaneal or talar local coordinate systems.

### 1.2.3 Rigid Segment Assumption

Any skin mounted external marker based multi-segmental foot model that defines multiple bones as a single rigid segment is making the assumption that the bones do not move with respect to one another. Any violation of the rigid body assumption results in overestimated inter-segmental motion or unreported intra-segmental motion. Verifying the rigid body assumption is difficult, as the methodologies required are beyond the use of external markers. Determining the motion between bones is the only way to confirm or refute the rigid body assumption. Cadaver studies are useful in determining and quantifying the motion between bones<sup>[36]</sup>, but it is difficult to ascertain from these studies if the motion observed would arise during natural weight-bearing gait. There have been *in vitro* bone pin studies reporting kinematics in which cadaveric feet were attached to walking simulators<sup>[30, 37-40]</sup>. Three of these studies report on the validity of the rigid body assumptions by multi-segmental foot models<sup>[30, 38, 40]</sup>. Nester et al. measured the kinematics of 22 anatomical foot joints and concluded that many of the rigid body models used to report *in vivo* kinematics may fail to capture the site of articulation<sup>[38]</sup>. In a later study, Nester et al. reported specifically on the error associated with rigid body violations of mid and forefoot segments and concluded that there was clear evidence of how different bone groupings influenced a segment's kinematics<sup>[40]</sup>. In a similar study on ten cadaveric feet, Okita et al. reported statistically significant segment angular deviations compared to the underlying bone for both the hindfoot and forefoot segments<sup>[30]</sup>. These studies would suggest that rigid body assumptions are being violated in current multi-segmental foot models that group bones together in segments which are assumed to be rigid.

The only way to correct for rigidity violations within a multi-bone segment via external markers is to subdivide the segment further. Defining a segment requires the placement of three non-collinear markers, but as these segments become smaller and smaller, or deeper within the foot (lacking palpable landmarks), finding locations to place three non-collinear markers becomes increasingly difficult. In light of these difficulties, current multi-segmental models using externally placed skin markers struggle in deviating from the rigid body assumptions that have been shown to contain error. The four most commonly reported multi-segmental foot models subdivide the shank/foot complex among four and nine rigid segments. In all of these models, at least three segments are composed of multiple bones<sup>[7-10]</sup>. Because of the fluoroscopic nature of the proposed study, the foot can be divided into individual bone segments, eliminating the need to make rigidity assumptions between bones.

### 1.3 Bone Marker Based Models

Bone marker based multi-segmental foot models circumvent the known errors associated with external markers by surgically attaching markers directly to the bone. This eliminates errors associated with skin motion artifact and marker misplacements as no external markers are directly attached to the skin. In addition, assumed rigidity between bones is avoided as each bone can define its own segment. Many studies appear in the literature quantifying and reiterating the methodological differences between bone pin and skin markers<sup>[12-17]</sup>. While there are obvious advantages to directly measuring bony motion via intra-cortical pins, their invasive nature and gait altering potential prevent widespread clinical use.

### 1.3.1 Invasive Nature

Insertion of intra-cortical pins requires the assistance of an experienced orthopaedic surgeon and is done under sterile operating conditions<sup>[13, 14]</sup>. Local anesthesia is used and care must be taken to avoid nerves and blood vessels<sup>[12-14, 17]</sup>. After pin removal, subjects are given antibiotics and/or pain medication<sup>[12-14, 17]</sup>, and some methodologies describe suturing of skin incisions<sup>[17]</sup>. While none of the studies report clinical complications, they all report subject pain and/or walking with a limp up to one week post analysis<sup>[12-14, 17]</sup>. While these methodologies were approved for research purposes on healthy male subjects, there is yet to be a bone pin study of the female foot, or based on the pediatric or pathologic foot. The currently proposed fluoroscopic study methods are non-invasive and achieve the same goals as bone marker based systems without the need for an invasive procedure.

### 1.3.2 Gait Pattern Alteration

Perhaps more concerning than the invasive nature of bone marker methods is their reported potential to alter gait. In a 2007 study, Nester et al. compared the stance time, ground reaction forces, and tibial kinematics between skin mounted, plate mounted (markers attached to plates mounted onto the skin), and bone anchored markers on six subjects<sup>[15]</sup>. Three statistically significant intra-subject differences in stance times were reported, and all were associated with bone implantation (one bone vs. skin, two bone vs. plate). For the seven ground reaction force parameters measured, 24 statistically significant intra-subject differences were reported, 17 of which were associated with bone

pins (eleven bone vs. skin, six bone vs. plate). And finally, the intra-subject difference in range of tibial motion in the major planes was statistically different in 25 instances. Eighteen of these were associated with bone pins (ten bone vs. skin, eight bone vs. plate). While it cannot be inferred from the results that the implantation process was the cause of the reported differences, it was the only methodology with invasive procedures. In addition to the reported differences, the methods of most bone marker based studies contain a period of time for subjects to acclimate to walking with markers implanted prior to testing<sup>[14-17]</sup>. This designated period implies that normal gait has been altered in some way through the marker implantation process, but can be restored after an adjustment period. Artifact errors associated with skin mounted external markers prevent quantification of the kinematic deviation from natural gait caused by pin insertion. Advances in radiographic models may be the key in measuring this deviation, if it exists.

In addition to the potential for directly altering natural gait, bone pin positions may be affected by soft tissue artifacts as well. Authors have reported an uncertainty as to whether the protruding pins have an anchoring effect on surrounding skin<sup>[17]</sup>, but methodologies describing the extension of incisions until skin no longer restricts pin motion<sup>[13]</sup> suggest that if care is not taken, skin can affect bone pin position. Because the current methodology does not require the invasive insertion of any device to define hindfoot segments, gait pattern alterations of any kind are avoided.

#### 1.4 Fluoroscopic Models

Dynamic radiography has emerged as another possible solution to the problems associated with skin mounted external marker based multi-segmental foot models. A

dynamic radiographic method, such as fluoroscopy, allows for the collection of radiographic images during dynamic motion. Numerous studies using this technology to characterize knee kinematics appear in the literature<sup>[41-45]</sup>, and the knee joint has received the most attention using this technology to date<sup>[46]</sup>. The application of dynamic radiography on the foot and ankle has proved challenging for multiple reasons and it does present the added challenge of ionizing radiation.

#### 1.4.1 Anatomic Limitations

Quantifying bony kinematics via radiographic images can be difficult, as bones have smooth, rounded contours making feature detection difficult<sup>[47]</sup>. The foot specifically is problematic because it involves numerous bones which overlap each other when viewed radiographically<sup>[46]</sup>, making the selection of a single view to capture its motion difficult. A transverse view may be appropriate for isolating the motion of the cuboid, navicular, and cuneiforms, but the tibia, talus and calcaneus would be stacked on top of each other in the radiograph, making it difficult to identify anatomic points of interest. Compounded with the difficulty in selecting a suitable view is the contralateral foot swinging through the field of view during mid-stance. It is noted in the literature, however, that lateral projections would show the talus and calcaneus clearly<sup>[46]</sup>, and may be appropriate for quantifying hindfoot sagittal plane kinematics.

### 1.4.2 Fluoroscopic Technology

The use of fluoroscopy on the foot during natural gait would require construction of robust walking platforms, as commercially available fluoroscopy units are nearly impossible to use at ground level<sup>[46]</sup>. Commercial fluoroscopic systems are C-arm in nature, with emitters mechanically and electronically tethered to image intensifiers. These C-arm systems capture motion in a small field of view, and obviate recording of natural motions such as gait<sup>[47]</sup>. Most C-arm systems sample at 25 Hz<sup>[47]</sup>, making the accurate acquisition of high speed motion impossible. Fluoroscopic images also suffer from ‘pin-cushioning’ effects which must be corrected for to ensure accurate linear tracking. This is typically done using polynomial functions which measure the distortion of a uniform marker array attached to the image intensifier surface<sup>[48-50]</sup>. Most of these limitations can be accounted for, as is done in the reported knee studies.

The use of ionizing radiation is also of concern when using fluoroscopy, though it poses a low radiation hazard to the patient<sup>[47]</sup>. Effective dose is a measure of the risk to the whole body due to ionizing radiation exposed non-uniformly to the body. Organs have different weighting factors when computing effective dose. A typical fluoroscopic protocol of 20 seconds exposes the patient to about 80  $\mu\text{Sv}$  of radiation<sup>[47]</sup>. Because the stance phase of gait in normal subjects occurs under one second, 80  $\mu\text{Sv}$  would be the effective dose of approximately 20 stance phases analyzed, or four  $\mu\text{Sv}$ /trial. Eighty  $\mu\text{Sv}$  exposure is approximately equivalent to the solar exposure during a 12 hour flight from London to Tokyo<sup>[51]</sup>, and according to the USNRC (United States Nuclear Regulatory Commission), whole body annual occupational limits are 5 rems (50,000  $\mu\text{Sv}$ ).

### 1.4.3 Foot and Ankle Fluoroscopy

While the difficulties involved with using fluoroscopy on the foot and ankle are recognized, they are being overcome and there are some limited reports of its use in the literature. The first pioneering study using fluoroscopy on foot biomechanics was done by Green et al. in 1975<sup>[52]</sup>. Fluoroscopic images were captured on 16 mm film and anatomic bony motion (non-quantitative) was described as subjects moved their foot from maximal pronation to maximal supination<sup>[52]</sup>. Since the work of Green et al., there have been several studies measuring both the osseous<sup>[19, 21, 53-57]</sup>, and soft tissue<sup>[58-61]</sup> characteristics of the foot and ankle. Of the bony fluoroscopic studies, two describe ankle joint kinematics associated with gait. In a 2000 study by Komistek et al., sagittal plane ankle kinematics were reported for ten subjects between static dorsiflexion and static plantar flexion positions<sup>[21]</sup>. Because of the static nature of the study methodology, only ranges of motion could be reported. In a bi-planar (dual-orthogonal fluoroscopy) study by de Asla et al., talocrural, subtalar, and tibiocalcaneal (calcaneus with respect to tibia) kinematics were reported among three static positions (heel strike, mid-stance, and toe-off)<sup>[19]</sup>. Similar to the Komistek et al. study, static positioning of the foot limits de Asla's reported results to ranges of motion. While these studies are valuable first steps, kinematics should be determined from foot positions derived with the subject walking at a freely selected pace in order to capture all the subtleties associated with gait. In the currently proposed study subjects are instructed to walk naturally, and kinematics are reported the entire time the foot is within the fluoroscopic field of view.

## 1.5 Hindfoot Specific Modeling

Hindfoot motion is typically defined as that between the calcaneus and tibia, anatomically encompassed by two articulations. The talocrural joint defines the motion between the talus and tibia while the subtalar joint defines the motion between the calcaneus and talus (Figure 1-1). A clear understanding of these articulations is critical in diagnosing/treating foot pathologies<sup>[62-64]</sup>, designing ankle prosthesis/implants<sup>[65-67]</sup>, and describing gait abnormalities. Recent literature confirms that quantifying the individual and combined motions of the talocrural and subtalar joints is a challenging task<sup>[68-70]</sup>.

### 1.5.1 Axes of Motion

The talocrural and subtalar joints work in unison to provide a smooth transfer of ground reaction forces to the rest of the body. The sequence of events required to achieve this smooth transition are quite complex and require an understanding of each joint. Conceptually, it is easiest to consider both the talocrural and subtalar joint motion occurring about fixed axes, but neither axis is truly fixed. In a cadaver study conducted by Inman, the angle between an empirical axis of the talocrural joint and the midline of the tibia in the coronal plane was measured in 107 specimens, and found to be  $82.7^\circ \pm 3.7^\circ$  (medial side)<sup>[71]</sup>. In the transverse plane, the talocrural joint is laterally and posteriorly directed  $20-30^\circ$ <sup>[36]</sup>. This axis can be reasonably represented by connecting the ends of the two malleoli. The obliquity of the talocrural axis results in the foot internally rotating when plantarflexed, and externally rotating when dorsiflexed. During the stance phase of gait, when the foot is static, this is observed as an external tibial rotation during

plantar flexion, and an internal tibial rotation during dorsiflexion<sup>[36]</sup>. These articulations are independent of subtalar motion<sup>[36]</sup>.

The subtalar axis is described by an inclination angle from the horizontal plane, and a deviation angle measured from the transverse plane to the midline of the foot<sup>[70]</sup>. Several early studies quantified the angle of inclination around 42° and the angle of deviation between 16-23°, depending on the definition of the midline of the foot<sup>[71-77]</sup>. It is also noted in the literature that some of the variability in subtalar axis location is accounted for by variations in foot type (pronation/supination)<sup>[72]</sup>. Difficulties in tracking bones, such as the talus, make quantification of subtalar motion during gait challenging<sup>[70]</sup>, but early studies noted initial pronation followed by supination towards the end of stance<sup>[72, 78]</sup>.

### 1.5.2 Kinematic Methodologies

Investigators initially modeled both the talocrural and subtalar joints as simple fixed hinges, and used various methodologies to locate and describe their orientations<sup>[71, 73, 74, 78-80]</sup>. Multiple subsequent studies have demonstrated this assumption to be invalid<sup>[67, 81-83]</sup>. In an eight subject *in vivo* study, Lundberg et al. concluded the non-uniform pattern of rotation in the talocrural joint indicated a shift in joint axis position<sup>[81]</sup>. In a 15 specimen *in vitro* study on both talocrural and subtalar motion, Siegler et al. concluded that neither the talocrural nor subtalar joint act as fixed axes<sup>[67]</sup>. With the advancement of more sophisticated 3D modeling techniques, the hinge joint assumptions have been eliminated, but differing opinions still exist as how to best model the talocrural and subtalar joints.

The current methodologies used to model hindfoot motion are the Euler angle method, the Joint Coordinate System (JCS) method, and the helical axis method. Studies using the Euler angle method to describe hindfoot motion<sup>[14, 15, 84, 85]</sup> require definition of three orthogonal axes for both the proximal and distal bones of interest. Because angular motion is defined about these fixed axes, rotation is sequence dependent<sup>[86]</sup>, and care must be taken when using them. The Euler angle method also requires the addition of a position vector to estimate translations, as it is only capable of rotational descriptions<sup>[85]</sup>. A modified Euler angle method known as the JCS method, developed by Grood and Suntay, uses non-orthogonal axes to define joint coordinate systems, is sequence independent, and accounts for both rotational and translational movement<sup>[86]</sup>. The JCS method was adopted by the International Society of Biomechanics (ISB) as the standard for reporting joint kinematics<sup>[87]</sup>, and several studies using this methodology to quantify hindfoot motion appear in the literature<sup>[46, 67, 69, 88-90]</sup>. The JCS method is quite useful in describing joint kinematics, but the non-orthogonality of axes can present a serious problem when joint forces and moments are to be determined<sup>[91]</sup>. The final method for determining joint kinematics is the helical axis method. This method describes the movement between bones as the rotation about and translation along a unique axis<sup>[92]</sup>. Several examples of its use in hindfoot motion appear in the literature<sup>[12, 13, 17, 67, 69, 88, 89, 93-96]</sup>. While the helical axis method is capable of accounting for both rotational and translational movement between bones, the parameters are difficult to interpret clinically, and may be less useful in describing joint kinematics<sup>[97]</sup>.

In a recent study by Choisine et al., the three methods for determining joint kinematics (Euler, JCS, and helical axis) were investigated for detecting subtalar and

ankle joint instability<sup>[98]</sup>. The study concluded that both the Euler angle and JCS methods led to the same conclusions in detecting instability, but the helical axis method was only suitable for detection of plantar/dorsiflexion instability at the talocrural joint, and inversion/eversion at the subtalar joint<sup>[98]</sup> (the major motions associated with these joints). Because the JCS method is ISB recommended<sup>[87]</sup>, and the results easily interpreted, it was used for the current study.

## 1.6 Kinetic Modeling

Lower extremity kinematics are used to quantitatively assess the segmental motion associated with activity. Kinetic analysis involves the forces associated with loadbearing and inertial motion of limbs, and is helpful in understanding why deviations are occurring<sup>[99]</sup>. An understanding of both kinematics and kinetics is essential in the comprehension of gait abnormalities<sup>[100]</sup>, but kinetic results are limited in multi-segmental foot models due to force measurement restrictions<sup>[101, 102]</sup> and inherent modeling assumptions. Given the results of modeling techniques such as intra-cortical bone pin and dynamic radiography, which are capable of dividing the foot into its individual bones, attempts should be made at estimating the inter-segmental dynamics. None of the aforementioned bone pin or radiographic models include kinetic analysis.

### 1.6.1 Force Measurement Technology

The ability to accurately measure ground reaction forces (normal and shear) under discrete subareas of the foot is critical in the development of kinetic multi-segmental foot

models, and can improve our understanding of foot and ankle function<sup>[101]</sup>.

Unfortunately, traditional force platforms are only capable of reporting a single resultant force vector and its locus<sup>[103]</sup>. Several researchers have developed miniature custom sensors<sup>[104, 105]</sup>, and even custom built transducer arrays<sup>[106, 107]</sup> suitable for measuring normal and shear forces under foot subareas, but nothing commercially available has been developed. Plantar pressure mats measure vertical pressure only and are incapable of determining shear contributions<sup>[105]</sup>. In light of these difficulties, a limited number of investigators have explored methods to discretize ground reaction forces using commercially available technology. Scott and Winters covered subjects' feet with carpenter's chalk and used the superposition of several targeted trials on a miniature force platform to estimate ground reaction forces at seven different loading sites under the foot<sup>[103]</sup>. This method was admittedly time consuming by the authors, and required laborious measurement over many trials. Other investigators used pressure mats in conjunction with standard force platforms to proportionally estimate subarea forces<sup>[9, 108]</sup>. While these methods are less arduous, concerns over their accuracy exist<sup>[101, 102]</sup>. More recent investigators have used adjacent platforms and targeted trials in which part of the foot is in contact with each platform during stance<sup>[109]</sup>. This approach limits the number of subareas being analyzed to two, and may not be practical for pathologic patients unable to perform targeted walking.

The proposed fluoroscopic system uses a single force platform and ground reaction forces were measured under the entire foot collectively. This method allows for an isolated kinetic analysis from heel strike through foot flat as the calcaneal segment is

the only segment in contact with the force platform during this time. After foot flat occurs, all force contributions are assumed to act on the calcaneal segment.

### 1.6.2 Body Segment Parameters

In conjunction with ground reaction force data, body segment parameters are used to determine intersegmental forces and moments utilizing inverse dynamics. These body segment parameters include mass, center of mass locus, and mass moments of inertia. A variety of methodologies exist for measuring these parameters. Some investigators make estimations by modeling body segments as geometric shapes<sup>[110]</sup>. Other models are based on cadaveric specimens<sup>[111, 112]</sup>, or *in vivo* mass scanning techniques<sup>[113-115]</sup>.

There is no consensus in the literature on the influence these estimated parameters have on reported kinetics during gait. Some investigators suggest they cannot be ignored, and can lead to significant variations in reported dynamics<sup>[116, 117]</sup>. Others minimize the effect misestimating these parameters can have on kinetic results<sup>[118-120]</sup>. Interestingly, authors from both groups suggest body segment parameters at the ankle joint play little role during stance phase. Ganley and Powers report a RMSE (root mean square error) of 0.005 for stance phase ankle kinetics when comparing two different body segment parameter methods in which foot mass and mass moment of inertia differed by over 35%<sup>[118]</sup>. In a similar study by Rao et al., the role of body segment parameters from six different models on gait inverse dynamics was analyzed<sup>[117]</sup>. In Rao's study, the largest difference in body segment parameters among models occurred at the foot ( $42.84 \pm 16.77\%$ ), but accounted for less than 1% of mean NRMS (normalized root mean square) moment at the ankle during stance phase<sup>[117]</sup>. Several additional authors have suggested

that lower extremity kinetics are dominated by ground reaction forces, and body inertial effects play a minimal role<sup>[109, 120, 121]</sup>. Part of the current study aims are to determine the role talar and calcaneal body segment parameters have on talocrural and subtalar joint kinetics during the stance phase of gait.

### 1.7 Hypotheses and Specific Aims

The purpose of this study was to determine the feasibility of using fluoroscopy to quantify *in vivo* intra-foot dynamics of the hindfoot during stance phase. It is hypothesized that:

1. Fluoroscopic sagittal plane dynamics of the talocrural and subtalar joints during barefoot stance are similar to those reported using other approaches (external skin marker, bone pin).
2. Talocrural and subtalar sagittal plane kinetics are dominated by ground reaction forces, rather than talar and calcaneal body segment parameters.
3. Fluoroscopic sagittal plane kinematics of the talocrural and subtalar joints during stance are different in barefoot and toe-only rocker conditions.

In order to validate the above hypotheses, the following specific aims were accomplished:

1. Develop a safe, portable single gantry fluoroscopic system capable of capturing gait dynamics during stance in normal adult subjects.
2. Synchronize a multi-camera video motion analysis system with the fluoroscopic system.

3. Synchronize a multi-axis force platform with the fluoroscopic system.
4. Calibrate and quantitatively evaluate the combined systems.
5. Develop a biomechanical model of the hindfoot for talocrural and subtalar sagittal plane dynamics.
6. Investigate the kinematic model sensitivity.
7. Investigate the role of talar and calcaneal body segment parameters on talocrural and subtalar joint sagittal plane kinetics during the stance phase of gait.
8. Characterize the sagittal plane hindfoot kinematics of a population of normal adult subjects when walking barefoot.
9. Characterize the sagittal plane hindfoot kinematics of a population of normal adult subjects when walking with toe-only rocker orthopaedic shoes.
10. Compare and contrast sagittal plane hindfoot kinematics in the normal adult when barefoot and wearing a toe-only rocker orthopaedic shoe.

## 2. A Model for Assessment of *In vivo* Hindfoot Motion During Gait

Fluoroscopic technology allows the direct visualization of underlying bony anatomy during gait, and circumvents the known limitations in skin mounted external marker multi-segmental foot models (skin motion artifact, marker misplacement sensitivity, rigid body assumption). This study introduces a fluoroscopic foot model suitable for assessment of *in vivo* hindfoot dynamics during gait. Sagittal plane talocrural and subtalar kinematics of five healthy subjects ( $22.8 \pm 4$  years,  $72.57 \pm 4.1$  kg,  $177.3 \pm 4.1$  cm), and the kinetics of one subject (25 years, 67.13 kg, 180.34 cm) are reported. Minimum and maximum talocrural plantar flexion and dorsiflexion occur at 12% cycle and 84% cycle respectively, with magnitudes of  $11.7^\circ$  and  $-8.4^\circ$  respectively (ROM =  $20.1^\circ$ ). Minimum and maximum subtalar plantar flexion and dorsiflexion occur at 96% cycle and 30% cycle respectively, with magnitudes of  $4.9^\circ$  and  $-4.4^\circ$  (ROM =  $9.3^\circ$ ). Kinematic results compare favorably with reported intra-cortical bone pin studies. Minimum and maximum talocrural moments occur at 8% cycle and 80% cycle respectively, with magnitudes of -0.32 and 1.32 Nm/kg. Minimum and maximum subtalar moments occur at 6% cycle and 81% cycle respectively, with magnitudes of -0.36 and 1.36 Nm/kg. Kinetic values are similar to other reported ankle/hindfoot moments.

### 2.1 Introduction

Gait analysis has become a powerful tool used by clinicians to assess the kinematics and kinetics of patients, pre- and post-operatively, for both rehabilitation and

research purposes. Historically, most of the models used by clinicians describe the lower extremity as a system of rigid segments with skin mounted external markers, whose most distal segment is a rigid representation of the entire foot <sup>[1-5]</sup>. A rigid body assumption of the foot fails to take into account the known major articulations, and can lead to errors regarding ankle and subtalar joint biomechanics, especially when applied to the deformed foot <sup>[122, 123]</sup>. Because of limitations associated with a single rigid representation of the entire foot, several multi-segmental models have been developed that divide the foot from anywhere among two and nine segments <sup>[6, 8-10, 124-126]</sup>. While dividing the foot into multiple segments via external skin markers allows for the biomechanical analysis of the major joints within the foot, doing so also introduces concerns about skin motion artifact, marker misplacement errors, and the continued problem of movement within an assumed to be rigid segment.

In the last two decades fluoroscopy has emerged as a means for directly visualizing the movement or position of the underlying foot anatomy <sup>[29, 55, 58-61, 127, 128]</sup>. The first 2D static kinematic model of the foot based on fluoroscopically collected images was done by Komistek et al. in 2000 <sup>[21]</sup>. The study measured the range of motion of ten ankles in the sagittal plane between two static positions (maximum flexion/extension). The first 3D static kinematic model of the hindfoot using fluoroscopic images was done by de Asla et al. in 2006 <sup>[19]</sup>. The model used MRI techniques to create a 3D model of the tibia, fibula, talus, and calcaneus. The fluoroscopic images were used to place the 3D models in the same orientations as seen by the fluoroscopic images. Coordinate systems were created for the bones and a kinematic analysis between different orientations was completed. The major drawbacks of de

Asla's study were the limited scope of gait studied (only heel strike, mid-stance, and toe-off were analyzed), the static nature of the analysis (subjects stopped moving while the fluoroscopic images were taken), and the limitation of the analysis to kinematics only.

The purpose of this study was to develop the techniques needed to collect and analyze *in vivo* hindfoot dynamics using fluoroscopy. The developed fluoroscopic system (FS) was designed to capture data as subjects walked at a natural, self-selected pace. The planar fluoroscopic images obtained from the system were corrected for foot progression angle and used to determine talocrural and subtalar dynamic components in the sagittal plane. A standard force plate was used to measure ground reaction force information for the kinetic model. Results were compared to invasive implant studies<sup>[12, 14]</sup>.

## 2.2 Materials and Methods

### 2.2.1 System Configuration

The system was set up so that marker motion data, fluoroscopic images, and ground reaction force (GRF) data could be collected in synchrony. The motion analysis system (MAS) consisted of 14 infra-red cameras (Vicon Motion Systems, Inc., Lake Forest, CA) that tracked standard 16 mm markers. The fluoroscopic images were collected at 120 fps using a Basler Aviator avA1000km camera (Basler Vision Technologies, Ahrensburg, Germany), XCAP imaging software (XCAPTM, Buffalo Grove, IL), and a reconfigured OEC 9000 C-arm fluoroscopy unit (GE, Fairfield, CT). During fluoroscopic data collection, radiation levels varied from 90-100 kVp, and 0.5-1.7

mA depending on patient-specific image quality analyses. GRF data was collected using a multi-axis AMTI OR6-5-1 force plate (AMTI, Watertown, MA) embedded in a raised walkway. All data processing was done in MATLAB or ImageJ.

Figure 2-1 illustrates the system configuration. The FS was reconfigured so that the emitter and image intensifier (II) were no longer attached and could be set on opposite sides of the walkway. In order to maximize the size and resolution of the foot in the collected images, as well as the size of the capture volume, the emitter collimator plates were altered so that the distance between the emitter and II could be increased to 32". The II was set parallel to the embedded AMTI force plate (global XZ plane), and positioned to capture heel strike and as much of stance phase as possible. Subjects walked along the global X direction.

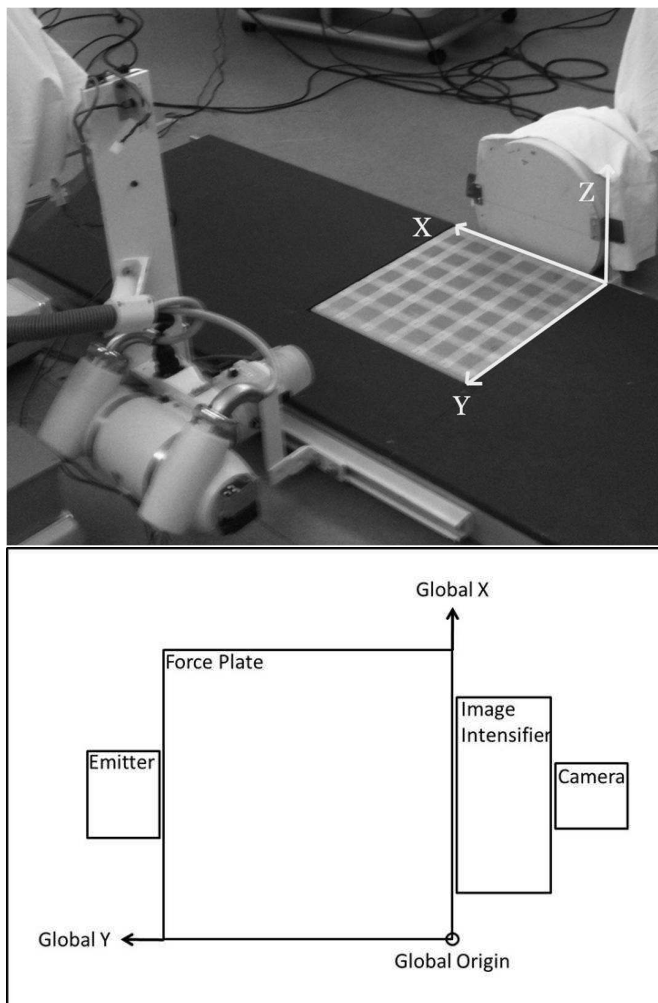


**Figure 2-1** System configuration. Embedded force plate with global coordinate system, emitter, image intensifier (II), and camera (behind II).

### 2.2.2 System Synchronization

The fluoroscopic images were synchronized to the MAS using a five volt TTL pulse. The pulse was generated by the fluoroscopy unit when activated, and sent to a relay circuit where the output voltage and current levels were reduced to acceptable levels for a computer's GPI (~3.3 volts, 200mA). This lower voltage was then inputted into the Vicon MX motion system as an external device analog signal, as well as the GPI of the computer with the XCAP imaging software, where it was used to trigger the recording of images. Code was written to analyze and quantify the number of frames between the five volt TTL trigger and force plate activation (heel strike). This number corresponded to the number of images collected fluoroscopically before heel strike occurred. High acceleration tests with an impact device were completed to ensure reliable detection of heel strike ( $\pm 1$  frame at 120 fps).

### 2.2.3 Image Construction

The characteristic pin cushion distortion of the II was mathematically corrected using a standard grid as defined by Karau et al.<sup>[49]</sup>. The correction algorithm determined the coefficients required to alter the image such that the calibration markers were at the same pixel distance in the calibration grid image. These coefficients were used to correct all collected fluoroscopic images in the processing phase of data analysis.

## 2.2.4 Global Referencing

Global referencing was used in the system design to allow for coincident identification of fluoroscopic points of interest as well as external skin markers. Equations 2.1-2.3 (Table 2.1) were used to translate point of interest (POI) locations in image coordinates ( $POIx'$ ,  $POIz'$ )

to POI locations in global coordinates ( $POIX$ ,  $POIY$ ,  $POIZ$ ) within the foot progression plane (vertical plane defined by subject foot progression angle). Figure 2-2 shows a typical fluoroscopic image with parameters identified. In order to validate the use of Equations 2.1-2.3, experiments were done to quantify the error between globally referenced points in fluoroscopic images and their known global locations (Section 2.3.1).



**Figure 2-2** Typical fluoroscopic image. POI locations are translated from image coordinates ( $POIx'$ ,  $POIz'$ ) to global ( $POIX$ ,  $POIY$ ,  $POIZ$ ) using an external marker's image ( $Hx'$ ,  $Hx'$ ) and global ( $HX$ ,  $HY$ ,  $HZ$ ) coordinate locations, as well as the image pixels per millimeter ( $ppm$ ) magnification, subject foot progression angle ( $\beta$ , calculated from external markers), and the camera's angular rotation from global ( $\theta$ ).

**Table 2.1** Equations used for global referencing.

$$POIX = HX + \left[ \left[ \frac{POIx' - Hx'}{ppm} \right] \cos \theta + \left[ \frac{POIz' - Hz'}{ppm} \right] \sin \theta \right] \quad (\text{Eq. 2.1})$$

$$POIY = HY + \left[ \left[ \frac{POIx' - Hx'}{ppm} \right] \cos \theta + \left[ \frac{POIz' - Hz'}{ppm} \right] \sin \theta \right] \tan \beta \quad (\text{Eq. 2.2})$$

$$POIZ = HZ + \left[ - \left[ \frac{POIx' - Hx'}{ppm} \right] \sin \theta + \left[ \frac{POIz' - Hz'}{ppm} \right] \cos \theta \right] \quad (\text{Eq. 2.3})$$

### 2.2.5 Kinematic Model

The model analyzes talocrural and subtalar joint kinematics, and therefore requires local coordinate systems to be defined for the tibia, talus and calcaneus. The tibia coordinate system is defined by external markers as it remains outside the II field of view for much of stance phase. The

talus and calcaneus coordinate systems are defined by virtual markers. Virtual markers are locations on fluoroscopic images that have been translated from image coordinates to global coordinates using global referencing (Table 2.1). Each bone (talus and calcaneus) requires two virtual markers to define its local coordinate system i-axis.

The locations on each bone used to



**Figure 2-3** Virtual marker locations. V1 and V2 represent typical virtual marker locations for the talus, while V3 and V4 represent typical virtual marker locations for the calcaneus.

derive the virtual markers needs to remain constant frame to frame so that i-axes are always defined using the same virtual marker locations. Figure 2-3 illustrates examples of virtual marker locations on the talus and calcaneus. After virtual marker locations are translated to global coordinates via global referencing, they are used in conjunction with external skin marker locations (Table 2.2) to define the local coordinate axes of the tibia, talus and calcaneus coordinate systems (Table 2.3).

**Table 2.2** External marker locations. Markers M1 and M2 are used to define the foot progression angle ( $\beta$ ) in Equation 2.2. Markers M3-M6 are used to define the axes of the tibial coordinate system.

Marker Name	Marker Location
M1	Calcaneal tuberosity
M2	Head of the 2 <sup>nd</sup> metatarsal
M3	Medial malleolus
M4	Lateral malleolus
M5	Medial femoral epicondyle
M6	Lateral femoral epicondyle

**Table 2.3** Segment coordinate system axes definition. Virtual markers have prefix V, external markers have prefix M. All marker locations (virtual and external) are defined in global coordinates.

Segment	i-axis	j-axis	k-axis
Calcaneus	$\frac{(V3 - V4)}{ (V3 - V4) }$	$\frac{(k_{axis} \times i_{axis})}{ (k_{axis} \times i_{axis}) }$	$\frac{(i_{axis} \times (0,0,1))}{ (i_{axis} \times (0,0,1)) }$
Talus	$\frac{(V1 - V2)}{ (V1 - V2) }$	$\frac{(k_{axis} \times i_{axis})}{ (k_{axis} \times i_{axis}) }$	$\frac{(i_{axis} \times (0,0,1))}{ (i_{axis} \times (0,0,1)) }$
Tibia	$\frac{(\frac{M5 + M6}{2}) - (\frac{M3 + M4}{2})}{\left  \left( \frac{M5 + M6}{2} \right) - \left( \frac{M3 + M4}{2} \right) \right }$	$\frac{\left( \left( M3 - \left( \frac{M3 + M4}{2} \right) \right) \times i_{axis} \right)}{\left  \left( \left( M3 - \left( \frac{M3 + M4}{2} \right) \right) \times i_{axis} \right) \right }$	$\frac{(i_{axis} \times j_{axis})}{ (i_{axis} \times j_{axis}) }$

After local coordinate definition, kinematic analysis is completed by using the Joint Coordinate System method, and motion is reported as distal segment movement with respect to proximal<sup>[129]</sup>. In addition to the dynamic images collected, the model is applied to a static x-ray image with the subject standing in single limb support with their foot placed at the same progression angle observed during dynamic data collection and the same virtual marker locations used. This is done to quantify the angles between segment coordinate systems during quiet standing. These measured angles during quiet standing are used for clinical reference and represent neutral position for reported kinematics.

#### 2.2.6 Kinematic Model Sensitivity

The virtual marker locations used to define talar and calcaneal local coordinate system i-axes are subject-unique, and chosen during data processing. Specific anatomic locations were not chosen so the model could be applied to a wider range of pathologies in which model defined anatomic locations may not be clearly visible in lateral view fluoroscopic images. The only requirement in selecting virtual marker locations is that the locale selected be identifiable in the entire dynamic fluoroscopic image sequence and the corresponding lateral view static x-ray. In general, virtual markers should be selected as far apart as possible. This increase in distance reduces the sensitivity in angular definition, and is similarly described for external marker models<sup>[130]</sup>. Because the proposed model uses subject specific virtual marker locations and quiet standing defines neutral joint angles, comparable kinematic results should be obtained when different POI

locations are used as virtual markers. Experiments were conducted to verify this empirically (Section 2.3.3).

### 2.2.7 Kinetic Model

GRF data was collected using an AMTI force plate, and standard center of pressure equations were used to describe the resultant reaction force vector in global coordinates. After foot flat occurs and multiple contact points exist between the force plate and the foot, GRF contributions distal to the calcaneal segment are included in estimating the force acting upon the calcaneal segment. Both the talocrural and subtalar joint locations were calculated for each frame of interest using global referencing (Table 2.1). Talus and calcaneus centroids, from the 2D fluoroscopic images, were used to define origins of segment masses (as opposed to center of mass locations). Centroid locations were determined by outlining each bone in a single static x-ray image and then using an ImageJ plugin (BoneJ) which outputted the 2D centroid pixel locations. In this static x-ray image, relationships of the each bone's centroid location and the virtual marker locations used to track the bone were created and used to mathematically determine the dynamic centroid location ( $C_d$ ) in dynamic images as described in:

$$C_d = V_d + D(R_1 \hat{u} + R_2 \hat{v}) \quad (\text{Eq. 2.4})$$

where (for the calcaneal segment),

$$\begin{aligned} V_d &= V3_d \\ D &= |V3_d - V4_d| \\ R_1 &= \frac{|V3_s - P_s|}{|V3_s - V4_s|} \\ R_2 &= \frac{|C_s - P_s|}{|V3_s - V4_s|} * \frac{C_{sz'} - P_{sz'}}{|C_{sz'} - P_{sz'}|} \\ \hat{u} &= \frac{V4_d - V3_d}{D} \\ \hat{v} &= \begin{bmatrix} 0 & -1 \\ 1 & 0 \end{bmatrix} \hat{u} \end{aligned}$$

- d denotes points in dynamic images,
- s denotes points in the static x-ray image, and
- z' denotes the z-component of a point's (x', z') pixel coordinates

Points  $C_d$ ,  $V3_d$ ,  $V4_d$ ,  $C_s$ ,  $V3_s$ ,  $V4_s$ , and  $P_s$  for a typical static x-ray and dynamic fluoroscopic image are illustrated in Figure 2-4. Similar equations were used to determine the dynamic talar centroid location by replacing point V3 with V1 and V4 with V2 (Eq. 2.4). These centroid pixel locations were then translated to global coordinates using global referencing (Table 2.1) and became the origins of segment masses in the kinetic analysis. The masses themselves were determined using a ratio of the area of the bone of interest to the area of the entire bony foot (from talus to distal phalanges) in the static x-ray. This value was then scaled by  $1.37\% \text{ BW}^{[113]}$  to estimate segment mass.

The mass estimation includes soft tissue weight at the same ratio as soft tissue to the entire foot. Table 2.4 shows the estimated mass of both the talus and calcaneus for a typical subject.

The final step before analyzing the hindfoot kinetically was estimating the mass moments of inertia for the talus and calcaneus. Each bone was modeled as a cylinder whose centroid coincided with the segment centroid, and whose cylindrical axis coincided with the local segment i-axis. The length of each cylinder was determined by measuring each bone using pixel locations and the magnification of the image (ppm in Figure 2-2). The cylindrical radius was determined by the relationship between mass, volume and density,

where segment density was assumed to be equivalent to overall foot density, was subject specific, and calculated per Contini's method<sup>[131]</sup>. Once the mass, length and radius of each cylinder was determined, mass moments of inertia were calculated using standard

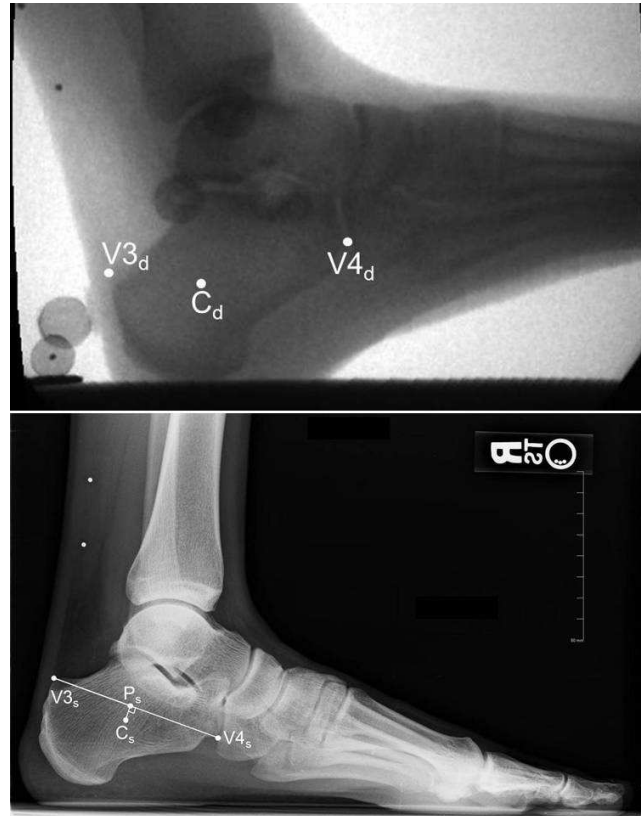


**Figure 2-4** Calcaneal segment centroid locus. Locus  $C_d$  in a dynamic fluoroscopic image (top) was calculated from various points as described in Equation 2.4.  $P_s$  is the locus on line segment  $\overline{V3_sV4_s}$  where a line through locus  $C_s$  perpendicularly intersects  $\overline{V3_sV4_s}$  in a static x-ray image (bottom).

cylinder equations. Table 2.4 shows the estimated mass moments of inertia for both the talus and calcaneus for a typical subject.

**Table 2.4** Body segment parameters.

Segment	Mass <i>kg</i>	Mass Moment of Inertia ( $10^{-4}$ )		
		Int/Ext <i>kg*m<sup>2</sup></i>	Abd/Add <i>kg*m<sup>2</sup></i>	Flx/Ext <i>kg*m<sup>2</sup></i>
Talus	0.12	0.2782	0.7685	0.7685
Calcaneus	0.20	0.5550	1.9590	1.9590

Linear mass accelerations were determined using five point numerical differentiation. Euler angles were used to define segment angular velocities and accelerations, which were in turn used to estimate change in segment angular momentum. Residual moments were calculated for the distal segment to the joint by determining the forces acting on the segment and multiplying them by the moment arm's they acted upon. The kinetic model followed the method of Vaughan et al.<sup>[129]</sup>.

### 2.2.8 Body Segment Parameters

A number of researchers have attempted to estimate lower extremity body segment parameters (mass locus, mass, mass moments of inertia)<sup>[110-115]</sup>, but none report talar or calcaneal specific data. For this reason, no comparisons could be made to the inertial estimates in the proposed kinetic model (Table 2.4). Any variability in the estimated body segment parameters are propagated through the kinetic model and are reflected in the reported results. In an attempt to quantify the role talar and calcaneal body segment parameters have on talocrural and subtalar kinetics, analyses were done

with and without their contributions. The differences when including and not including these body segment parameters are presented in Section 2.3.5.

### 2.2.9 Subject Selection

For the kinematic model, the right feet of five male subjects were tested after institutional review approval and informed consent (mean age  $22.8 \pm 4$  years, mean weight  $72.57 \pm 4.12$  kg, mean height  $177.3 \pm 4.1$  cm). One of these subjects (age 25 years, weight 67.13 kg, height 180.34 cm) was randomly selected and their right foot was analyzed using the kinetic model. All subjects were screened for exclusion criteria, and demonstrated a normal gait pattern.

## 2.3 Results

### 2.3.1 Global Referencing

POIs were globally referenced with the FS and compared to their known tri-axial coordinates as determined with the MAS. Resolution and accuracy of motion systems have been established for both adult and pediatric foot capture volumes in prior studies<sup>[8, 132]</sup>. For evaluation, a global referencing matrix of 81 equally spaced radiopaque markers (2 mm DIA) was imaged (Figure 2-5). The markers were located in a 9x9 matrix array (rows and columns spaced at an interval of 25.4 mm). Each marker was globally referenced using equations 2.1-2.3 (Table 2.1). The 2D matrix was rotated in 5° increments in the global XY plane and swept through a 90° angle ( $\pm 45^\circ$ ) in order to approximate extreme variations in foot progression angle. Figure 2-6 shows the results of these tests for foot progression angles seen during data collection (neutral to 10° external

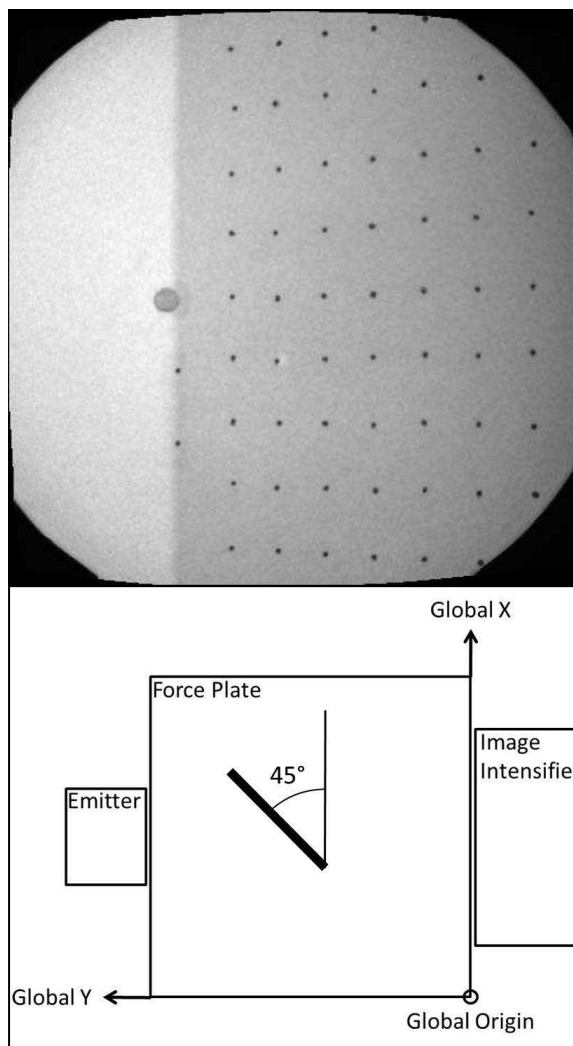


**Figure 2-5** Global referencing matrix. The fluoroscopic image of the global referencing matrix (top) was taken at an angle of 45° to the global X-axis in the global XY plane (bottom).

rotation). As progression angle increased, averaged marker position error increased with distance away from the point of rotation. At a progression angle of  $0^\circ$  an averaged marker position error less than 0.25 mm was noted 40 mm distal to the point of rotation, and an error of 0.75 mm was noted 120 mm distal to the point of rotation. As the progression angle increased to  $10^\circ$  external rotation, averaged marker position errors of 0.50 mm and 2.75 mm, respectively, were reported at distances of 40 mm and 120 mm distal to the point of rotation.

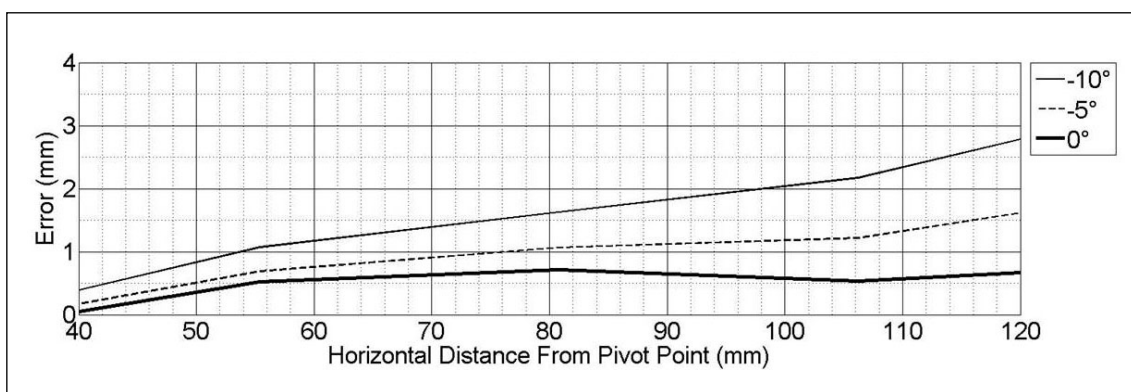


**Figure 2-6** Global referencing error based on position in capture volume. Lines represent tests at three different progression angles.

### 2.3.2 Joint Kinematics

Sagittal plane kinematic results for both the talocrural and subtalar joints are presented in Figure 2-7. Standardized phases of gait<sup>[133]</sup> were normalized to stance, and vertical lines represent divisions in phases. The missing fluoroscopic data between 97-100% of stance phase corresponds to the subject's foot vacating the II field of view. Comparison values displayed in Figure 2-7 are derived from an invasive bone pin study<sup>[14]</sup>. Table 2.5 presents the kinematic results of the fluoroscopic study and that of existing bone pin studies reporting talocrural and subtalar motion<sup>[12, 14, 134]</sup>.

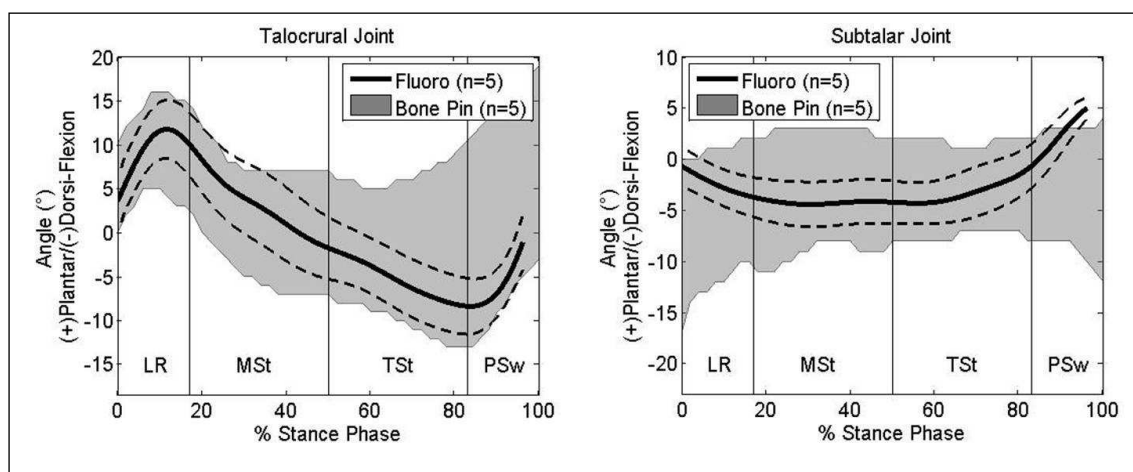


**Figure 2-7** Sagittal plane kinematic results. Black solid lines represent mean angle of all five fluoroscopic subjects. Dashed lines represent fluoroscopic subjects' mean  $\pm$  1 SD. The grey bands depict the standard deviation ranges in Lundgren's study of five adult males<sup>[14]</sup>.

**Table 2.5** Fluoroscopic and bone pin kinematics.

	Talocrural Joint		
	Fluoroscopic (n=5)	Bone Pin <sup>[12, 134]</sup> (n=3)	Bone Pin <sup>[14]</sup> (n=5)
	Max (% Stance Phase)	Max (% Stance Phase)	Max (% Stance Phase)
Plantar flexion	11.2° (11)	7.2° (13)	-
Dorsiflexion	-6.9° (85)	-4.6° (80)	-
ROM	18.1°	11.8°	15.3°
	Subtalar Joint		
	Fluoroscopic (n=5)	Bone Pin <sup>[12, 134]</sup> (n=3)	Bone Pin <sup>[14]</sup> (n=5)
	Max (% Stance Phase)	Max (% Stance Phase)	Max (% Stance Phase)
Plantar flexion	4.8° (96)	1.5° (97)	-
Dorsiflexion	-3.6° (30)	-1.3° (23)	-
ROM	8.4°	2.8°	6.8°

### 2.3.3 Kinematic Model Sensitivity

Table 2.6 shows the mean and standard deviation of the absolute difference between kinematic results of the same subject and same examiner using different virtual marker locations over five trials. All results are sub-divided into standardized phases of

gait: Loading Response (LR, 0-10%), Mid Stance (MSt, 10-30%), Terminal Stance (TSt, 30-50%), and Pre Swing (PSw, 50-60%)<sup>[133]</sup>. Maximum talocrural angular difference occurred during MSt, and was 2.37°. Maximum subtalar angular difference also occurred during MSt, and was 3.32°.

**Table 2.6** Kinematic model sensitivity. Absolute difference in sagittal plane kinematic results for the same subject using different virtual marker locations (n=5 trials). Mean values and standard deviation in parentheses are presented.

	LR	MSt	TSt	PSw
Talocrural	1.78° (0.82°)	2.37° (1.51°)	1.89° (1.00°)	2.04° (1.11°)
Subtalar	1.75° (0.97°)	3.32° (1.75°)	2.22° (1.67°)	2.08° (1.81°)

#### 2.3.4 Joint Kinetics

Talocrural and subtalar kinetic results for an individual subject are presented in Figure 2-8. Each of the five trials is plotted. Minimum and maximum talocrural moments occur at 8% and 80% cycle, respectively, with magnitudes of -0.32 and 1.32 Nm/kg. Minimum and maximum subtalar moments occur at 6% and 81% cycle, respectively, with magnitudes of -0.36 and 1.36 Nm/kg.

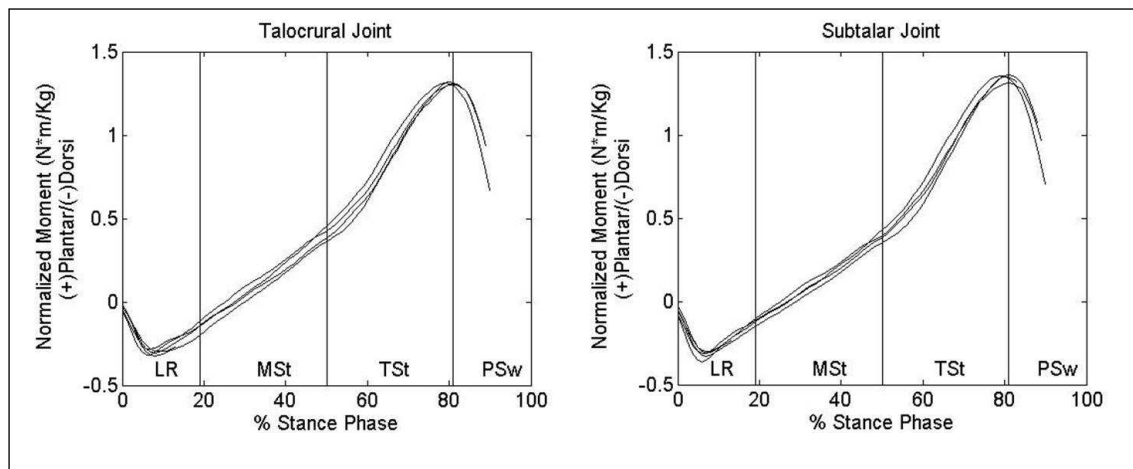


**Figure 2-8** Sagittal plane kinetic results. Black lines represent individual trials for a single subject.

### 2.3.5 Kinetic Body Segment Parameter Effects

Table 2.7 shows the mean and standard deviation of the absolute difference between talocrural and subtalar kinetic results of the same subject when including and not including talar and calcaneal body segment parameters. Maximum talocrural kinetic difference occurred during PSw, and was  $1.10 \text{ e}^{-3} \text{ Nm/kg}$ . Maximum subtalar kinetic difference occurred during MSt, and was  $6.45 \text{ e}^{-4} \text{ Nm/kg}$ .

**Table 2.7** Kinetic body segment parameter effects. Absolute difference in sagittal plane kinetic results for the same subject when including and not including talar and calcaneal body segment parameters (n=5 trials). Mean values and standard deviations in parentheses are presented (units:  $10^{-4} \text{ Nm/kg}$ ).

	LR	MSt	TSt	PSw
Talocrural	7.75 (5.68)	4.48 (1.06)	5.69 (1.07)	11.00 (1.87)
Subtalar	3.58 (2.34)	6.45 (0.63)	5.52 (0.83)	3.92 (0.41)

## 2.4 Discussion

The global referencing method used to translate virtual markers from a single 2D image to global 3D space utilizes the foot progression angle acquired from external markers. The foot progression angle in conjunction with a jointly known external marker location, both in the FS and MAS, is used to determine the 3D coordinates of POIs. Errors can be introduced in the global referencing equations if a single image magnification factor (ppm) is assumed for an object that is not parallel to the II during image collection. Such errors are measurable as illustrated in Figure 2-6. Typical progression angles, as observed in our study (neutral to 10° external rotation), demonstrate similar dynamic position errors to those reported with other MAS systems (1.42-2.96 mm)<sup>[8, 132]</sup>. In determining POI loci, the error associated with assuming a single image magnification factor is measurable and repeatable. Thus, correction algorithms can be used for even larger progression angles as well as POI locations more distal to the known external marker location.

Most of the current kinematic models using external skin markers report only ankle joint motion, or that of a hindfoot segment with respect to a shank segment. There are a handful of studies in the literature estimating talocrural and subtalar joint motion on the basis of external skin marker locations and assumed anatomic relationships<sup>[126, 135]</sup>. It is generally accepted in the field of biomechanics that the talus cannot be accurately tracked by markers attached to the surface of the skin<sup>[9]</sup>. Bone pin methodologies do allow discrete talar isolation and are capable of reporting talocrural and subtalar motion as noted in the current study.

Results from these invasive studies compare favorably to that of this work.

Figure 2-7 illustrates the results of the fluoroscopic study and estimates those of bone pin work by Lundgren et al.<sup>[14]</sup>. The fluoroscopic and bone pin results show the talocrural joint going from neutral to plantar flexion during load response followed by a return to neutral and into dorsiflexion during mid-stance and terminal stance. Both studies also report talocrural joint motion going from dorsiflexion to neutral/plantar flexion during pre-swing. The fluoroscopic study and an earlier (2004) bone pin study also illustrate maximum plantar flexion during load response (Table 2.5). The bone pin study reports maximum dorsiflexion during terminal stance<sup>[12, 134]</sup>, whereas the fluoroscopic study reports maximum dorsiflexion during pre-swing. The two differ by only 4% of the gait cycle.

A similar comparison for the subtalar joint reveals that fluoroscopic results show neutral to dorsiflexion during load response, while the bone pin study shows a wider region of motion gradually increasing from dorsiflexion to neutral. Both studies illustrate subtalar dorsiflexion during mid and terminal stance. The bone pin study depicts much larger motion variation. The fluoroscopic results show a return to neutral/plantar flexion during pre-swing, while the bone pin results remain dorsiflexed (Figure 2-7).

Differences in kinematics between the two methodologies may be attributed to the invasive nature of bone pin insertion effecting natural gait or age differences among study subjects. Westblad et al. have reported discrepancies between magnitudes of rotation when comparing superficial skin mounted and bone anchored markers. Results for tibio-calcaneal rotations inversion/eversion, plantar/dorsiflexion, and abduction/adduction were 2.5°, 1.7° and 2.8° respectively<sup>[17]</sup>. The authors hypothesize

discrepancies may be the result of pain, anesthetic or soft tissue impingement. In another comparison of surface and bone-anchored foot markers, Nester et al. reported differences greater than  $3^\circ$  throughout the gait cycle<sup>[15]</sup>.

The fluoroscopic study group consisted of younger individuals (22.8 years) than the bone pin kinematic studies (39.3 and 38 years)<sup>[12, 14]</sup>. Oberg et al. has described differences in gait kinematics with aging for 233 healthy subjects aged 10-79 years<sup>[136]</sup>. While these differences are small, the effects of age upon *in vivo* bony kinematics of the foot and ankle have not been studied.

Another contributing factor in reporting kinematics is marker placement (virtual or external). External skin marker placement repeatability is critical in models where marker locations are used to define non-zero joint positions during quiet standing. The advantage of these models is they allow for measurement of foot deformity<sup>[137]</sup> as long as markers are placed accurately on subjects and precisely among subjects. The disadvantage of these models is that if markers are misplaced, kinematic results can be affected. In a four-segmental foot model developed by Carson et al., inter-segmental angles as high as  $6^\circ$  were reported for inter-day repeatability<sup>[7]</sup>. Alternative models, like the proposed fluoroscopic, define joint neutrality with a static trial. The ramification of this is a potential offset in kinematic results when compared to models that define non-zero joint neutrality. The advantages of using quiet standing to define joint neutrality in the proposed fluoroscopic model are twofold. The first advantage is virtual marker locations are subject unique and can be defined as the most clearly visible and distinguishable anatomic locations in the fluoroscopic image sequence. The second advantage is that because kinematic results are reported relative to joint neutrality,

different virtual marker locations will produce the same kinematics results, as illustrated in Table 2.6. The largest angular difference reported when using alternate virtual marker locations to analyze the talocrural and subtalar joints was  $3.32^\circ$  and occurred during mid-stance of the subtalar joint.

The proposed fluoroscopic model uses subject unique virtual marker locations, and kinematic results are dependent on these unique locations being correctly identified in subsequent images. Any variability in virtual marker loci frame to frame would be reflected in the kinematic results. Because there is no way to determine the true position of virtual marker locations frame to frame, quantifying this error is impossible. It is noted in the literature, however, that intra-rater reliability of several radiographic angular and linear parameters of the foot have been reported as high as  $R = 0.82\sim 0.99$ <sup>[138]</sup>.

The fluoroscopic kinetic results (Figure 2-8) cannot be directly compared to literature as there are no reported *in vivo* kinetic results regarding the talocrural and subtalar joints. In a 1991 study by Scott and Winter, talocrural and subtalar joint kinetics were reported on the basis of anatomic estimates of talar position<sup>[135]</sup>. The talar locus was mathematically estimated assuming two monocentric hinge joints and tracking the tibia and calcaneus with external markers. The error associated with the two monocentric hinges was estimated at less than 4 mm<sup>[135]</sup>. Despite methodological differences, the reported talocrural results compare favorably with the fluoroscopic results, both in morphology and magnitude. Scott and Winter report peak talocrural moment around 80% stance between 1.59 and 1.62 Nm/kg (after normalizing their results to subject weight). The fluoroscopic talocrural peak moment is 1.32 Nm/kg and occurs at 80% stance. The subtalar results reported by Scott and Winter, while morphologically similar,

are smaller in magnitude than those of the fluoroscopic model. Scott and Winter report peak subtalar moment near 75% stance at a value of 0.47 Nm/kg (after normalizing their results to subject weight). The fluoroscopic subtalar peak moment is 1.36 Nm/Kg and occurs at 81% stance. Differences in reported subtalar kinetics may be attributed to the talar position being directly measured in the current fluoroscopic study, and estimated by tibial and calcaneal position in the Scott and Winter study<sup>[135]</sup>.

Other external skin marker studies report ankle joint kinetics (kinetics between a shank segment and an adjoining foot or hindfoot segment) which anatomically compares to the talocrural joint. MacWilliams et al. report averaged minimum and maximum hindfoot extension moments of 0.25 and 1.2 Nm/kg respectively<sup>[9]</sup>. Bruening reports averaged minimum and maximum ankle moments of 0.1 and 1.2 Nm/kg<sup>[109]</sup>, while Dixon reports averaged minimum and maximum ankle internal moments of 0.2 and 1.46 Nm/kg<sup>[139]</sup>. From these studies, minimum moments at the ankle are somewhat lower than minimum talocrural moments in the current fluoroscopic model, while maximum ankle moments are similar.

Differences in the reported kinetic results are likely related to limitations in current kinetic instrumentation<sup>[109]</sup> or modeling assumptions. The biggest instrumentation challenge has been measuring complete GRF data for the subareas of the foot. Each of the reported kinetic models has a different approach for doing this. The fluoroscopic model assumes the calcaneal segment to be in isolated contact with the ground through load response and includes the force contributions of all contact points in estimating the calcaneal reaction forces following load response. The MacWilliams model uses a pressure mat and proportionally divides the overall reaction force among

each segment contacting the ground. Bruening uses two adjacent force plates and targeting trials to isolate contributions between hindfoot and forefoot segments. The Dixon study assumes a rigid foot until after heel rise.

In addition, assumptions in body segment parameter estimation can play a role in reported kinetic discrepancies. The proposed fluoroscopic kinetic model estimates mass locus, mass, and mass moments of inertia for both the talus and calcaneus. In conjunction with GRF data, these body segment parameters are used to determine intersegmental forces and moments during stance phase utilizing inverse dynamics. Table 2.7 suggests these parameters play an incidental role in reported kinetics. When not including body segment parameters, maximum differences in talocrural and subtalar flexion/extension moments of  $1.10 \times 10^{-3}$  and  $6.45 \times 10^{-4}$  Nm/kg, respectively, are observed. These results compare favorably with current literature on the influence of body segment parameters in ankle joint kinetics. Ganley and Powers report a RMSE (root mean square error) of 0.005 for stance phase ankle kinetics when comparing two different body segment parameter methods for which foot mass and mass moment of inertia differed by over 35%<sup>[118]</sup>. In a similar study by Rao et al., the role of body segment parameters from six different models on gait inverse dynamics was analyzed<sup>[117]</sup>. In Rao's study, the largest difference in body segment parameters among models occurred at the foot ( $42.84 \pm 16.77\%$ ), but accounted for less than 1% of mean NRMS (normalized root mean square) at the ankle during stance phase<sup>[117]</sup>. Both of the aforementioned studies show large decreases in body segment parameter influences on joint kinetics from hip to knee and knee to ankle<sup>[117, 118]</sup>. These large decreases can be attributed to segmental masses decreasing from thigh to shank and shank to foot. It is hypothesized that this further

reduction from foot to talus and calcaneus mass is the reason why body segment parameters have an incidental role on the currently reported talocrural and subtalar stance phase kinetics.

It should also be noted that while the fluoroscopic and Scott study subjects were of similar ages (25 and 24.3 years respectively), subjects in the other studies were much younger (MacWilliams: 12.4 years, Bruening: 12.6 years, Dixon: 14.4 years). Age related kinetic changes using rigid foot models have been reported in the literature<sup>[140]</sup>, but no such studies have been done on multi-segmental models.

## 2.5 Conclusion

Talar anatomy does not accommodate external skin marker placement<sup>[9]</sup> and has challenged researchers and clinicians for years with respect to subtalar joint dynamics and hindfoot motion. Bone pin studies are capable of isolating the talus and calcaneus, although their invasive nature, risk of infection and gait altering potential limit widespread clinical application. The current fluoroscopic results are promising, and offer a viable non-invasive method suitable for quantifying talocrural and subtalar dynamics.

Study limitations include a narrow sample of adult male subjects aged 18 to 28 with no reported gait deficiencies or prior bony foot injury. The current study is also limited to a single plane (sagittal) analysis of hindfoot motion components. A further limitation is the use of ionizing radiation with current levels estimated at 10  $\mu\text{Sv}/\text{trial}$ . According to the USNRC, whole body annual occupational limits are 5 rems (50,000  $\mu\text{Sv}$ ).

It is concluded on the basis of the current study that controlled fluoroscopy within a motion analysis environment is appropriate for assessment of *in vivo* hindfoot bony dynamics. The methodology has the potential for assessment of other *in vivo* segmental joints as well as high speed motion applications for sports related activities. The technology is also capable of assessment of *in vivo* bony motion with footwear and pedorthics/orthotics. Further evolution of the technology will allow 3D reconstruction and examination of *in vivo* bony foot kinematics during natural gait.

### 3. Pilot Investigation: *In Vivo* Hindfoot Kinematics During Normal Barefoot Gait

Complex hindfoot anatomy makes quantification of *in vivo* talocrural and/or subtalar motion during gait using standard surface marker tracking technology challenging. This study uses fluoroscopy and a previously described hindfoot model to overcome these challenges, and reports the *in vivo* talocrural and subtalar kinematics of 13 healthy subjects ( $22.9 \pm 2.9$  years,  $77.2 \pm 6.9$  kg,  $178.2 \pm 3.7$  cm). Minimum and maximum talocrural plantar flexion and dorsiflexion occur at 11% cycle and 85% cycle respectively, with magnitudes of  $11.2^\circ$  and  $-6.9^\circ$  respectively (ROM =  $18.1^\circ$ ). Minimum and maximum subtalar plantar flexion and dorsiflexion occur at 96% and 30% cycle, respectively, with magnitudes of  $4.8^\circ$  and  $-3.6^\circ$  (ROM =  $8.4^\circ$ ). Kinematic results compare favorably with reported intra-cortical bone pin studies. In addition, summary measurements (minimum position, maximum position, range) and sources of variability are reported, as well as intra-class correlation (ICC) values for inter-subject variability. It is concluded that inter-subject variability for the sagittal plane motion of normal subjects is higher for the talocrural joint than the subtalar joint. The fluoroscopic system is recommended for continued clinical application and expansion to include three-dimensional (3D) kinematics.

#### 3.1 Introduction

The kinematic sequence of events that occur in the hindfoot during normal ambulation are quite complex, and have long been a challenge for investigators to quantify. Clinically, this is the motion between the calcaneus and tibia, contributed by

two articulations. The talocrural joint defines the motion between the talus and tibia while the subtalar joint defines the motion between the calcaneus and talus. A clear understanding of these articulations is critical in diagnosing and treating foot pathologies<sup>[62-64]</sup>, designing ankle prosthesis/implants<sup>[65-67]</sup>, and describing gait abnormalities.

Because talar position cannot be tracked via surface mounted markers<sup>[9]</sup>, *in vivo* talocrural and subtalar motion is impossible to quantify using standard stereophotogrammetry. For this reason, the majority of kinematic data available on hindfoot motion come from *in vitro* studies<sup>[37-39, 67-69, 84, 85, 88, 90, 98]</sup>, and lacks information in regards to natural weight-bearing gait. While some of these studies have attempted to replicate natural gait using robotic walking simulators<sup>[37-39]</sup>, they are only capable of “near-physiologic” conditions<sup>[39]</sup>, and their kinematic results are more a description of isolated cadaveric foot motion<sup>[38]</sup>.

Most *in vivo* studies quantifying hindfoot motion place the foot in either static non-weight-bearing positions<sup>[20, 89, 93, 94, 96]</sup> or static weight-bearing positions<sup>[19, 21, 81, 82]</sup>. These studies are useful in quantifying joint ROM, but don’t offer much insight into motion attributed to natural gait. Static positioning fails to account for all the subtle foot motions between heel strike and toe-off. In addition, ankle alignment has been shown to change as a result of weight-bearing<sup>[141-144]</sup>. There are a limited number of studies in the literature quantifying hindfoot motion during natural gait using intra-cortical bone pins<sup>[12, 14]</sup>. The invasive nature of these studies limits widespread clinical use.

Fluoroscopy has emerged as an alternative to bone pins to quantify hindfoot motion, but only studies in which the foot was statically placed appear in the literature<sup>[19,</sup>

<sup>21]</sup>. The exception is a study by Yamaguchi et al. in 2009 using fluoroscopy to quantify hindfoot motion at 7.5 fps. Images were collected as subjects moved their foot from maximal plantar flexion to maximal dorsiflexion while their forefoot was in contact with a stair<sup>[57]</sup>. While this methodology is capable of quantifying dynamic hindfoot kinematics, the movement pattern itself is not a direct representation of natural gait.

The purpose of the immediate study was to quantify and characterize both talocrural and subtalar joint motion of the normal foot from heel strike through terminal stance. Fluoroscopic images were collected at 120 fps as subjects walked at a natural, self-selected pace, and reported kinematic data are a direct representation of the bony motion of the hindfoot during gait.

### 3.2 Materials and Methods

Motion analysis testing was conducted by synchronizing a reconfigured OEC 9000 C-arm fluoroscopy unit (GE, Fairfield, CT) with a 14 camera motion analysis system (Vicon Motion Systems, Inc., Lake Forest, CA). Fluoroscopic and motion data were additionally synchronized with analog ground reaction force data captured using a multi-axis AMTI OR6-5-1 force plate (AMTI, Watertown, MA). Once synchronized, the combined fluoroscopic data ( $f_s = 120$  Hz), motion data ( $f_s = 120$  Hz), and force plate data ( $f_s = 3000$  Hz) were used in conjunction with a hindfoot kinematic model to calculate sagittal plane motion from heel strike through terminal stance. Details of the system configuration, synchronization process, and kinematic model can be found in Section 2.2.

### 3.2.1 Subject Selection

Thirteen normal male volunteers (mean age  $22.9 \pm 2.9$  years, mean weight  $77.2 \pm 6.9$  kg, mean height  $178.2 \pm 3.7$  cm) were recruited for this study. All subjects were screened for exclusion criteria, and demonstrated a normal gait pattern. This study was approved by the Institutional Review Boards of Marquette University (Milwaukee, WI), and the Medical College of Wisconsin. All subjects provided informed consent prior to testing.

### 3.2.2 Testing Protocol

The right leg and foot of each subject were instrumented with six reflective markers ( $d = 16$  mm) placed over specific bony landmarks as outlined in Table 2.2. Simultaneous motion analysis, fluoroscopic, and ground reaction force data were collected as subjects walked at a self-selected pace along a six meter walkway. The fluoroscopic system was manually activated just prior to the subject's foot contacting the force plate and de-activated just after toe-off. During fluoroscopic data collection radiation levels varied from 90-110 kVp, and 0.5-1.7 mA depending on patient-specific image quality analyses. A maximum of five barefoot trials were completed with minimum radiation exposure as approved by the IRB. Following dynamic data collection, subjects were escorted to a nearby x-ray suite where a single limb support barefoot x-ray was taken of their right foot placed at the same foot progression angle observed during dynamic image collection.

Synchronized force plate data were used to detect fluoroscopic images between heel strike and toe-off. For each of these images, virtual marker locations were selected for both the talus and calcaneus and translated into global coordinates via global referencing (Section 2.2.4). These translated virtual marker locations, in conjunction with reflective marker positions, were used to define local coordinate systems for the tibia, talus, and calcaneus (Table 2.3). After coordinate definition, a kinematic analysis was completed by using the Joint Coordinate System method<sup>[129]</sup>. Kinematic results were normalized to stance phase (0-100%). Additional kinematics were calculated (with the same virtual marker locations) using the static weight-bearing x-ray. These static kinematic values represent quiet standing and are used for clinical reference (0° on reported kinematic plots). An in-depth description of the kinematic model appears in Section 2.2.5.

Due to the IRB restriction of five radiation exposures per subject, trials in which the subject was exposed but the foot was not within the image intensifier field of view could not be re-imaged. For this reason, six subjects had five trials of data to analyze, six subjects had four trials, and one subject had three trials (n = 57 trials). Foot placement also affected the percentages of stance phase analyzed for each trial, as the talus and calcaneus may not have been in the field of view at heel strike or toe-off. Therefore, trials were grouped together according to Perry's phases of gait: Loading Response (LR, 0-10%), Mid Stance (MSt, 10-30%), and Terminal Stance (TSt, 30-50%)<sup>[133]</sup>. An additional phase was analyzed called loading response through terminal stance (LR-TSt, 0-50%), which combines LR, MSt, and TSt. In order to be included, the trial needed to span the entire phase. LR had 52 trials, MSt had 52 trials, TSt had 41 trials and LR-TSt

had 37 trials. With the exception of LR-TSt, in which 12 subjects were represented, all 13 subjects had at least one trial in each phase analyzed.

### 3.2.3 Statistical Methods

For each joint (talocrural, subtalar) and phase (LR, MSt, TSt, LR-TSt), three summary measures were calculated (minimum position, maximum position, and range) on trials that spanned a given phase. Temporal spatial parameters of walking speed, cadence, and stride length were also analyzed.

All statistical analyses were performed in R 2.13 ([www.r-project.org](http://www.r-project.org)). A random effects linear regression model was used to perform variance components analysis on each summary measurement (minimum position, maximum position, range, walking speed, cadence, and stride length). The model included random effects for subject and measurement as described in:

$$y_{ij} = \beta_0 + \alpha_i + \varepsilon_{ij} \quad (\text{Eq. 3.1})$$

where

- $i$  enumerates subjects ( $i=1:13$ ),
- $j$  enumerates trials within subjects ( $j=1:n_i$ , where  $n_i$  is the number of trials for the  $i^{\text{th}}$  subject).
- $\beta_0$  represents an overall mean among subjects,
- $\alpha_i$  represents random subject effect with Normal distribution ( $\mu = 0$ ,  $\sigma^2 = \sigma_s^2$ ), and
- $\varepsilon_{ij}$  represents random measurement error with Normal distribution ( $\mu = 0$ ,  $\sigma^2 = \sigma^2$ )

Variability was reported as the estimated standard deviations of each of the random effects (subject, measurement), and the estimated standard deviation of  $y_{ij}$ .

$$SD(y_{ij}) = \sqrt{\sigma_s^2 + \sigma^2} \quad (\text{Eq. 3.2})$$

Intra-class correlation (ICC) values represent the percentage of total variability accounted for by subject variability.

$$ICC = \frac{\sigma_s^2}{\sigma_s^2 + \sigma^2} \quad (\text{Eq. 3.3})$$

As described in Equation 3.1,  $\beta_0$  represents the overall mean among subjects for each summary measurement (minimum position, maximum position, range, walking speed, cadence, and stride length). This overall mean differs from the overall mean among trials in that it accounts for subjects having different numbers of trials.  $SD(y_{ij})$  is the standard deviation of  $y_{ij}$ , as described in Equation 3.2. This standard deviation can be thought of as the standard deviation of each summary measurement. Because it has contributions from both subject variation and measurement error,  $SD(y_{ij})$  will be larger than reported subject variability or measurement variability. ICC values represent the percentage of total variability accounted for by subject variability (Eq. 3.3), and can be thought of as a summary measure of ability to detect differences among subjects. Higher ICC values indicate a stronger ability to detect differences.

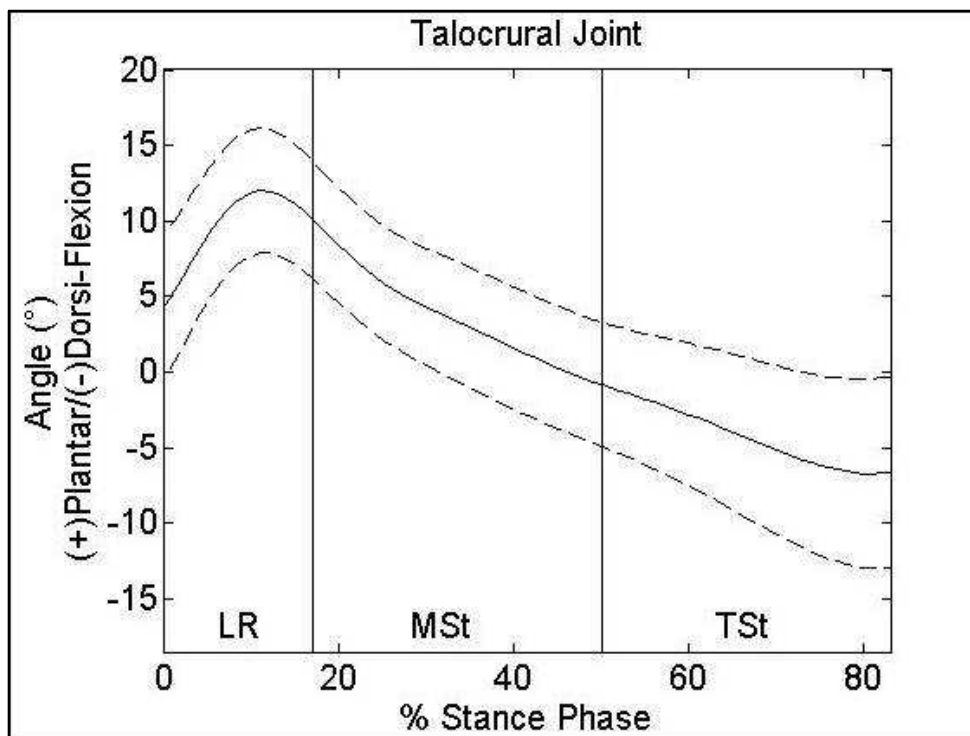
### 3.3 Results

#### 3.3.1 Joint Kinematics

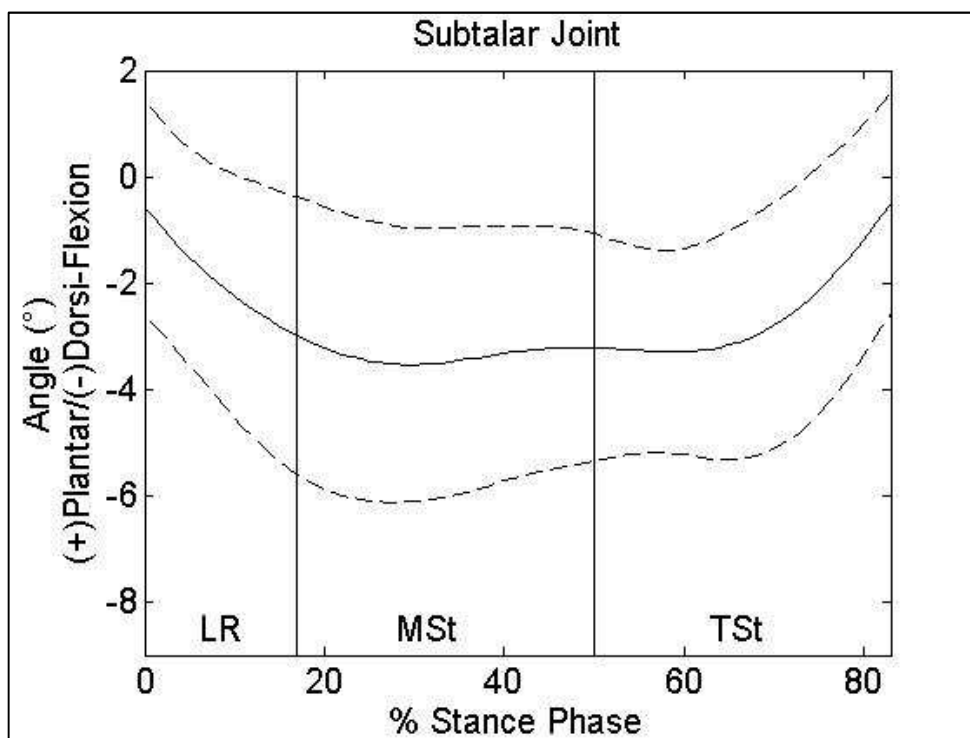
Sagittal plane kinematic results for the talocrural and subtalar joints are presented in Figures 3-1 and 3-2, respectively. Averaged joint angles for the 37 trials that spanned LR through TSt ( $\pm 1$  standard deviation) are reported. Vertical lines represent divisions in Perry's phases of gait<sup>[133]</sup> after normalizing them to stance phase. Talocrural joint motion is reported as talus with respect to tibia, and subtalar motion as calcaneus with respect to talus. Lateral weight-bearing x-rays during quiet standing were used to calculate neutral position ( $0^\circ$ ). Plantar flexion (+) and dorsiflexion (-) represent deviations from this neutral position.

Figure 3.1 presents talocrural joint sagittal plane motion from heel strike through terminal stance. At heel strike the talocrural joint is plantar flexed and increases to a maximal value during LR. After foot flat, the tibia begins to rotate over the talus in the sagittal plane which is depicted as the talocrural joint returning to  $0^\circ$  during MSt. As the tibia continues to rotate over the talus during TSt, the talocrural joint becomes dorsiflexed in preparation for push-off.

Subtalar joint sagittal plane motion from heel strike through terminal stance is depicted in Figure 3.2. At heel strike the subtalar joint is in a relatively neutral position and becomes dorsiflexed during LR. Maximal dorsiflexion is achieved during MSt followed by a slight rocker motion. This rocker motion is completed during TSt, followed by a return to neutral position before PSw.



**Figure 3-1** Talocrural sagittal plane kinematics. Solid line represents mean angle. Dashed lines represent mean  $\pm$  1 SD (n=37 trials).



**Figure 3-2** Subtalar sagittal plane kinematics. Solid line represents mean angle. Dashed lines represent mean  $\pm$  1 SD (n=37 trials).

### 3.3.2 Statistics

Statistical results from the random effects linear regression model (Eq 3.1) on talocrural joint summary measurements (minimum position, maximum position, range) are presented in Table 3.1.  $\beta_0$  values represent an overall mean among subjects for each summary measurement, and  $SD(y_{ij})$  are reported as described in Equation 3.2. Subject SD represents the estimated variability associated with the random subject effect, and Error SD represents the estimated variability associated with the random measurement error. ICC values are the percentage of total variability accounted for by subject variability (Eq. 3.3). For all phases analyzed (LR, MSt, TSt, and LR-TSt), talocrural minimum position and maximum position ICC values exceeded 0.91. This indicates a large variability in these summary measurements among subjects. This trend can also be seen in the much larger subject SD values when compared to error SD. Range of motion (ROM) ICC values for each phase was lower than reported minimum position or maximum position ICC values. This reduction in ICC was associated with a reduction in subject SD, and not an increase in error SD (Table 3.1). While talocrural ROM variability among subjects was strong (ICC = 0.68~0.87), it was lower than minimum position or maximum position variability (ICC = 0.91~0.96).

Similar results using the random effects model (Eq. 3.1) on subtalar motion are presented in Table 3.2. The largest variability among subjects was associated with minimum position. ICC values for this summary measure ranged from 0.4520 to 0.6605. Across all phases analyzed (LR, MSt, TSt, LR-TSt), subtalar error SD exceeded subject SD for maximum position and ROM measurements. This is indicated by ICC values

**Table 3.1** Talocrural kinematic statistics.

	Phase	LR	MSt	TSt	LR-TSt
	Trials	n = 52	n = 52	n = 41	n = 37
Minimum	B <sub>0</sub> [SD(y <sub>ij</sub> )]	3.94° [4.69°]	-1.23° [4.32°]	-6.64° [6.54°]	-7.49° [6.51°]
	Subject SD	4.53°	4.14°	6.36°	6.38°
	Error SD	1.23°	1.23°	1.53°	1.29°
	ICC	0.9314	0.9183	0.9455	0.9608
Maximum	B <sub>0</sub> [SD(y <sub>ij</sub> )]	11.27° [4.45°]	8.53° [4.21°]	-0.77° [5.16°]	11.33° [4.76°]
	Subject SD	4.25°	4.02°	4.99°	4.58°
	Error SD	1.32°	1.24°	1.32°	1.29°
	ICC	0.9124	0.9136	0.9346	0.9264
ROM	B <sub>0</sub> [SD(y <sub>ij</sub> )]	7.33° [2.18°]	9.76° [2.87°]	5.90° [2.82°]	18.83° [5.63°]
	Subject SD	1.80°	2.61°	2.55°	5.25°
	Error SD	1.24°	1.20°	1.19°	2.02°
	ICC	0.6784	0.8260	0.8202	0.8709

**Table 3.2** Subtalar kinematic statistics.

	Phase	LR	MSt	TSt	LR-TSt
	Trials	n = 52	n = 52	n = 41	n = 37
Minimum	B <sub>0</sub> [SD(y <sub>ij</sub> )]	-3.16° [2.24°]	-4.30° [2.33°]	-3.69° [2.02°]	-4.35° [2.48°]
	Subject SD	1.82°	1.83°	1.36°	1.91°
	Error SD	1.31°	1.44°	1.50°	1.58°
	ICC	0.6605	0.6183	0.4520	0.5949
Maximum	B <sub>0</sub> [SD(y <sub>ij</sub> )]	-0.28° [1.97°]	-2.20° [2.15°]	-0.25° [1.99°]	0.29° [1.95°]
	Subject SD	1.28°	1.44°	1.10°	0.94°
	Error SD	1.50°	1.59°	1.66°	1.71°
	ICC	0.4223	0.4478	0.3060	0.2312
ROM	B <sub>0</sub> [SD(y <sub>ij</sub> )]	2.94° [1.37°]	2.13° [1.30°]	3.46° [1.17°]	4.75° [1.59°]
	Subject SD	0.61°	0.80°	0.64°	1.03°
	Error SD	1.23°	1.02°	0.98°	1.21°
	ICC	0.1993	0.3782	0.3031	0.4175

**Table 3.3** Temporal spatial statistics.

	Current Study	Majumdar et al. <sup>[145]</sup>	Lythgo et al. <sup>[146]</sup>
Population Size	13	8	82
Walking Speed [SD] <i>m/s</i>	1.083 [0.146]	1.089 [0.068 <sup>α</sup> ]	1.414 [0.031 <sup>β</sup> ]
Cadence [SD] <i>Steps/min</i>	100.1 [7.61]	105.4 [5.79 <sup>α</sup> ]	118.4 [116.2-119.8 <sup>β</sup> ]
Stride length [SD] <i>m</i>	1.305 [0.111]	1.244 <sup>α</sup> [0.058 <sup>α</sup> ]	1.430 [0.029 <sup>β</sup> ]

<sup>α</sup> Averaged from right/left sided parameters

<sup>β</sup> Represent 95% Confidence Intervals (not SD).

ranging from 0.1993 to 0.4478. This reduction in ICC was associated with a reduction in subject SD, and not an increase in error SD (Table 3.2).

The statistical results ( $\beta_0$ ,  $SD(y_{ij})$ ) on the temporal spatial parameters of walking speed, cadence, and stride length of the current study are presented in Table 3.3 along with results measured from two additional barefoot studies<sup>[145, 146]</sup>. The current study used a random effects model (Eq. 3.1 and 3.2) to define these parameters, while the Majumdar study used the statistical mean/standard deviation<sup>[145]</sup>, and the Lythgo study used statistical mean and 95% Confidence Interval<sup>[146]</sup>. The current fluoroscopic study reports the slowest walking speed, lowest cadence and median stride length.

### 3.4 Discussion

Direct kinematic comparisons with other studies is difficult as differences in methodologies exist. Foot models using externally mounted surface markers either combine the talus with the calcaneus in a lumped “hindfoot” segment, or report calcaneal motion relative to the tibia<sup>[7-10]</sup>. These methodologies are incapable of reporting true talocrural or subtalar motion. It is noted, however, that the reported sagittal plane motion of the hindfoot or calcaneus relative to tibia in all of the aforementioned studies is morphologically similar to the currently reported talocrural joint motion<sup>[7-10]</sup>. Vertical offset shifts exist, which is an indication of differences in local coordinate system definition<sup>[9]</sup>.

The only current studies that report *in vivo* talus relative to tibia and calcaneus relative to talus kinematics over the entire stance phase are intra-cortical bone pin studies. These studies isolate both talocrural and subtalar motion by inserting bone pins in the

tibia, talus, and calcaneus with the assistance of an orthopaedic surgeon. At the end of each inserted bone pin, a triad of external markers is affixed whose motions are tracked using standard stereophotogrammetry. The kinematic results of five of the 13 participants in the current fluoroscopic study were previously compared in depth to the kinematic results of multiple invasive bone pin studies<sup>[12, 14]</sup> (Section 2.4). Figure 3-3 and Table 3.4 represent updates to Figure 2-7 and Table 2.5, with the addition of eight previously unreported fluoroscopic subjects. Comparison values displayed in Figure 3-3 are derived from an invasive bone pin study<sup>[14]</sup>. Table 3.4 presents the kinematic results of the fluoroscopic study and that of existing bone pin studies reporting talocrural and subtalar motion<sup>[12, 14, 134]</sup>.

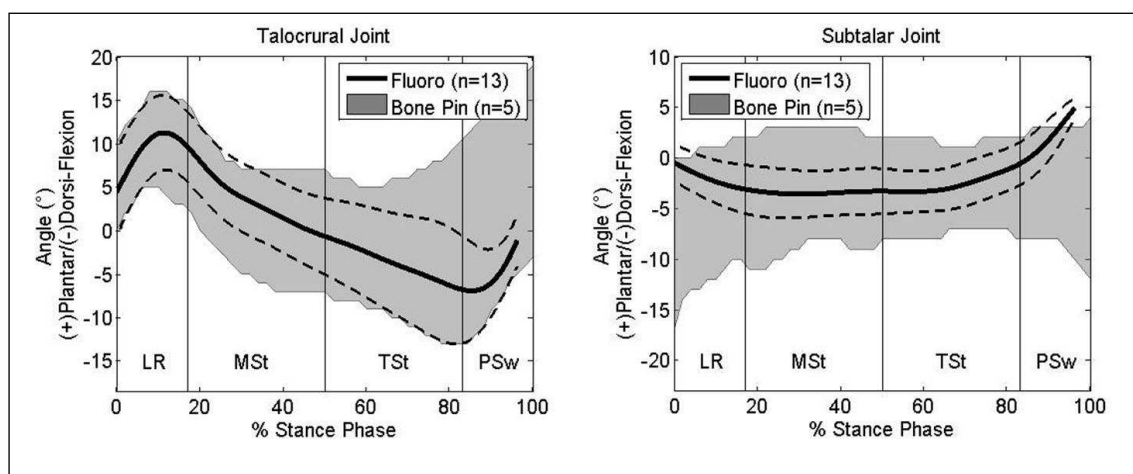


**Figure 3-3** Sagittal plane kinematic results. Black solid lines represent mean angle of all 13 fluoroscopic subjects. Dashed lines represent fluoroscopic subjects' mean  $\pm 1$  SD. The grey bands depict the standard deviation ranges in Lundgren's study of 5 adult males<sup>[14]</sup>.

**Table 3.4** Fluoroscopic and bone pin kinematics.

	Talocrural Joint		
	Fluoroscopic (n=13)	Bone Pin <sup>[12, 134]</sup> (n=3)	Bone Pin <sup>[14]</sup> (n=5)
	Max (% Stance Phase)	Max (% Stance Phase)	Max (% Stance Phase)
Plantar flexion	11.2° (11)	7.2° (13)	-
Dorsiflexion	-6.9° (85)	-4.6° (80)	-
ROM	18.1°	11.8°	15.3°
	Subtalar Joint		
	Fluoroscopic (n=13)	Bone Pin <sup>[12, 134]</sup> (n=3)	Bone Pin <sup>[14]</sup> (n=5)
	Max (% Stance Phase)	Max (% Stance Phase)	Max (% Stance Phase)
Plantar flexion	4.8° (96)	1.5° (97)	-
Dorsiflexion	-3.6° (30)	-1.3° (23)	-
ROM	8.4°	2.8°	6.8°

The comparisons made in Chapter 2 (Section 2.4) between talocrural and subtalar kinematics derived from bone pin methodologies and the currently proposed fluoroscopic method are further strengthened by the addition of eight fluoroscopic subjects. As shown in Figure 3-3, the fluoroscopic and bone pin results still depict the talocrural joint going from neutral to plantar flexion during LR followed by a return to neutral and into dorsiflexion during MSt and TSt. Both methodologies also continue to report talocrural joint motion going from dorsiflexion to neutral/plantar flexion during pre-swing (PSw). The updated fluoroscopic results and an earlier (2004) bone pin study illustrate maximum plantar flexion during LR (Table 3.4). The bone pin study reports maximum dorsiflexion during TSt<sup>[12, 134]</sup>, whereas the fluoroscopic study still reports maximum dorsiflexion during PSw. The two differ by only 5% gait cycle (up from 4% in Chapter 2, when only five fluoroscopic subjects were reported).

A similar comparison for the subtalar joint reveals that the fluoroscopic results (Figure 3-3) continue to show neutral to dorsiflexion during LR, while the bone pin study shows a wider region of motion gradually increasing from dorsiflexion to neutral. Both

studies illustrate subtalar dorsiflexion during mid and terminal stance. The bone pin study depicts much larger motion variation. The fluoroscopic results show a return to neutral/plantar flexion during pre-swing, while the bone pin results remain dorsiflexed.

The fluoroscopic study group consisted of younger individuals (22.9 years) than the bone pin kinematic studies (39.3 and 38 years)<sup>[12, 14]</sup>. Oberg et al. have described differences in gait kinematics with aging for 233 healthy subjects aged 10-79 years<sup>[136]</sup>. While these differences are small, the effects of age upon *in vivo* bony kinematics of the foot and ankle have not been studied.

Kadaba et al. originally introduced a method for statistical analysis between gait waveforms<sup>[33]</sup> that has been subsequently adopted by other investigators for reporting foot/ankle kinematics<sup>[9, 10, 14, 124, 130, 147]</sup>. While this method has become the standard for statistically comparing kinematic results among studies, it has been shown to be less reliable for inter-segmental joints with small ranges of motion<sup>[7, 130]</sup>. The current study reports subtalar ROM values as low as 2.13° during MSt (Table 3.2). In addition, Kadaba's method requires all subjects to have the same number of trials over the phase analyzed. The non-uniform distribution of trials among subjects, as well as the small subtalar ROM in the current study, obviated using Kadaba's method. In an effort to include as many subjects and trials as possible in the statistical analysis, a new model was created (Eq. 3.1). The novelty of the currently reported statistical model prevents direct comparisons with other studies, but general trends can be commented on.

In this study, the largest ICC value associated with subtalar kinematics (0.6605) was lower than the smallest ICC value associated with talocrural kinematics (0.6784). These results suggest there is a larger variability among normal subjects in sagittal plane

talocrural kinematics than subtalar kinematics. This conflicts with a 2008 bone pin study by Lundgren et al., in which the sagittal plane inter-subject talocrural CMC value (using the Kadaba et al. method<sup>[33]</sup> where higher CMC values indicated a lower variability between waveforms) was much higher than the subtalar CMC value (0.6 vs. <0.2)<sup>[14]</sup>. The results of the current study may be expected, as the major plane of motion attributed to the talocrural joint is sagittal, while the major plane of motion attributed to the subtalar joint is coronal<sup>[98]</sup>. Because of this, there may be less variability in subtalar motion among subjects in the sagittal plane. In addition, average sagittal plane talocrural ROM among subjects from heel strike through TSt in the current study was three times larger than that of the subtalar joint (18.83° vs. 5.75°). This increased ROM strengthens the possibility of detecting differences among subjects as the region for potential differences to exist is larger. Another possibility for the decreased variability among subjects in currently reported sagittal plane subtalar kinematics is the influence of measurement error. The average error SD for all kinematic summary measures was 1.36° (0.98° min, 2.02° max). It is possible that sagittal plane subtalar variability among subjects is larger than that reported by current ICC values, but differences are smaller than measurement error.

Temporal spatial statistics for the 13 volunteer subjects are provided in Table 3.3, along with similar parameters from two additional barefoot studies<sup>[145, 146]</sup>. Majumdar et al. reports mean walking speed, cadence, and stride length values within 10% of those being currently reported. With the exception of walking speed (31%), Lythgo et al. reports temporal spatial mean values within 20% of those being currently reported. Because all three studies reported in Table 3.3 (including the current fluoroscopic) were

non-invasive and subjects were asked to walk at a self-selected pace, temporal spatial parameters should be similar. Differences may be related to population age, as most temporal spatial parameters are affected by maturation<sup>[146]</sup>. The fluoroscopic study group consisted of older individuals (22.9 years) than those in the Lythgo study (19.6)<sup>[146]</sup>, but younger than those of the Majumdar study (26.7)<sup>[145]</sup>.

### 3.5 Conclusion

The currently reported talocrural joint kinematic data are morphologically similar to hindfoot/calcaneal relative to tibia motion described by previous studies using externally mounted surface markers. Invasive bone pin studies capable of reporting true talocrural and subtalar motion compare even more favorably to the talocrural and subtalar kinematics currently being reported. It is additionally concluded that sagittal plane talocrural inter-subject variability among normal adult male subjects is larger than that of the subtalar joint. The reduction of inter-subject variability at the subtalar joint is hypothesized to be the result of the coronal plane (not sagittal) being its primary plane of motion. Because of this, subtalar ROM in the sagittal plane is greatly reduced when compared to the talocrural joint.

Study limitations include a narrow sample of adult male subjects aged 18 to 28 with no reported gait deficiencies or prior bony foot injury. A further limitation is the use of ionizing radiation with current levels estimated at 10  $\mu\text{Sv}$ /trial. Based on the IRB restriction of five trials per subject, each subject was exposed to approximately 50  $\mu\text{Sv}$ . The USNRC (United States Nuclear Regulatory Commission) places whole body annual occupation limits at 5 rems (50,000  $\mu\text{Sv}$ ).

On the basis of the current study, it is concluded that single plane fluoroscopic technology is appropriate for the sagittal plane measurement of both talocrural and subtalar kinematics. This technology is recommended for further clinical applications, including the assessment of *in vivo* motion with footwear. It is additionally recommended to expand this analysis with a second fluoroscopic system, therefore capable of assessing 3D kinematics.

#### **4. Pilot Investigation: Comparing Barefoot and Toe-Only Rocker Soled Shoe Hindfoot Kinematics**

Rocker profiled shoes have proven efficacy in the reduction of foot plantar pressures, but the exact biomechanical reason they work is not well understood. The current study was designed to quantify *in vivo* hindfoot sagittal plane kinematics from the use of toe-only rocker soled shoes and to compare with previously reported barefoot motion. Compared to barefoot, toe-only rocker shoes increase talocrural dorsiflexion during loading response, and increase subtalar plantar flexion during loading response, mid-stance and terminal stance. These results are similar to kinematic differences reported by others between barefoot and normal shoes. Based on these findings it is concluded that hindfoot sagittal plane kinematics may not significantly contribute to the reduction in reported plantar pressures associated with toe-only rocker shoes. It was additionally found that toe-only rocker use decreased inter-subject kinematic variability compared to barefoot walking. The fluoroscopic technology outlined in this study is recommended for further clinical applications including *in vivo* assessment with pedorthics and orthotics.

##### 4.1 Introduction

According to the Center for Disease Control, 8.3% of the total United States population in 2010 were suffering from diabetes mellitus (25.8 million, 7 million undiagnosed)<sup>[148]</sup>. In 2007, the estimated direct medical cost associated with the disease was \$116 billion<sup>[148]</sup>. While classified as a metabolic disease, diabetes has numerous

complications, all of which pose medical risk and financial cost to the patient. Among these complications, plantar ulcerations are common, and diagnosed prior to 85% of all diabetic amputations<sup>[149]</sup>. One of the leading causes of plantar ulcerations is peripheral neuropathy, which causes a loss of distal extremity sensation, combined with increased plantar pressure<sup>[150]</sup>. Prophylactic shoes have been shown to decrease plantar pressure and are often prescribed for this reason<sup>[151, 152]</sup>, with rocker soled shoes being the most common<sup>[153]</sup>. In 1998, in an attempt to reduce foot ulcers, and ultimately foot amputation, congress passed the therapeutic shoe bill (PL-100-203sec4072) which authorized Medicare coverage for one pair of shoes per diabetic patient per calendar year.

Historically, rocker soled shoes were prescribed on the basis of theoretical considerations, but the advances of gait analysis have provided empirical evidence about their efficacy. Several researchers have investigated the effect of rocker soled shoes on plantar pressure and temporal-spatial parameters. Schaff et al. noted shifts in forefoot peak pressure from medial to lateral as well as significant changes in temporal parameters<sup>[154]</sup>. Xu et al. studied center of pressure locus changes associated with rocker soled heel design and found a strong correlation<sup>[155]</sup>. Kavros et al. noted a reduction in peak plantar pressure at the hallux, metatarsal head, and heel regions when comparing rocker soled shoes to flat soled<sup>[156]</sup>. Brown et al. concluded rocker soles were imperative in reducing pressure in the diabetic foot<sup>[151]</sup>.

Three-dimensional kinematic studies on the efficacy of rocker sole shoes are limited. Van Bogart et al. concluded that while many statistically significant changes were observed between baseline and toe-only rocker shoes, they were small in magnitude, and the major benefit of their use seemed to be the maintenance of walking

speed<sup>[153]</sup>. Myers et al. reports similar findings using a negative heel rocker soled shoe<sup>[157]</sup>, as well as Long et al. using double rocker soled shoes<sup>[158]</sup>. In light of these studies, the reduction of plantar pressure is assumed to be achieved by minimizing the sagittal plane motion of specific joints of the foot<sup>[159]</sup>; however, the kinematic effect rocker soled shoes have on the foot itself are not well understood.

Standard multi-segmental foot models require the placement of external markers to the surface of the skin, which is not easily achieved during shod motion. Current methodologies measuring foot mechanics during shod ambulation use sandals, so that anatomic locations are still exposed<sup>[160, 161]</sup>, place markers on the outer surface of the shoe<sup>[162]</sup>, or remove shoe material to expose the anatomic area for marker placement<sup>[163]</sup>. These approaches are of limited value in quantifying foot kinematics in rocker shoes. Rocker soled shoes are not manufactured as sandals, and any custom made sandals may not have the same properties as the actual shoes patients would wear. Studies have shown that markers placed on the outer surface of a shoe cannot accurately track motion of the foot inside the shoe<sup>[164, 165]</sup>, and removal of material to expose underlying landmarks could jeopardize shoe integrity<sup>[166]</sup>. These methodological challenges make quantifying foot kinematics in rocker sole shoes difficult.

Fluoroscopy allows direct *in vivo* visualization of bony motion. Several studies using this technology on the foot are reported<sup>[19, 21, 55, 56, 167]</sup>. Of the studies measuring foot kinematics, none have looked at the motion inside rocker soled shoes. The immediate study was designed to quantify hindfoot kinematics caused by the use of toe-only rocker soled shoes using fluoroscopic technology. In addition, hindfoot kinematics from toe-only rocker shoes are compared to barefoot kinematics.

## 4.2 Materials and Methods

### 4.2.1 Subject Selection

Thirteen normal male volunteers (mean age  $22.9 \pm 2.9$  years, mean weight  $77.2 \pm 6.9$  kg, mean height  $178.2 \pm 3.7$  cm) were recruited for this study. The same subjects were previously tested barefoot and kinematic results have been reported (Chapter 3). All subjects were screened for exclusion criteria, and demonstrated a normal gait pattern. This study was approved by the Institutional Review Boards of Marquette University (Milwaukee, WI), and the Medical College of Wisconsin. All subjects provided informed consent prior to testing.

### 4.2.2 Testing Protocol

Following informed consent, subjects were fitted with a commercially available New Balance MW927 toe-only rocker soled shoe (Figure 4-1). The toe-rocker shoe provides a flat contour under the rear and mid-foot regions of the foot, followed by a tapered portion under the forefoot and toes. This design provides a means of rocking the foot from heel strike to toe-off as the weight of the body passes over the fulcrum of the shoe. In addition to the toe-only rocker, these shoes contain a rigid shank within the sole that maintains shoe integrity for added motion control throughout the gait cycle (Figure 4-1).

The right leg and shoe of each subject were instrumented with six reflective markers ( $d = 16$  mm) placed over the specific bony landmarks outlined in Table 2.2. Markers M1 and M2 were placed on the outer surface of the rocker shoe after palpation of the landmark. Simultaneous motion analysis, fluoroscopic, and ground reaction force data were collected as subjects



**Figure 4-1** Toe-only rocker shoe (top). Note the rigid shank in the x-ray image (bottom).

walked at a self-selected pace along a six meter walkway. The fluoroscopic system was manually activated just prior to the subject's shoe contacting the force plate and deactivated just after toe-off. During fluoroscopic data collection radiation levels varied from 80-110 kVp and 0.5-1.7 mA depending on patient-specific image quality analyses. A maximum of five trials wearing toe-only rocker soled shoes were completed with minimum radiation exposure as approved by the IRB. Following dynamic data collection, subjects were escorted to a nearby x-ray suite where a single limb support x-ray was taken of their right foot, still wearing the toe-only rocker shoe, placed at the same foot progression angle observed during dynamic image collection.

Synchronized force plate data were used to detect fluoroscopic images between heel strike and toe-off. For each of these images, virtual marker locations were selected for both the talus and calcaneus and translated into global coordinates via global

referencing (Section 2.2.4). These translated virtual marker locations, in conjunction with reflective marker positions, were used to define local coordinate systems for the tibia, talus, and calcaneus (Table 2.3). After coordinate definition, a kinematic analysis was completed by using the Joint Coordinate System method<sup>[129]</sup>. All kinematic results were normalized to stance phase (0-100%). Additional kinematics were calculated (with the same virtual marker locations) using the static weight-bearing x-ray. These static kinematic values represent quiet standing and are used for clinical reference (0° on reported kinematic plots). Details of the system configuration, synchronization process, and kinematic model can be found in Section 2.2.

Due to the IRB restriction of five radiation exposures per subject, trials in which the subject was exposed but the foot was not within the image intensifier field of view could not be re-imaged. For this reason, each of the 13 subjects had, on average, three trials of motion analyzed ( $n = 37$  trials). Foot placement also affected the percentages of stance phase analyzed for each trial, as the talus and calcaneus may not have been in the field of view at heel strike or toe-off. Therefore, trials were grouped together according to Perry's phases of gait: Loading Response (LR, 0-10%), Mid Stance (MSt, 10-30%), and Terminal Stance (TSt, 30-50%)<sup>[133]</sup>. In order to be included, the trial needed to span the entire phase. LR had 17 trials, MSt had 31 trials, and TSt had 12 trials.

#### 4.2.3 Statistical Methods

For each joint (talocrural, subtalar) and phase (LR, MSt, TSt), three summary measures were calculated (minimum position, maximum position, and range) on trials

that spanned a given phase. Temporal spatial parameters walking speed, cadence, and stride length were also analyzed.

All statistical analyses were performed in R 2.13 ([www.r-project.org](http://www.r-project.org)). A random effects linear model (Eq. 3.1) was used to perform variance components analysis on each summary measurement (minimum position, maximum position, range, walking speed, cadence, and stride length). This model is described in-depth in Section 3.2.3.

Subjects in the current study were previously analyzed during barefoot ambulation (Chapter 3), and the kinematics results are directly compared to those of the current study. To compare the two conditions (barefoot and toe-only rocker) a linear mixed model was used. The model included random effects for subject and measurement, and a fixed effect for condition as described in:

$$y_{ijk} = \beta_0 + \delta_k + \alpha_{ik} + \varepsilon_{ijk} \quad (\text{Eq. 4.1})$$

where

- $i$  enumerates subjects ( $i=1:13$ ),
- $j$  enumerates trials within subjects ( $j=1:n_i$ , where  $n_i$  is the number of trials for the  $i^{\text{th}}$  subject),
- $k$  enumerates condition ( $k=1:2$ , where 1 = barefoot, 2 = toe-only rocker),
- $\beta_0$  represents an overall mean among barefoot subjects,
- $\varepsilon_{ijk}$  represents random measurement error with Normal distribution ( $\mu = 0$ ,  $\sigma^2 = \sigma^2$ ), and
- $\alpha_{ik}$  represents a 2D random subject effect with Normal distribution:

$$\begin{pmatrix} \alpha_{i1} \\ \alpha_{i2} \end{pmatrix} d = \begin{pmatrix} 0 \\ 0 \end{pmatrix}, \begin{pmatrix} \sigma_{i1}^2 & \sigma_{i1}\sigma_{i2}\rho \\ \sigma_{i1}\sigma_{i2}\rho & \sigma_{i2}^2 \end{pmatrix} \quad (\text{Eq. 4.2})$$

where

- $\alpha_{i1}$  is the variance of the subject effect barefoot,
- $\alpha_{i2}$  is the variance of the subject effect for toe-only rocker, and
- $\rho$  accounts for the possible subject correlation between the two conditions.
- $\delta_k$  represents a fixed effect term for condition, where  $\delta_1 = 0$  (the barefoot effect), and  $\delta_2 = \delta$  (the effect for toe-only rocker shoes).

A likelihood ratio test was used to determine p-values. For all comparisons, a level of significance (p-value) of 0.01 was chosen with regard to the population size and number of trials.

## 4.3 Results

### 4.3.1 Joint Kinematics

Figures 4-2, 4-3, and 4-4 present talocrural and subtalar sagittal plane kinematic results during LR, MSt, and TSt, respectively. Black solid lines represent mean angle of toe-only rocker motion, and dashed lines represent mean  $\pm 1$  SD. Grey banded comparison values in each figure are the barefoot kinematic standard deviations of the same 13 volunteer subjects. Talocrural joint motion is reported as talus with respect to tibia, and subtalar motion as calcaneus with respect to talus. Lateral weight-bearing x-

rays during quiet standing were used to calculate neutral position ( $0^\circ$ ). Plantar flexion (+) and dorsiflexion (-) represent deviations from this neutral position.

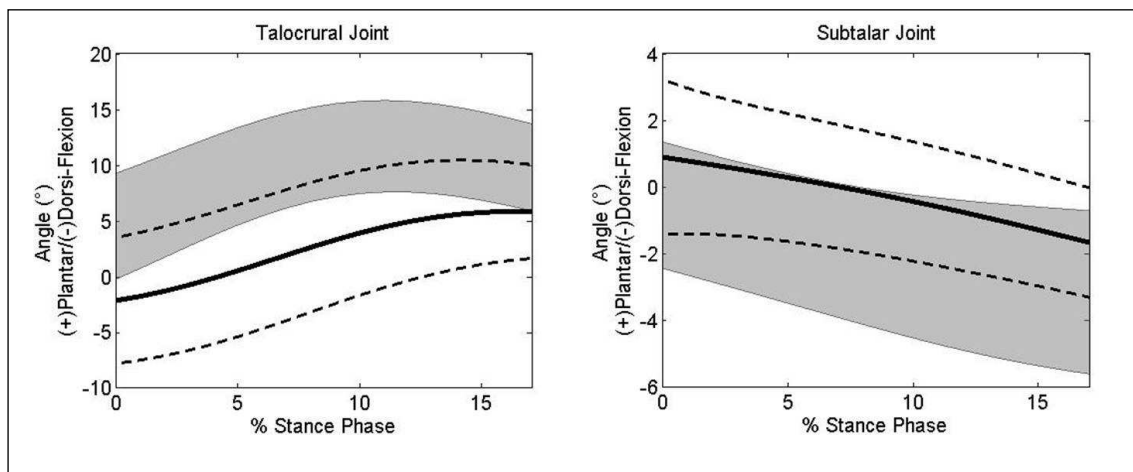


**Figure 4-2** Sagittal plane kinematic results during LR. Black solid lines represent mean angle of 17 trials of toe-only rocker motion. Dashed lines represent toe-only rocker mean  $\pm 1$  SD. The grey bands depict the standard deviation range of 52 trials of barefoot motion.

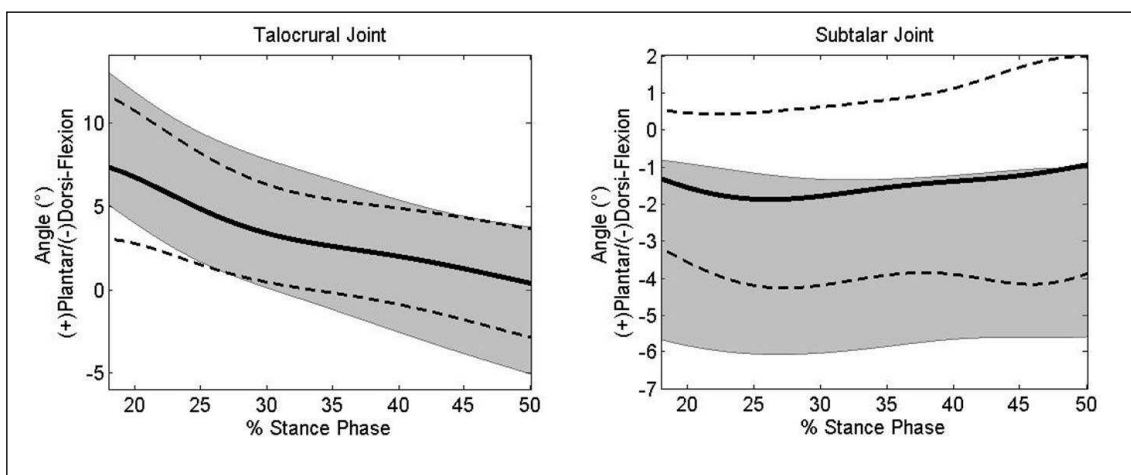


**Figure 4-3** Sagittal plane kinematic results during MSt. Black solid lines represent mean angle of 31 trials of toe-only rocker motion. Dashed lines represent toe-only rocker mean  $\pm 1$  SD. The grey bands depict the standard deviation range of 52 trials of barefoot motion.

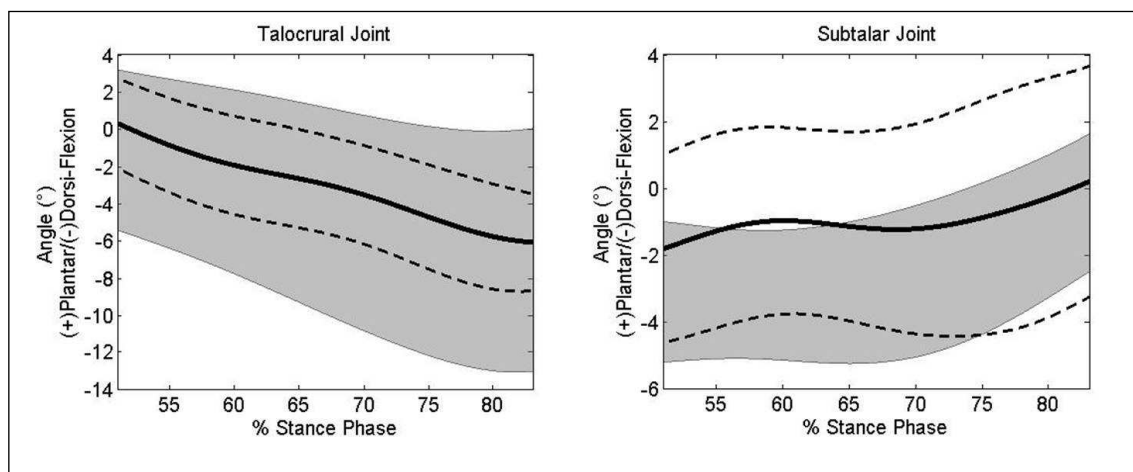


**Figure 4-4** Sagittal plane kinematic results during TSt. Black solid lines represent mean angle of 12 trials of toe-only rocker motion. Dashed lines represent toe-only rocker mean  $\pm$  1 SD. The grey bands depict the standard deviation range of 41 trials of barefoot motion.

As depicted in Figure 4-2, toe-only rocker talocrural kinematics during LR start slightly dorsiflexed and become progressively plantar flexed throughout LR. Compared to barefoot, toe-only rocker kinematics are more dorsiflexed throughout the entire phase, and maximal plantar flexion is shifted to the very end of LR. During mid and terminal stance, sagittal plane talocrural kinematics between barefoot and toe-only rocker motion are virtually identical as depicted in Figures 4-3 and 4-4. At MSt the talocrural joint goes from a plantar flexed position to neutral, followed by a neutral to dorsiflexed position during TSt.

Sagittal plane subtalar kinematics during LR are present in Figure 4-2 and show toe-only rocker motion going from slight plantar flexion to slight dorsiflexion. Barefoot kinematics are similar, but slightly dorsiflexed in comparison. During MSt the subtalar joint remains in a slightly dorsiflexed position throughout. This motion is similar between both conditions, but more dorsiflexed in barefoot. At TSt the subtalar joint has a slight rocker motion as it goes from slight dorsiflexion to neutral. Barefoot kinematics

are similar to toe-only rocker during TSt, but once again are more dorsiflexed in comparison.

#### 4.3.2 Statistics

Statistical results using a random effects linear regression model (Eq. 3.1) on joint summary measurements (minimum position, maximum position, range) during LR, MSt, and TSt are delineated in Tables 4.1, 4.2, and 4.3, respectively. The model was applied to the current toe-only rocker kinematics and the previously reported barefoot kinematics (Chapter 3), and results of both are presented for comparison.  $\beta_0$  values represent an overall mean among subjects for each summary measurement, and  $SD(y_{ij})$  is reported as described in Equation 3.2. Subject SD represents the estimated variability associated with the random subject effect, and Error SD represents the estimated variability associated with the random measurement error. ICC values are the percentage of total variability accounted for by subject variability (Eq. 3.3).

For each condition (barefoot, toe-only rocker), three summary measures were made (minimum position, maximum position, and range) for each phase analyzed (LR, MSt, TSt) at each joint (talocrural, subtalar). Of these 18 measurements, 11 (61.1%) depict a reduction in ICC value by use of the toe-only rocker shoe (Table 4.1, 4.2, 4.3). Of these 11 ICC value reductions, eight (72.7%) were associated with reduction in inter-subject SD (as opposed to an increase in error SD). The combination of these trends indicates a decreased variability among subjects from barefoot to toe-only rocker kinematics.

**Table 4.1** Kinematic statistics during LR.

		Talocrural Joint		Subtalar Joint	
		Barefoot	Toe-only	Barefoot	Toe-only
Trials		n = 52	n = 17	n = 52	n = 17
Minimum	B <sub>0</sub> [SD(y <sub>ij</sub> )]	3.94° [4.69°]	-2.40° [5.34°]	-3.16° [2.24°]	-1.75° [1.74°]
	Subject SD	4.53°	5.10°	1.82°	1.32°
	Error SD	1.23°	1.59°	1.31°	1.14°
	ICC	0.9314	0.9118	0.6605	0.5734
	p	0.0004 <sup>α</sup>		0.0827	
Maximum	B <sub>0</sub> [SD(y <sub>ij</sub> )]	11.27° [4.45°]	6.49° [4.77°]	-0.28° [1.97°]	1.22° [2.21°]
	Subject SD	4.25°	4.09°	1.28°	1.16°
	Error SD	1.32°	2.45°	1.50°	1.88°
	ICC	0.9124	0.7364	0.4223	0.2776
	p	0.0014 <sup>α</sup>		0.0919	
ROM	B <sub>0</sub> [SD(y <sub>ij</sub> )]	7.33° [2.18°]	8.88° [2.77°]	2.94° [1.37°]	2.91° [1.43°]
	Subject SD	1.80°	2.28°	0.61°	<sup>β</sup>
	Error SD	1.24°	1.57°	1.23°	1.43°
	ICC	0.6784	0.6797	0.1993	<sup>β</sup>
	p	0.0069 <sup>α</sup>		1	

<sup>α</sup> Statistically significant<sup>β</sup> Subject SD ≤ 0 (ICC value not reliable)**Table 4.2** Kinematic statistics during MSt.

		Talocrural Joint		Subtalar Joint	
		Barefoot	Toe-only	Barefoot	Toe-only
Trials		n = 52	n = 31	n = 52	n = 31
Minimum	B <sub>0</sub> [SD(y <sub>ij</sub> )]	-1.23° [4.32°]	-0.11° [3.36°]	-4.30° [2.33°]	-2.67° [2.33°]
	Subject SD	4.14°	2.78°	1.83°	1.92°
	Error SD	1.23°	1.88°	1.44°	1.31°
	ICC	0.9183	0.6869	0.6183	0.6829
	p	0.8066		0.0482	
Maximum	B <sub>0</sub> [SD(y <sub>ij</sub> )]	8.53° [4.21°]	7.20° [4.07°]	-2.20° [2.15°]	0.09° [2.46°]
	Subject SD	4.02°	3.83°	1.44°	1.62°
	Error SD	1.24°	1.38°	1.59°	1.85°
	ICC	0.9136	0.8855	0.4478	0.4327
	p	0.2344		0.0105	
ROM	B <sub>0</sub> [SD(y <sub>ij</sub> )]	9.76° [2.87°]	8.19° [4.17°]	2.13° [1.30°]	2.78° [1.54°]
	Subject SD	2.61°	3.87°	0.80°	0.43°
	Error SD	1.20°	1.58°	1.02°	1.48°
	ICC	0.8260	0.8574	0.3782	0.0766
	p	0.0506		0.0569	

**Table 4.3** Kinematic statistics during TSt.

		Talocrural Joint		Subtalar Joint	
		Barefoot	Toe-only	Barefoot	Toe-only
Trials		n = 41	n = 12	n = 41	n = 12
Minimum	$B_0$ [ $SD(y_{ij})$ ]	-6.64° [6.54°]	-5.76° [3.11°]	-3.69° [2.02°]	-2.95° [2.91°]
	Subject SD	6.36°	2.88°	1.36°	2.52°
	Error SD	1.53°	1.19°	1.50°	1.46°
	ICC	0.9455	0.8545	0.4520	0.7487
	p	0.7269		0.5249	
Maximum	$B_0$ [ $SD(y_{ij})$ ]	-0.77° [5.16°]	0.31° [2.87°]	-0.25° [1.99°]	0.80° [3.54°]
	Subject SD	4.99°	2.46°	1.10°	2.87°
	Error SD	1.32°	1.49°	1.66°	2.08°
	ICC	0.9346	0.7312	0.3060	0.6543
	p	0.8483		0.5294	
ROM	$B_0$ [ $SD(y_{ij})$ ]	5.90° [2.82°]	6.48° [2.21°]	3.46° [1.17°]	3.42° [1.59°]
	Subject SD	2.55°	<sup>β</sup>	0.64°	0.64°
	Error SD	1.19°	2.21°	0.98°	1.46°
	ICC	0.8202	<sup>β</sup>	0.3031	0.1610
	p	0.9161		1	

<sup>β</sup> Subject SD  $\leq$  0 (ICC value not reliable)

To compare the two conditions a linear mixed model was used (Eq. 4.1). For all comparisons, a level of significance of 0.01 was chosen with regard to population size and number of trials. The only statistically significant kinematic deviations occurred at the talocrural joint during load response. All talocrural summary measures during LR were significantly different, with both minimum and maximum position becoming more dorsiflexed, and ROM increasing as the result of toe-only rocker use (Table 4.1). The statistical results ( $\beta_0$ ,  $SD(y_{ij})$ ) on the temporal spatial parameters of walking speed, cadence, and stride length are presented in Table 4.4. In addition to talocrural kinematics during LR, all temporal spatial parameters analyzed were significantly different between the two conditions. As the result of toe-only rocker use, both walking speed and stride length increased, while cadence decreased.

**Table 4.4** Temporal spatial statistics.

	Barefoot	Toe-only Rocker	p
Walking Speed [SD] <i>m/s</i>	1.083 [0.146]	1.130 [0.162]	0.0021 <sup>a</sup>
Cadence [SD] <i>Steps/min</i>	100.1 [7.61]	95.5 [7.60]	0.0001 <sup>a</sup>
Stride length [SD] <i>m</i>	1.305 [0.111]	1.412 [0.102]	0 <sup>a</sup>

<sup>a</sup> Statistically significant

#### 4.4 Discussion

Graphically comparing sagittal plane kinematics between the two conditions it can be observed that the majority of kinematic differences occur at the talocrural joint during LR (Figure 4-2). At heel strike, the talocrural joint is over 5° dorsiflexed from toe-only rocker use compared to barefoot, and continues to be more dorsiflexed throughout LR. In addition to the vertical shift, the position of talocrural maximal plantar flexion moved from 11% stance to 17% as the result of toe-only rocker use. This vertical and horizontal shift is noted in other studies quantifying the kinematic differences between barefoot and normal shod gait. In a 14 subject study conducted by Oeffinger et al., a decrease in ankle plantar flexion was observed, as well as a horizontal delay of gait events from the use of shoes<sup>[168]</sup>. A similar horizontal delay can be noted between the tibia and hindfoot in an 18 subject study conducted by Wolf et al. comparing barefoot and shod walking<sup>[169]</sup>. Based on these previous studies and the current results, it appears toe-only rocker use does not affect talocrural kinematics any differently than normal shoes.

The subtalar joint is slightly plantarflexed as the result of toe-only rocker use (Figure 4-2, 4-3, and 4-4). While this vertical offset is perceived graphically, the statistical summary measurements of the subtalar joint show no significant difference in

kinematics between the two conditions. This result is confirmed by the only other study to report subtalar rotation between barefoot and normal shod walking. In the 2008 study by Wolf et al., hindfoot motion relative to tibia is reported about an axis “close to the functional axis of the subtalar joint” and found to have no kinematic influence from the use of footwear<sup>[169]</sup>. These results in conjunction with the current study, indicate that subtalar motion is unaffected by the use of toe-only rocker shoes compared to normal shoes.

The fluoroscopic study group consisted of older individuals (22.9 years) than the Oeffinger or Wolf studies (6-10 years). Oberg et al. has described differences in gait kinematics with aging for 233 healthy subjects aged 10-79 years<sup>[136]</sup>. While these differences are small, the effects of age upon *in vivo* bony kinematics of the foot and ankle have not been studied.

The only statistically significant kinematic differences between the two conditions were observed at the talocrural joint during LR (Table 4.1). As previously discussed, the literature demonstrates normal footwear has been shown to alter ankle joint kinematics<sup>[168]</sup>. Wolf et al. specifically noted a statistically significant increase in talocrural ROM in the shod condition compared to barefoot<sup>[169]</sup>. This increase in talocrural range of motion is observed during LR and TSt of the current study (Table 4.1, 4.3), and is found to be statistically significant during LR (Table 4.1).

Based on the statistical results, it is additionally observed that inter-subject variability decreases from use of toe-only rocker shoes. Eleven of the 18 kinematic summary measurements depicted a reduction in ICC value from barefoot to toe-only rocker. Of these 11 reductions in ICC, eight were associated with a reduction in subject

SD. It is unclear if this reduction in inter-subject variability is similar to shod motion in general as no studies reporting on inter-subject variability between barefoot and normal shod motion exist in the literature. It is noted, however, that the toe-only rocker shoes used in this study (New Balance MW927) are deemed to control motion during gait, which may account for the reduction in inter-subject variability statistically observed.

All temporal spatial parameters analyzed were statistically different between the two conditions (Table 4.4). As the result of toe-only rocker use, walking speed increased by 0.047 m/s, stride length increased by 0.107 m, and cadence decreased by 4.6 steps/min. Similar results have been reported in studies comparing barefoot to shod motion. In an 980 subject study of children (5-27 years old), Lythgo et al. reports an increase in walking speed of 0.08 m/s, an increase of stride length of 0.111 m, and a decrease in cadence of 3.9 steps/min<sup>[146]</sup>. This trend has been observed elsewhere in the literature<sup>[145, 168-170]</sup>. Based on these earlier studies and the current results, it appears the natural response to footwear is an increase in walking speed and stride length while reducing cadence.

#### 4.5 Conclusion

Compared to barefoot, toe-only rocker shoes increase talocrural dorsiflexion during LR, and increase subtalar plantar flexion during LR, MSt and TSt. These results are common to other studies comparing barefoot to general shod motion, and are therefore thought to have little influence from the toe-only rocker shoe. These findings may be expected as the toe-only rocker is designed such that new stability positions are only required of the forefoot/metatarsal region after the body center of pressure moves

anteriorly to the fulcrum<sup>[153]</sup>. Because of this, hindfoot motion from toe-only rocker shoes may be unaffected compared to baseline shoes, as the current study results suggest.

While rocker shoes are thought to minimize plantar pressures by reducing sagittal plane motion in specific joints of the foot<sup>[159]</sup>, it is yet unclear as to which joints are affected by their use. The current study suggests that both talocrural and subtalar sagittal plane motion is altered by toe-only rocker shoes in a similar manner to normal shoes. These anatomic joints would therefore not be the locations in which sagittal plane motion contributes to the reduction in reported plantar pressures. Based on these findings, any sagittal plane kinematic changes because of toe-only rocker use are occurring distal to the hindfoot. This may be expected as the majority of plantar pressure reduction by use of rocker profiled shoes occurs at the forefoot<sup>[159]</sup>. While this study did not measure kinematics distal to the hindfoot, the described fluoroscopic methodology would be appropriate for such an undertaking.

Study limitations include a narrow sample of adult male subjects aged 18 to 28 with no reported gait deficiencies or prior bony foot injury. A further limitation is the use of ionizing radiation with current levels estimated at 10  $\mu\text{Sv}$ /trial. Based on the IRB restriction of five trials per subject, each subject was exposed to approximately 50  $\mu\text{Sv}$ . The USNRC (United States Nuclear Regulatory Commission) places whole body annual occupation limits at 5 rems (50,000  $\mu\text{Sv}$ ).

On the basis of the current study, it is concluded that single plane fluoroscopic technology is appropriate for the sagittal plane measurement of both talocrural and subtalar kinematics within a shoe. This technology is recommended for further clinical applications, including the assessment of *in vivo* motion with pedorthics and orthotics. It

is additionally recommended to expand this analysis with an additional fluoroscopic system, therefore capable of assessing 3D kinematics.

## 5. Conclusion

Current multi-segmental foot models that use externally mounted skin markers are incapable of tracking the individual bones of the foot. As such, these models group adjoining bones in segments that are assumed to be rigid. Any intra-segmental motion is either not accounted for, or incorrectly ascribed to a neighboring intersegmental joint. The subtalar joint is clinically significant in many pathologies, including pes planovalgus and tarsal coalition, but because the talus cannot be tracked with skin mounted markers<sup>[9]</sup>, these models are incapable of tracking subtalar motion. Bone marker based models that are adequate in measuring individual bone position do report subtalar motion, but their invasive nature prevents widespread clinical use. The purpose of this dissertation was to determine the feasibility of using fluoroscopy to quantify *in vivo* dynamics of the hindfoot during the stance phase of gait. The developed system proved capable of non-invasively quantifying both talocrural and subtalar sagittal plane dynamics. Preliminary results compared favorably with the kinematics and kinetics reported by other authors, and led to the undertaking of two pilot investigations. The first investigation quantified and statistically analyzed the sagittal plane talocrural and subtalar kinematics of barefoot ambulation during stance. The second investigation compared stance phase sagittal plane hindfoot kinematics between barefoot and toe-only rocker walking conditions, and examined the role hindfoot motion played in the reported reduction of plantar pressures from toe-only rocker use.

## 5.1 Summary of Findings

Based on the results of this dissertation, all hypotheses outlined in Section 1.7 were verified. These verifications were completed by accomplishing all the specific aims additionally outlined in Section 1.7. The application of fluoroscopic technology on the foot during gait required construction of an elevated walkway, and the reconfiguration of a C-arm fluoroscopy unit (Section 2.2.1). Custom algorithms, in conjunction with a relay circuit, were developed to synchronize the system with a standard motion analysis system and multi-axis force platform (Section 2.2.2). After the removal of fluoroscopic image distortion (Section 2.2.3), a method of global referencing was introduced to translate points of interest from fluoroscopic image coordinates to lab global coordinates (2.2.4). Experiments were conducted to measure and quantify errors associated with the global referencing method (Section 2.3.1). From these experiments it was concluded that for typical foot progression angles (neutral to 10° external rotation), errors in translating hindfoot fluoroscopic points of interest to global coordinates were similar to dynamic position errors reported for standard motion analysis systems (Section 2.4). It was additionally concluded that algorithms could be developed to correct for global referencing error, as these errors were measurable and repeatable (Section 2.4).

Using the fluoroscopy system and global referencing method, a hindfoot kinematic foot model was developed (Section 2.2.5). This model used external skin marker locations to define a local tibial coordinate system, and virtual marker locations (globally referenced fluoroscopic points of interest) to define local coordinate systems for the talus and calcaneus. Once defined, these local coordinate systems were used to quantify talocrural and subtalar sagittal plane kinematics during stance phase by

implementing the Joint Coordinate System method<sup>[129]</sup>. The preliminary results using this kinematic model on a population of five normal adult subjects during barefoot walking compared favorably to the barefoot kinematics reported by other authors (Section 2.4), as hypothesized in Section 1.7.

The developed kinematic model was designed to use subject specific virtual marker locations so the most visible and distinguishable anatomic locations in the fluoroscopic image sequence could be selected. Kinematic model sensitivity was determined by comparing the kinematic results of the same subject using different virtual marker locations. These angular differences were found to be less than the reported inter-session angular variability of existing skin mounted external marker based multi-segmental foot models (Section 2.4).

Similar to the kinematic model, a hindfoot kinetic model was developed to quantify talocrural and subtalar sagittal plane stance phase dynamics (Section 2.2.7). This model used algorithms developed to track talar and calcaneal centroid loci based on fluoroscopic points of interest. These centroid locations were subsequently used as origins of segment masses. Custom methods were introduced to estimate talar and calcaneal mass and mass moments of inertia as described in Section 2.2.7. After talar and calcaneal body segment parameter estimation (mass locus, mass, mass moments of inertia), the kinetic model followed the methods of Vaughn et al.<sup>[129]</sup>. The preliminary results compared favorably to kinetics reported by other authors (Section 2.4). In order to determine the role of body segment parameters on talocrural and subtalar kinetics, analyses were done with and without the addition of talar and calcaneal parameters. It was concluded that talar and calcaneal body segment parameters play only an incidental

role in sagittal plane talocrural and subtalar kinetics during stance (Section 2.4), as hypothesized in Section 1.7.

Based on the results of Chapter 2, the developed kinematic model was applied to data collected from a larger population of normal adult subjects walking barefoot. The kinematic results from this pilot investigation further strengthened the favorable comparison to kinematics reported by other authors (Section 3.4), as hypothesized (Section 1.7). It was concluded that subject variability in sagittal plane kinematics was higher for the talocrural joint than the subtalar joint (Section 3.4). This increased variability may be attributed to the subtalar joint major plane of motion being coronal rather than sagittal.

The final pilot investigation was conducted to determine if differences existed in talocrural and subtalar stance phase kinematics between barefoot and toe-only rocker use. Compared to barefoot, toe-only rocker shoes increased talocrural dorsiflexion during loading response, and increased subtalar plantar flexion during loading response, mid-stance and terminal stance (Section 4.4). It was additionally observed that toe-only rocker use decreased subject kinematic variability compared to barefoot walking (Section 4.4). Based on these results, it was concluded that both the talocrural and subtalar joints were influenced by toe-only rocker use (compared to barefoot), as hypothesized in Section 1.7. Because the differences between barefoot and toe-only rocker use were similar to differences reported by other authors between barefoot and normal shoes, it was additionally noted that hindfoot sagittal plane kinematics may not contribute substantially to reductions in reported plantar pressures associated with toe-only rocker shoe usage (Section 4.5).

## 5.2 Limitations and Future Directions

This study represents the first report of fluoroscopy being used to quantify *in vivo* intra-foot dynamics during the stance phase of gait. This non-invasive process allows for the kinematic evaluation of subcutaneous joints of the foot previously unattainable with standard stereophotogrammetry methods. While this study assessed the talocrural and subtalar dynamics of healthy adult subjects, the technology developed is capable of examining many of the soft tissue and bony abnormalities associated with the pathologic foot of both adult and pediatric populations. Characterization of the intra-foot kinematics associated with pathologies such as equinovarus or pes planovalgus could play a crucial role in the pre- and post-operative evaluation of patients, and may lead to improved surgical techniques.

As a result of this study, it was concluded that hindfoot sagittal plane kinematics acquired from fluoroscopic technology compare favorably to the kinematics reported by authors using more invasive methodologies. Based on this conclusion, it is recommended that this technology be further developed for dynamic analysis of the foot and ankle. The introduction and synchronization of an additional fluoroscopy system would allow for a three-dimensional kinematic analysis. Larger image intensifiers would expand the fluoroscopic field of view, and use of custom triggering techniques to terminate exposure if the foot is not projected to be within the capture volume would increase the amount of fluoroscopic data collected per subject. In addition, high speed cameras would allow for the evaluation of sports-related activities.

The sagittal plane hindfoot kinetics reported in this study compare favorably with those reported by other authors. As noted in the current study, the role of body segment

parameters in stance phase hindfoot kinetics is negligible compared to ground reaction force contributions. Unfortunately, limitations in force plate technology hamper a true kinetic evaluation of the multi-segmental foot. Traditional force platforms are only capable of reporting a single resultant vector, and plantar pressure mats only measure vertical force components. This inability to apportion vertical and shear ground reaction force components among multiple foot segments requires modeling assumptions to be made that propagate into estimated kinetics. Though several custom devices suitable for measuring normal and shear forces under foot subareas appear in the literature<sup>[104-107]</sup>, nothing commercially available has been developed.

The foot model introduced in this study requires the use of ionizing radiation. This radiation was minimal, with per trial subject exposure levels conservatively estimated at 10  $\mu\text{Sv}$ . The USNRC (United States Nuclear Regulatory Commission) places whole body annual occupation limits at 5 rems (50,000  $\mu\text{Sv}$ ). Reaching this threshold based on the currently described methodology would require more than ten trials per day for 365 consecutive days. This minimal radiation exposure allows for the direct visualization of bony motion within the foot. As demonstrated, fluoroscopic technology is suitable for quantifying inter-segmental foot motion in the shod condition, and would be capable of such an evaluation in orthotic or pedorthic applications as well. Such use of ionizing radiation has the potential of revolutionizing the way assistive devices are evaluated and prescribed.

## Bibliography

1. Apkarian, J., S. Naumann, and B. Cairns, *A three-dimensional kinematic and dynamic model of the lower limb*. J Biomech, 1989. **22**(2): p. 143-55.
2. Cappozzo, A., T. Leo, and A. Pedotti, *A general computing method for the analysis of human locomotion*. J Biomech, 1975. **8**(5): p. 307-20.
3. Kadaba, M.P., H.K. Ramakrishnan, and M.E. Wootten, *Measurement of lower extremity kinematics during level walking*. J Orthop Res, 1990. **8**(3): p. 383-92.
4. Ounpuu, S., J.R. Gage, and R.B. Davis, *Three-dimensional lower extremity joint kinetics in normal pediatric gait*. J Pediatr Orthop, 1991. **11**(3): p. 341-9.
5. White, S.C., H.J. Yack, and D.A. Winter, *A three-dimensional musculoskeletal model for gait analysis. Anatomical variability estimates*. J Biomech, 1989. **22**(8-9): p. 885-93.
6. Leardini, A., et al., *Rear-foot, mid-foot and fore-foot motion during the stance phase of gait*. Gait Posture, 2007. **25**(3): p. 453-62.
7. Carson, M.C., et al., *Kinematic analysis of a multi-segment foot model for research and clinical applications: a repeatability analysis*. J Biomech, 2001. **34**(10): p. 1299-307.
8. Kidder, S.M., et al., *A system for the analysis of foot and ankle kinematics during gait*. IEEE Trans Rehabil Eng, 1996. **4**(1): p. 25-32.
9. MacWilliams, B.A., M. Cowley, and D.E. Nicholson, *Foot kinematics and kinetics during adolescent gait*. Gait Posture, 2003. **17**(3): p. 214-24.
10. Leardini, A., et al., *An anatomically based protocol for the description of foot segment kinematics during gait*. Clin Biomech (Bristol, Avon), 1999. **14**(8): p. 528-36.
11. Bishop, C., G. Paul, and D. Thewlis, *Recommendations for the reporting of foot and ankle models*. J Biomech, 2012. **45**(13): p. 2185-94.
12. Arndt, A., et al., *Ankle and subtalar kinematics measured with intracortical pins during the stance phase of walking*. Foot Ankle Int, 2004. **25**(5): p. 357-64.
13. Arndt, A., et al., *Intrinsic foot kinematics measured in vivo during the stance phase of slow running*. J Biomech, 2007. **40**(12): p. 2672-8.
14. Lundgren, P., et al., *Invasive in vivo measurement of rear-, mid- and forefoot motion during walking*. Gait & Posture, 2008. **28**(1): p. 93-100.

15. Nester, C., et al., *Foot kinematics during walking measured using bone and surface mounted markers*. J Biomech, 2007. **40**(15): p. 3412-23.
16. Wolf, P., et al., *Functional units of the human foot*. Gait Posture, 2008. **28**(3): p. 434-41.
17. Westblad, P., et al., *Differences in ankle-joint complex motion during the stance phase of walking as measured by superficial and bone-anchored markers*. Foot Ankle Int, 2002. **23**(9): p. 856-63.
18. Johnson, J.E., et al., *Hindfoot coronal alignment: a modified radiographic method*. Foot Ankle Int, 1999. **20**(12): p. 818-25.
19. de Asla, R.J., et al., *Six DOF in vivo kinematics of the ankle joint complex: Application of a combined dual-orthogonal fluoroscopic and magnetic resonance imaging technique*. J Orthop Res, 2006. **24**(5): p. 1019-27.
20. Imai, K., et al., *In vivo three-dimensional analysis of hindfoot kinematics*. Foot Ankle Int, 2009. **30**(11): p. 1094-100.
21. Komistek, R.D., et al., *A determination of ankle kinematics using fluoroscopy*. Foot & Ankle International, 2000. **21**(4): p. 343-350.
22. Andriacchi, T.P. and E.J. Alexander, *Studies of human locomotion: past, present and future*. Journal of Biomechanics, 2000. **33**(10): p. 1217-1224.
23. Chiari, L., et al., *Human movement analysis using stereophotogrammetry: Part 2: Instrumental errors*. Gait & Posture, 2005. **21**(2): p. 197-211.
24. Hoschek, J., et al., *Mathematical kinematics in engineering of endoprostheses. Evaluation of the results of gait analysis*. Arch Orthop Trauma Surg, 1984. **103**(5): p. 342-7.
25. Leardini, A., et al., *Human movement analysis using stereophotogrammetry: Part 3. Soft tissue artifact assessment and compensation*. Gait & Posture, 2005. **21**(2): p. 212-225.
26. Cappozzo, A., et al., *Position and orientation in space of bones during movement: experimental artefacts*. Clin Biomech (Bristol, Avon), 1996. **11**(2): p. 90-100.
27. Shultz, R., A.E. Kedgley, and T.R. Jenkyn, *Quantifying skin motion artifact error of the hindfoot and forefoot marker clusters with the optical tracking of a multi-segment foot model using single-plane fluoroscopy*. Gait Posture, 2011. **34**(1): p. 44-8.
28. Tranberg, R. and D. Karlsson, *The relative skin movement of the foot: a 2-D roentgen photogrammetry study*. Clin Biomech (Bristol, Avon), 1998. **13**(1): p. 71-76.

29. Wrbaskic, N. and J.J. Dowling, *An investigation into the deformable characteristics of the human foot using fluoroscopic imaging*. Clinical Biomechanics, 2007. **22**(2): p. 230-238.
30. Okita, N., et al., *An objective evaluation of a segmented foot model*. Gait Posture, 2009. **30**(1): p. 27-34.
31. Reinschmidt, C., et al., *Tibiofemoral and tibiocalcaneal motion during walking: external vs. skeletal markers*. Gait & Posture, 1997. **6**(2): p. 98-109.
32. Della Croce, U., et al., *Human movement analysis using stereophotogrammetry: Part 4: assessment of anatomical landmark misplacement and its effects on joint kinematics*. Gait & Posture, 2005. **21**(2): p. 226-237.
33. Kadaba, M.P., et al., *Repeatability of kinematic, kinetic, and electromyographic data in normal adult gait*. J Orthop Res, 1989. **7**(6): p. 849-60.
34. Della Croce, U., A. Cappozzo, and D.C. Kerrigan, *Pelvis and lower limb anatomical landmark calibration precision and its propagation to bone geometry and joint angles*. Med Biol Eng Comput, 1999. **37**(2): p. 155-61.
35. Caravaggi, P., et al., *Repeatability of a multi-segment foot protocol in adult subjects*. Gait Posture, 2011. **33**(1): p. 133-5.
36. Stiehl, J.B. and V.T. Inman, *Inman's Joints of the Ankle*. 1991: Williams & Wilkins.
37. Hamel, A.J., et al., *Relative motions of the tibia, talus, and calcaneus during the stance phase of gait: a cadaver study*. Gait Posture, 2004. **20**(2): p. 147-53.
38. Nester, C.J., et al., *In vitro study of foot kinematics using a dynamic walking cadaver model*. Journal of Biomechanics, 2007. **40**(9): p. 1927-1937.
39. Whittaker, E.C., P.M. Aubin, and W.R. Ledoux, *Foot bone kinematics as measured in a cadaveric robotic gait simulator*. Gait & Posture, 2011. **33**(4): p. 645-650.
40. Nester, C., et al., *Error in the description of foot kinematics due to violation of rigid body assumptions*. Journal of Biomechanics, 2010. **43**(4): p. 666-672.
41. Banks, S.A. and W.A. Hodge, *Accurate measurement of three-dimensional knee replacement kinematics using single-plane fluoroscopy*. IEEE Trans Biomed Eng, 1996. **43**(6): p. 638-49.
42. Komistek, R.D., D.A. Dennis, and M. Mahfouz, *In vivo fluoroscopic analysis of the normal human knee*. Clin Orthop Relat Res, 2003(410): p. 69-81.

43. Li, G., et al., *New fluoroscopic imaging technique for investigation of 6DOF knee kinematics during treadmill gait*. J Orthop Surg Res, 2009. **4**: p. 6.
44. You, B.M., et al., *In vivo measurement of 3-D skeletal kinematics from sequences of biplane radiographs: application to knee kinematics*. IEEE Trans Med Imaging, 2001. **20**(6): p. 514-25.
45. Zihlmann, M.S., et al., *Three-dimensional kinematics and kinetics of total knee arthroplasty during level walking using single plane video-fluoroscopy and force plates: a pilot study*. Gait Posture, 2006. **24**(4): p. 475-81.
46. Yamokoski, J. and S. Banks, *Dynamic radiographic measurement of three-dimensional skeletal motion*. 2008, Foot and ankle motion analysis: clinical treatment and technology. Boca Raton, FL: CRC Press.
47. Ackland, D.C., F. Keynejad, and M.G. Pandy, *Future trends in the use of X-ray fluoroscopy for the measurement and modelling of joint motion*. Proceedings of the Institution of Mechanical Engineers Part H-Journal of Engineering in Medicine, 2011. **225**(H12): p. 1136-1148.
48. Garlinga, E.H., et al., *Marker Configuration Model-Based Roentgen Fluoroscopic Analysis*. Journal of Biomechanics, 2005. **38**: p. 893-901.
49. Karau, K.L., et al., *Microfocal X-ray CT imaging and pulmonary arterial distensibility in excised rat lungs*. Am J Physiol Heart Circ Physiol, 2001. **281**(3): p. H1447-57.
50. Weng, J., P. Cohen, and M. Herniou, *Camera calibration with distortion models and accuracy evaluation*. IEEE Transactions on pattern analysis and machine intelligence, 1992. **14**(10): p. 965-980.
51. Bottollier-Depois, J.F., et al., *Assessing exposure to cosmic radiation during long-haul flights*. 2009.
52. Green, D., T. Sgarlato, and M. Wittenberg, *Clinical biomechanical evaluation of the foot: a preliminary radiocinematographic study*. Journal of the American Podiatry Association, 1975. **65**(8): p. 732-755.
53. Gefen, A., et al., *Biomechanical analysis of the three-dimensional foot structure during gait: a basic tool for clinical applications*. J Biomech Eng, 2000. **122**(6): p. 630-9.
54. Giddings, V.L., et al., *Calcaneal loading during walking and running*. Medicine and science in sports and exercise, 2000. **32**(3): p. 627-634.
55. Wearing, S.C., et al., *Errors in measuring sagittal arch kinematics of the human foot with digital fluoroscopy*. Gait & Posture, 2005. **21**(3): p. 326-332.

56. Wearing, S.C., et al., *Sagittal plane motion of the human arch during gait: a videofluoroscopic analysis*. Foot Ankle Int, 1998. **19**(11): p. 738-42.
57. Yamaguchi, S., et al., *Ankle and subtalar kinematics during dorsiflexion-plantarflexion activities*. Foot & Ankle International, 2009. **30**(4): p. 361.
58. de Asla, R.J., et al., *Function of anterior talofibular and calcaneofibular ligaments during in-vivo motion of the ankle joint complex*. J Orthop Surg Res, 2009. **4**: p. 7.
59. Gefen, A., *The in vivo elastic properties of the plantar fascia during the contact phase of walking*. Foot Ankle Int, 2003. **24**(3): p. 238-44.
60. Wan, L., et al., *In vivo cartilage contact deformation of human ankle joints under full body weight*. J Orthop Res, 2008. **26**(8): p. 1081-9.
61. Wearing, S.C., et al., *Bulk compressive properties of the heel fat pad during walking: a pilot investigation in plantar heel pain*. Clin Biomech (Bristol, Avon), 2009. **24**(4): p. 397-402.
62. Bozkurt, M. and M.N. Doral, *Anatomic factors and biomechanics in ankle instability*. Foot and ankle clinics, 2006. **11**(3): p. 451.
63. Daniels, T. and R. Thomas, *Etiology and biomechanics of ankle arthritis*. Foot and Ankle Clinics of North America, 2008. **13**(3): p. 341-352.
64. Karlsson, J. and M. Sancone, *Management of acute ligament injuries of the ankle*. Foot and ankle clinics, 2006. **11**(3): p. 521.
65. Chou, L.B., et al., *Osteoarthritis of the ankle: the role of arthroplasty*. Journal of the American Academy of Orthopaedic Surgeons, 2008. **16**(5): p. 249-259.
66. Leardini, A., et al., *Mobility of the human ankle and the design of total ankle replacement*. Clinical orthopaedics and related research, 2004. **424**: p. 39-46.
67. Siegler, S., J. Chen, and C. Schneck, *The three-dimensional kinematics and flexibility characteristics of the human ankle and subtalar joints--Part I: Kinematics*. Journal of biomechanical engineering, 1988. **110**(4): p. 364.
68. Leardini, A., et al., *A geometric model of the human ankle joint*. J Biomech, 1999. **32**(6): p. 585-91.
69. Leardini, A., R. Stagni, and J.J. O'Connor, *Mobility of the subtalar joint in the intact ankle complex*. J Biomech, 2001. **34**(6): p. 805-9.
70. Piazza, S.J., *Mechanics of the subtalar joint and its function during walking*. Foot and ankle clinics, 2005. **10**(3): p. 425.

71. Inman, V.T., *The joints of the ankle*. 1976: Williams & Wilkins Baltimore.
72. Close, J., et al., *The Function of the Subtalar Joint*. Clinical orthopaedics and related research, 1967. **50**: p. 159-180.
73. Hicks, J., *The mechanics of the foot: I. The joints*. Journal of Anatomy, 1953. **87**(Pt 4): p. 345.
74. Isman, R.E., V.T. Inman, and P. Poor, *Anthropometric studies of the human foot and ankle*. Bulletin of prosthetics research, 1969. **11**: p. 97-108.
75. Manter, J.T., *Movements of the subtalar and transverse tarsal joints*. The anatomical record, 1941. **80**(4): p. 397-410.
76. Root, M., et al., *Axis of motion of the subtalar joint*. J Am Podiatry Assoc, 1966. **56**(4): p. 149-155.
77. Smith, J., *The ligamentous structures in the canalis and sinus tarsi*. Journal of Anatomy, 1958. **92**(Pt 4): p. 616.
78. Wright, D.G., S.M. Desai, and W.H. Henderson, *Action of the subtalar and ankle-joint complex during the stance phase of walking*. The Journal of Bone & Joint Surgery, 1964. **46**(2): p. 361-464.
79. Dul, J. and G.E. Johnson, *A kinematic model of the human ankle*. Journal of Biomedical Engineering, 1985. **7**(2): p. 137-143.
80. Procter, P. and J. Paul, *Ankle joint biomechanics*. Journal of Biomechanics, 1982. **15**(9): p. 627-634.
81. Lundberg, A., et al., *Kinematics of the ankle/foot complex: plantarflexion and dorsiflexion*. Foot & ankle, 1989. **9**(4): p. 194.
82. Lundberg, A., et al., *The axis of rotation of the ankle joint*. Journal of Bone & Joint Surgery, British Volume, 1989. **71**(1): p. 94-99.
83. Sammarco, J., *Biomechanics of the ankle I. Surface velocity and instant center of rotation in the sagittal plane*. The American journal of sports medicine, 1977. **5**(6): p. 231-234.
84. Ringleb, S.I., et al., *Effects of lateral ligament sectioning on the stability of the ankle and subtalar joint*. Journal of orthopaedic research, 2011. **29**(10): p. 1459-1464.
85. Wong, Y., W. Kim, and N. Ying, *Passive motion characteristics of the talocrural and the subtalar joint by dual Euler angles*. J Biomech, 2005. **38**(12): p. 2480-5.

86. Grood, E.S. and W.J. Suntay, *A joint coordinate system for the clinical description of three-dimensional motions: application to the knee*. Journal of biomechanical engineering, 1983. **105**(2): p. 136.
87. Wu, G., et al., *ISB recommendation on definitions of joint coordinate system of various joints for the reporting of human joint motion* part I: ankle, hip, and spine. Journal of Biomechanics, 2002. **35**(4): p. 543-548.
88. Ringleb, S., et al., *The effect of ankle ligament damage and surgical reconstructions on the mechanics of the ankle and subtalar joints revealed by three-dimensional stress MRI*. Journal of orthopaedic research, 2005. **23**(4): p. 743-749.
89. Siegler, S., et al., *Mechanics of the ankle and subtalar joints revealed through a 3D quasi-static stress MRI technique*. Journal of Biomechanics, 2005. **38**(3): p. 567-578.
90. Weindel, S., et al., *Subtalar instability: a biomechanical cadaver study*. Archives of orthopaedic and trauma surgery, 2010. **130**(3): p. 313-319.
91. Zatsiorsky, V., *Kinematics of Human Motion*. 1998, Champaign, IL: Human Kinetics.
92. Berme, N., A. Capozzo, and J. Meglan, *Rigid body mechanics as applied to human movement studies*. Biomechanics of Human Movement: Applications in Rehabilitation, Sports and Ergonomics, 1990: p. 89-107.
93. Beimers, L., et al., *In-vivo range of motion of the subtalar joint using computed tomography*. Journal of Biomechanics, 2008. **41**(7): p. 1390-1397.
94. Goto, A., et al., *Three-dimensional in vivo kinematics of the subtalar joint during dorsi-plantarflexion and inversion-eversion*. Foot & Ankle International, 2009. **30**(5): p. 432.
95. Sheehan, F.T., *Research The instantaneous helical axis of the subtalar and talocrural joints: a non-invasive in vivo dynamic study*. 2010.
96. Tuijthof, G.J.M., et al., *Determination of consistent patterns of range of motion in the ankle joint with a computed tomography stress-test*. Clinical biomechanics (Bristol, Avon), 2009. **24**(6): p. 517-523.
97. Ramakrishnan, H.K. and M.P. Kadaba, *On the estimation of joint kinematics during gait*. J Biomech, 1991. **24**(10): p. 969-77.
98. Choisne, J., et al., *Influence of kinematic analysis methods on detecting ankle and subtalar joint instability*. J Biomech, 2012. **45**(1): p. 46-52.

99. Gage, J.R. and T.F. Novacheck, *An update on the treatment of gait problems in cerebral palsy*. J Pediatr Orthop B, 2001. **10**(4): p. 265-74.
100. Davis, R.B., *Reflections on clinical gait analysis*. J Electromyogr Kinesiol, 1997. **7**(4): p. 251-257.
101. Bruening, D.A., et al., *Measured and estimated ground reaction forces for multi-segment foot models*. J Biomech, 2010. **43**(16): p. 3222-6.
102. Yavuz, M., G. Botek, and B.L. Davis, *Plantar shear stress distributions: comparing actual and predicted frictional forces at the foot-ground interface*. J Biomech, 2007. **40**(13): p. 3045-9.
103. Scott, S.H. and D.A. Winter, *Biomechanical model of the human foot: kinematics and kinetics during the stance phase of walking*. Journal of Biomechanics, 1993. **26**(9): p. 1091.
104. Chen, W.-M., et al., *A novel gait platform to measure isolated plantar metatarsal forces during walking*. Journal of Biomechanics, 2010. **43**(10): p. 2017-2021.
105. Heywood, E., D. Jeutter, and G. Harris. *Tri-axial plantar pressure sensor: design, calibration and characterization*. in *Engineering in Medicine and Biology Society, 2004. IEMBS'04. 26th Annual International Conference of the IEEE*. 2004: IEEE.
106. Davis, B., et al., *A device for simultaneous measurement of pressure and shear force distribution on the plantar surface of the foot*. Journal of Applied Biomechanics, 1998. **14**: p. 93-104.
107. Perry, J.E., J.O. Hall, and B.L. Davis, *Simultaneous measurement of plantar pressure and shear forces in diabetic individuals*. Gait & Posture, 2002. **15**(1): p. 101-107.
108. Giacomozzi, C. and V. Macellari, *Piezo-dynamometric platform for a more complete analysis of foot-to-floor interaction*. Rehabilitation Engineering, IEEE Transactions on, 1997. **5**(4): p. 322-330.
109. Bruening, D.A., K.M. Cooney, and F.L. Buczek, *Analysis of a kinetic multi-segment foot model part II: kinetics and clinical implications*. Gait Posture, 2012. **35**(4): p. 535-40.
110. Hanavan, E.P., *A mathematical model of the human body*. Vol. 32. 1964: Aerospace Medical Research Laboratories, Aerospace Medical Division, Air Force Systems Command.
111. Chandler, R., et al., *Investigation of inertial properties of the human body*. 1975, DTIC Document.

112. Dempster, W.T., *Space requirements of the seated operator: geometrical, kinematic, and mechanical aspects of the body, with special reference to the limbs*. 1955.
113. de Leva, P., *Adjustments to Zatsiorsky-Seluyanov's segment inertia parameters*. J Biomech, 1996. **29**(9): p. 1223-30.
114. Zatsiorsky, V. and V. Seluyanov, *The mass and inertia characteristics of the main segments of the human body*. Biomechanics VIII-B, 1983. **56**(2): p. 1152-1159.
115. Zatsiorsky, V., V. Seluyanov, and L. Chugunova, *In vivo body segment inertial parameters determination using a gamma-scanner method*. Biomechanics of human movement: Applications in rehabilitation, sports and ergonomics (Edited by Berme, N. and Cappozzo, A.), 1990: p. 187-202.
116. Andrews, J.G. and S.P. Mish, *Methods for investigating the sensitivity of joint resultants to body segment parameter variations*. Journal of Biomechanics, 1996. **29**(5): p. 651-654.
117. Rao, G., et al., *Influence of body segments' parameters estimation models on inverse dynamics solutions during gait*. Journal of Biomechanics, 2006. **39**(8): p. 1531-1536.
118. Ganley, K.J. and C.M. Powers, *Determination of lower extremity anthropometric parameters using dual energy X-ray absorptiometry: the influence on net joint moments during gait*. Clinical Biomechanics, 2004. **19**(1): p. 50-56.
119. Pearsall, D. and P. Costigan, *The effect of segment parameter error on gait analysis results*. Gait & Posture, 1999. **9**(3): p. 173-183.
120. Silva, M. and J.A. Ambrósio, *Sensitivity of the results produced by the inverse dynamic analysis of a human stride to perturbed input data*. Gait & Posture, 2004. **19**(1): p. 35-49.
121. Wells, R., *The projection of the ground reaction force as a predictor of internal joint moments*. Bulletin of prosthetics research, 1981. **10**: p. 15.
122. Harris, G.F., *Analysis of Ankle and Subtalar Motion During Human Locomotion*, in *Inman's Joints of the Ankle*, J.B. Stiehl, Editor. 1991, Williams & Wilkins. p. 75-84.
123. Davis, R.B., et al., *The Design, Development, and Initial Evaluation of a Multisegment Foot Model for Routine Clinical Gait Analysis*, in *Foot and Ankle Motion Analysis: Clinical Treatment and Technology*, G.F. Harris, P.A. Smith, and R.M. Marks, Editors. 2008, CRC Press. p. 425-444.
124. Hunt, A.E., et al., *Inter-segment foot motion and ground reaction forces over the stance phase of walking*. Clin Biomech (Bristol, Avon), 2001. **16**(7): p. 592-600.

125. Jenkyn, T.R. and A.C. Nicol, *A multi-segment kinematic model of the foot with a novel definition of forefoot motion for use in clinical gait analysis during walking*. J Biomech, 2007. **40**(14): p. 3271-8.
126. Hwang, S.J., H.S. Choi, and Y.H. Kim, *Motion analysis based on a multi-segment foot model in normal walking*. Conf Proc IEEE Eng Med Biol Soc, 2004. **7**: p. 5104-6.
127. De Clercq, D., P. Aerts, and M. Kunnen, *The mechanical characteristics of the human heel pad during foot strike in running: an in vivo cineradiographic study*. J Biomech, 1994. **27**(10): p. 1213-22.
128. Perlman, P.R., P. Dubois, and V. Siskind, *Validating the process of taking lateral foot x-rays*. J Am Podiatr Med Assoc, 1996. **86**(7): p. 317-21.
129. Vaughan, C.L., B. Davis, and J.C. O'Connor, *Dynamics of human gait / Christopher L. Vaughan, Brian L. Davis, Jeremy C. O'Connor*. 1992, Champaign : Human Kinetics Publishers.
130. Simon, J., et al., *The Heidelberg foot measurement method: development, description and assessment*. Gait Posture, 2006. **23**(4): p. 411-24.
131. Contini, R., *Body Segment Parameters, Part III*. Artificial limbs, 1972: p. 1.
132. Myers, K.A., et al., *Validation of a multisegment foot and ankle kinematic model for pediatric gait*. IEEE Trans Neural Syst Rehabil Eng, 2004. **12**(1): p. 122-30.
133. Perry, J., *Gait analysis: normal and pathological function*. Slack, Thorofare, NJ, 1992.
134. Arndt, A., *Personal Communication* 2012.
135. Scott, S.H. and D.A. Winter, *Talocrural and talocalcaneal joint kinematics and kinetics during the stance phase of walking*. J Biomech, 1991. **24**(8): p. 743-52.
136. Oberg, T., A. Karsznia, and K. Oberg, *Joint angle parameters in gait: reference data for normal subjects, 10-79 years of age*. J Rehabil Res Dev, 1994. **31**(3): p. 199-213.
137. Stebbins, J., et al., *Repeatability of a model for measuring multi-segment foot kinematics in children*. Gait & Posture, 2006. **23**(4): p. 401-410.
138. Taranto, M.J., et al., *Radiographic investigation of angular and linear measurements including first metatarsophalangeal joint dorsiflexion and rearfoot to forefoot axis angle*. J Foot Ankle Surg, 2005. **44**(3): p. 190-9.
139. Dixon, P.C., H. Bohm, and L. Doderlein, *Ankle and midfoot kinetics during normal gait: a multi-segment approach*. J Biomech, 2012. **45**(6): p. 1011-6.

140. Ganley, K.J. and C.M. Powers, *Gait kinematics and kinetics of 7-year-old children: a comparison to adults using age-specific anthropometric data*. *Gait Posture*, 2005. **21**(2): p. 141-5.
141. Kitaoka, H., et al., *Kinematics of the normal arch of the foot and ankle under physiologic loading*. *Foot & ankle international/American Orthopaedic Foot and Ankle Society [and] Swiss Foot and Ankle Society*, 1995. **16**(8): p. 492.
142. Michelson, J., H. Clarke, and R. Jinnah, *The effect of loading on tibiotalar alignment in cadaver ankles*. *Foot & ankle*, 1990. **10**(5): p. 280.
143. Shereff, M., et al., *A comparison of nonweight-bearing and weight-bearing radiographs of the foot*. *Foot Ankle*, 1990. **10**(6): p. 306-311.
144. Tochigi, Y., et al., *Influence of the interosseous talocalcaneal ligament injury on stability of the ankle-subtalar joint complex--a cadaveric experimental study*. *Foot & ankle international/American Orthopaedic Foot and Ankle Society [and] Swiss Foot and Ankle Society*, 2000. **21**(6): p. 486.
145. Majumdar, D., et al., *Temporal spatial parameters of gait with barefoot, bathroom slippers and military boots*. *Indian journal of physiology and pharmacology*, 2006. **50**(1): p. 33.
146. Lythgo, N., C. Wilson, and M. Galea, *Basic gait and symmetry measures for primary school-aged children and young adults whilst walking barefoot and with shoes*. *Gait & Posture*, 2009. **30**(4): p. 502-506.
147. Long, J.T., et al., *Repeatability and sources of variability in multi-center assessment of segmental foot kinematics in normal adults*. *Gait & Posture*, 2010. **31**(1): p. 32-36.
148. CDC. *National Diabetes Fact Sheet, 2011*. Available from: [http://www.cdc.gov/diabetes/pubs/pdf/ndfs\\_2011.pdf](http://www.cdc.gov/diabetes/pubs/pdf/ndfs_2011.pdf).
149. Singh, N., D.G. Armstrong, and B.A. Lipsky, *Preventing foot ulcers in patients with diabetes*. *JAMA: the journal of the American Medical Association*, 2005. **293**(2): p. 217-228.
150. Boulton, A.J.M., *The diabetic foot: from art to science. The 18th Camillo Golgi lecture*. *Diabetologia*, 2004. **47**(8): p. 1343-1353.
151. Brown, D., et al., *Effect of rocker soles on plantar pressures*. *Archives of physical medicine and rehabilitation*, 2004. **85**(1): p. 81-86.
152. Fuller, E., S. Schroeder, and J. Edwards, *Reduction of peak pressure on the forefoot with a rigid rocker-bottom postoperative shoe*. *Journal of the American Podiatric Medical Association*, 2001. **91**(10): p. 501-507.

153. Van Bogart, J.J., et al., *Effects of the toe-only rocker on gait kinematics and kinetics in able-bodied persons*. Neural Systems and Rehabilitation Engineering, IEEE Transactions on, 2005. **13**(4): p. 542-550.
154. Schaff, P. and P. Cavanagh, *Shoes for the insensitive foot: the effect of a "rocker bottom" shoe modification on plantar pressure distribution*. Foot & ankle, 1990. **11**(3): p. 129.
155. Xu, H., et al., *Effect of shoe modifications on center of pressure and in-shoe plantar pressures*. American journal of physical medicine & rehabilitation/Association of Academic Physiatrists, 1999. **78**(6): p. 516.
156. Kavros, S.J., et al., *Forefoot plantar pressure reduction of off-the-shelf rocker bottom provisional footwear*. Clinical Biomechanics, 2011. **26**(7): p. 778-782.
157. Myers, K., et al., *Biomechanical implications of the negative heel rocker sole shoe: Gait kinematics and kinetics*. Gait & Posture, 2006. **24**(3): p. 323-330.
158. Long, J.T., et al., *Biomechanics of the double rocker sole shoe: gait kinematics and kinetics*. Journal of Biomechanics, 2007. **40**(13): p. 2882-2890.
159. Hutchins, S., et al., *The biomechanics and clinical efficacy of footwear adapted with rocker profiles-Evidence in the literature*. The Foot, 2009. **19**(3): p. 165-170.
160. Eslami, M., et al., *Forefoot-rearfoot coupling patterns and tibial internal rotation during stance phase of barefoot versus shod running*. Clinical biomechanics (Bristol, Avon), 2007. **22**(1): p. 74.
161. Morio, C., et al., *The influence of footwear on foot motion during walking and running*. Journal of Biomechanics, 2009. **42**(13): p. 2081-2088.
162. Bishop, C., G. Paul, and D. Thewlis, *The reliability, accuracy and minimal detectable difference of a multi-segment kinematic model of the foot-shoe complex*. Gait & Posture, 2012.
163. Butler, R.J., J. Hamill, and I. Davis, *Effect of footwear on high and low arched runners' mechanics during a prolonged run*. Gait & Posture, 2007. **26**(2): p. 219.
164. McCulloch, M., D. Brunt, and D. Vander Linden, *The effect of foot orthotics and gait velocity on lower limb kinematics and temporal events of stance*. The Journal of orthopaedic and sports physical therapy, 1993. **17**(1): p. 2.
165. Stacoff, A., et al., *Effects of shoe sole construction on skeletal motion during running*. Medicine and science in sports and exercise, 2001. **33**(2): p. 311-319.
166. Shultz, R. and T. Jenkyn, *Determining the maximum diameter for holes in the shoe without compromising shoe integrity when using a multi-segment foot model*. Medical engineering & physics, 2012. **34**(1): p. 118-122.

167. Cenni, F., et al., *Kinematics of the three components of a total ankle replacement: in vivo fluoroscopic analysis*. Foot & ankle international/American Orthopaedic Foot and Ankle Society [and] Swiss Foot and Ankle Society, 2012. **33**(4): p. 290.
168. Oeffinger, D., et al., *Comparison of gait with and without shoes in children*. Gait & Posture, 1999. **9**(2): p. 95-100.
169. Wolf, S., et al., *Foot motion in children shoes-A comparison of barefoot walking with shod walking in conventional and flexible shoes*. Gait & Posture, 2008. **27**(1): p. 51-59.
170. Moreno-Hernandez, A., et al., *Temporal and spatial gait parameters analysis in non-pathological Mexican children*. Gait & Posture, 2010. **32**(1): p. 78-81.

## Appendices

**Appendix A: Raw kinematic data**

The following raw kinematic data represents the five subjects that underwent barefoot fluoroscopic analyses as described in Chapter 2.

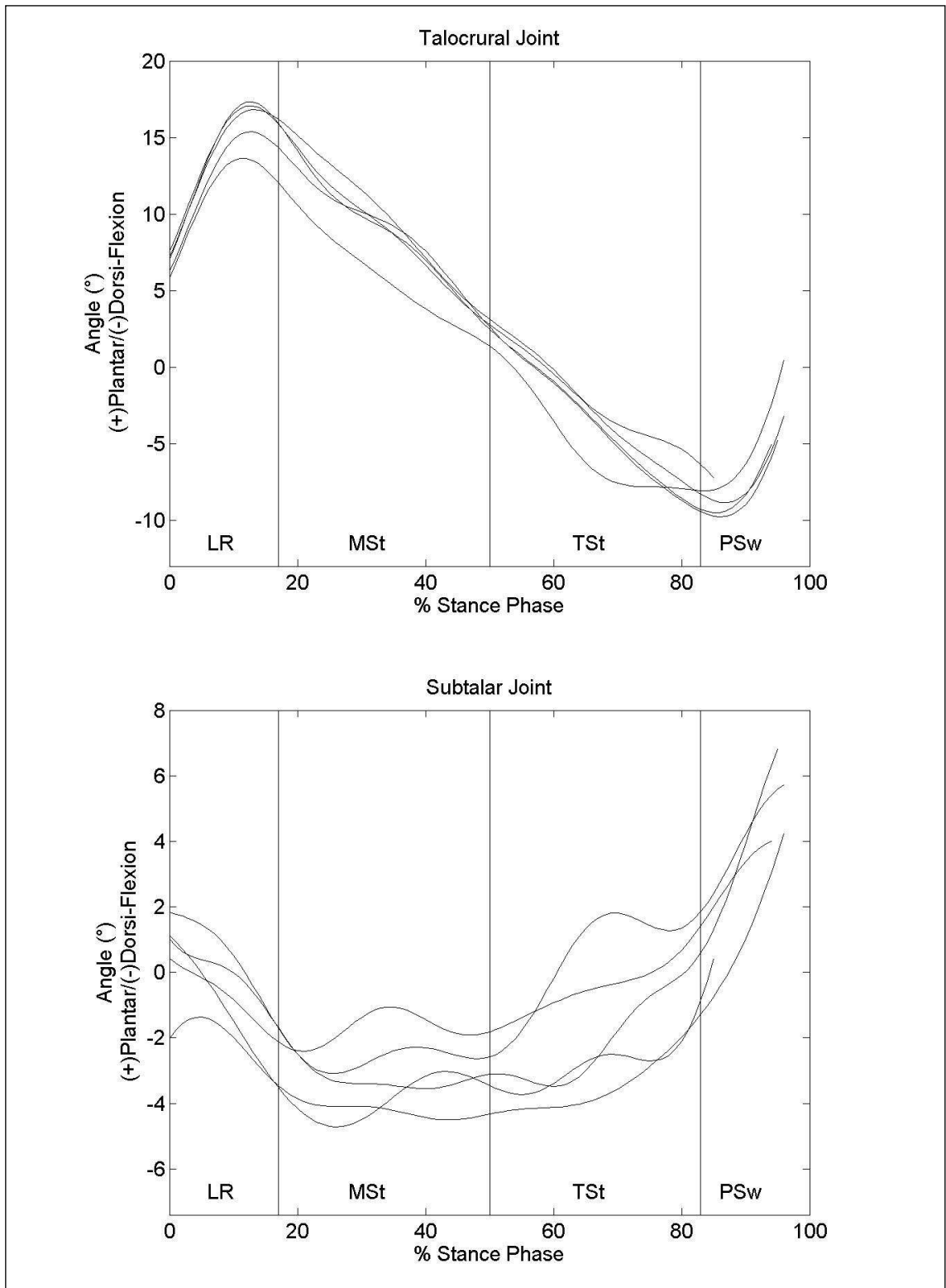


**Figure A-1** Raw kinematics: Subject 1. Subject 1 had 5 trials of barefoot motion analyzed.

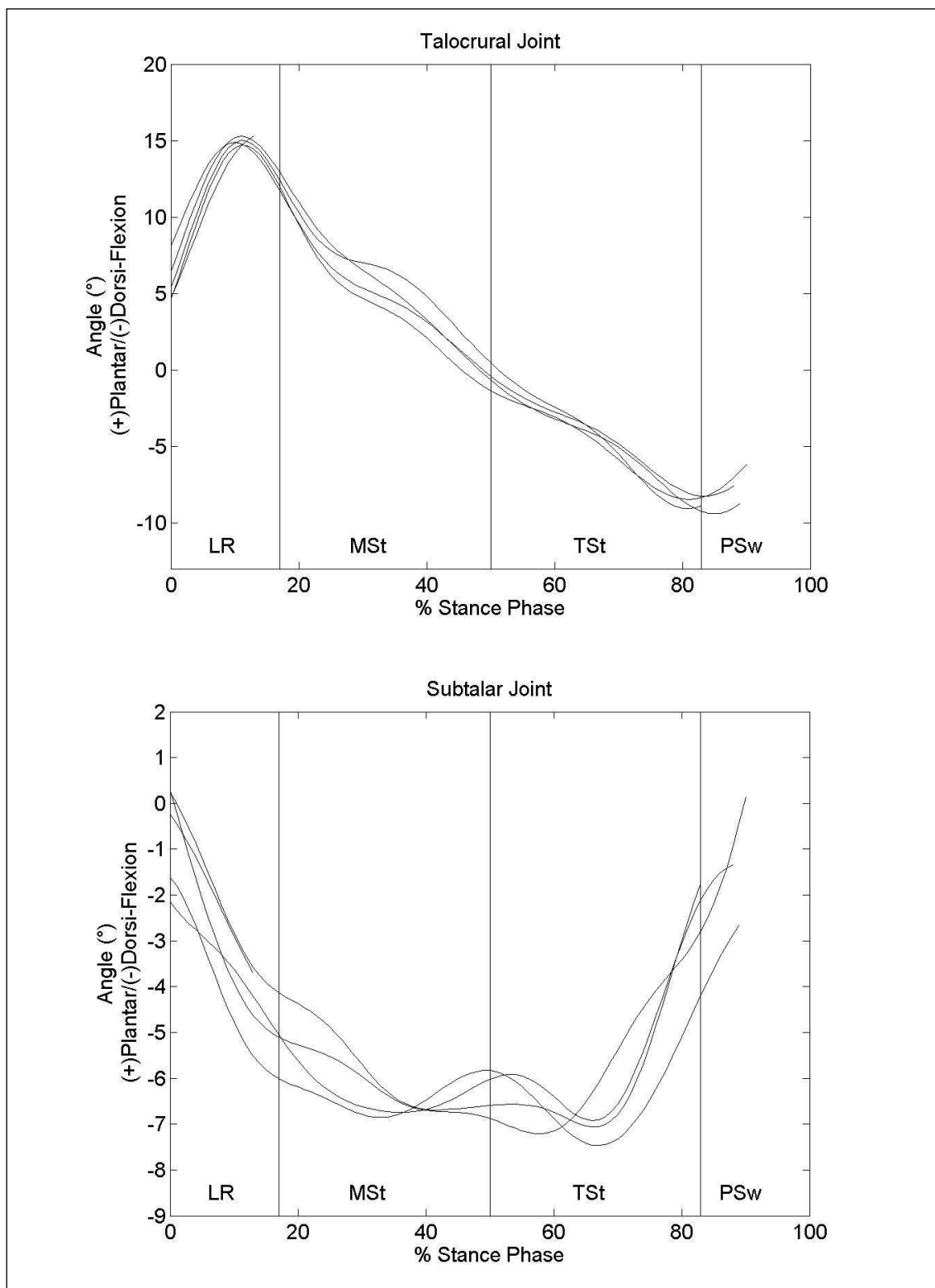


**Figure A-2** Raw kinematics: Subject 2. Subject 2 had 5 trials of barefoot motion analyzed.

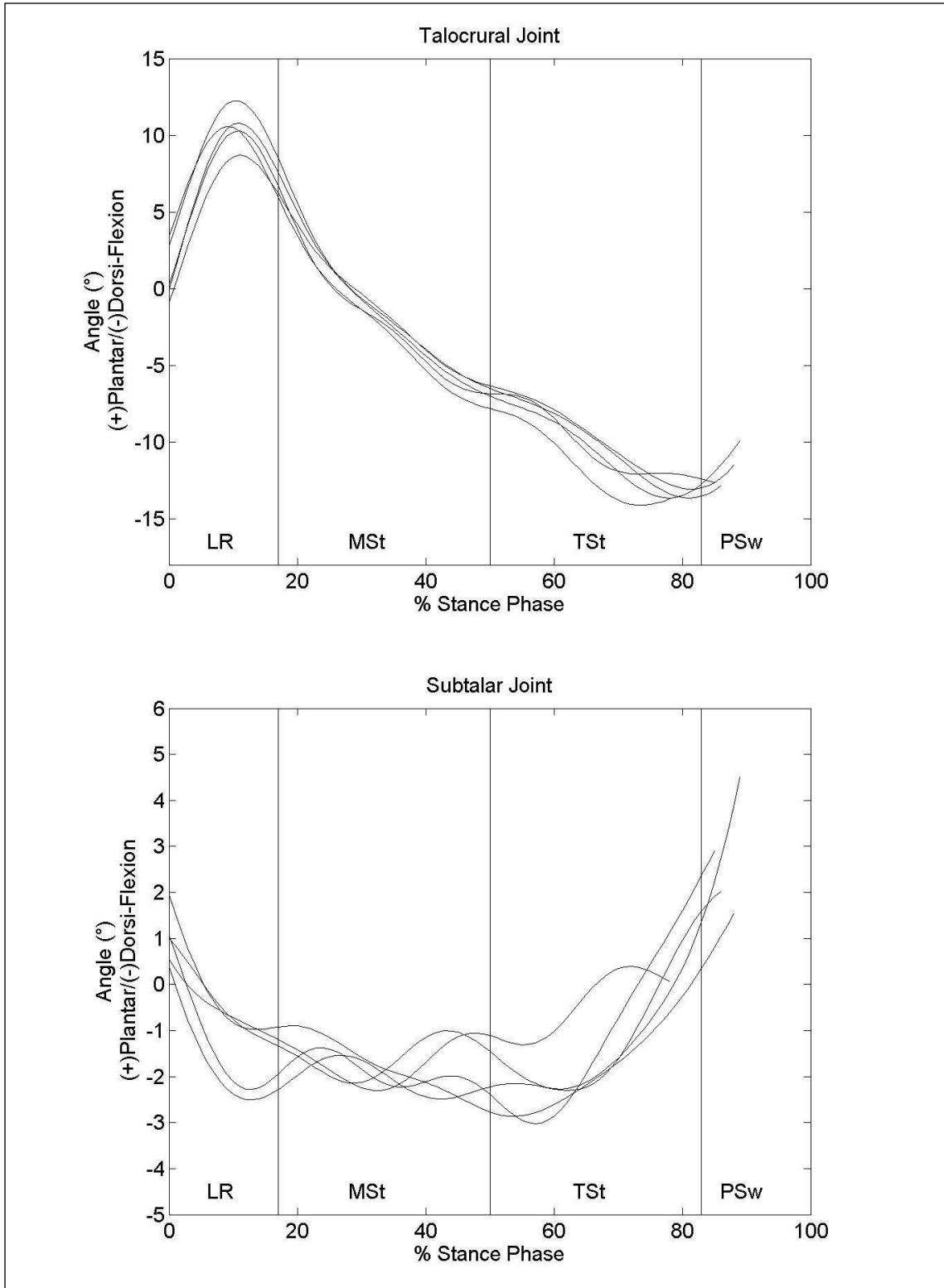


**Figure A-3** Raw kinematics: Subject 3. Subject 3 had 5 trials of barefoot motion analyzed.

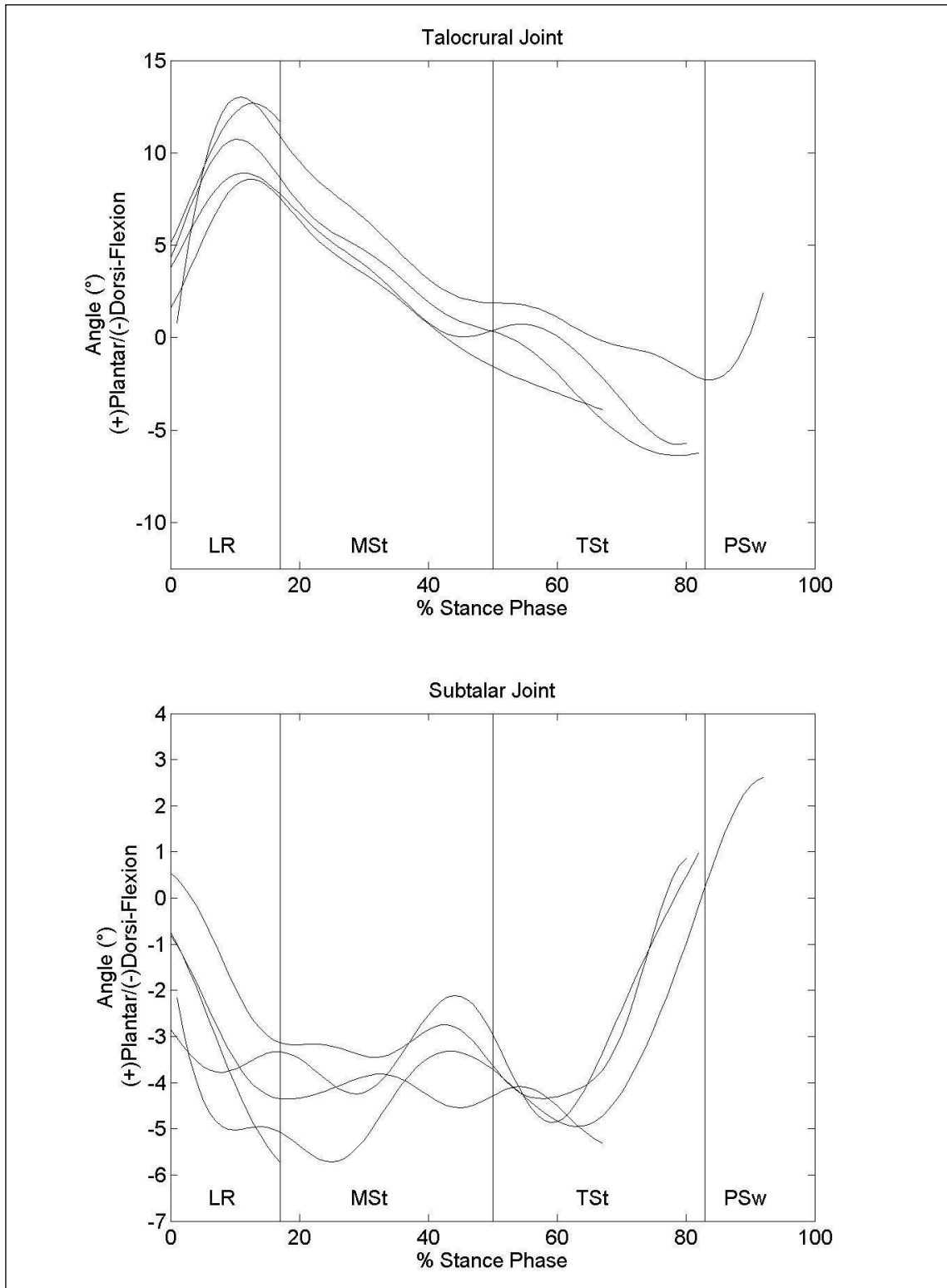


**Figure A-4** Raw kinematics: Subject 4. Subject 4 had 5 trials of barefoot motion analyzed.

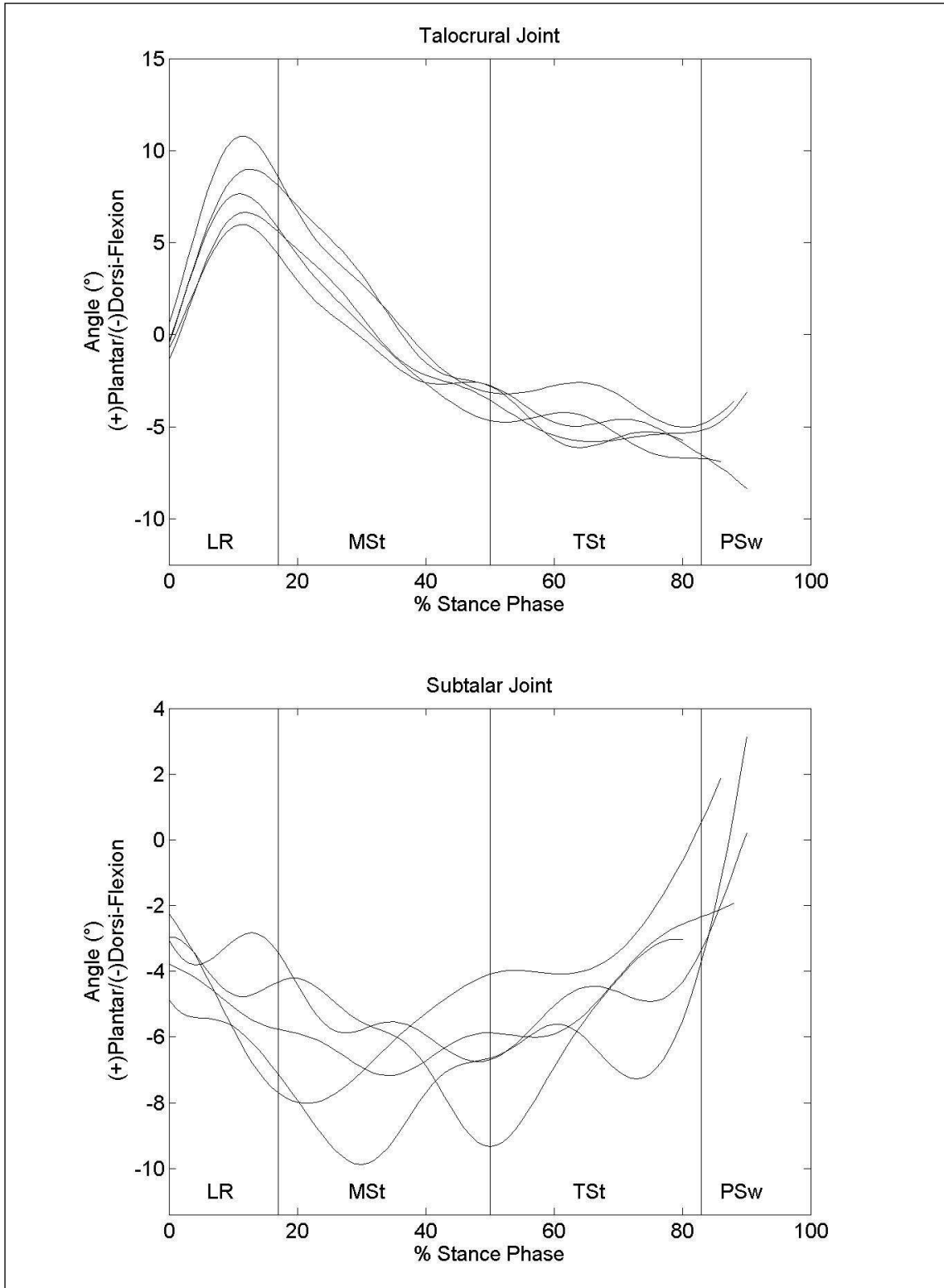


**Figure A-5** Raw kinematics: Subject 5. Subject 5 had 5 trials of barefoot motion analyzed.

**Appendix B: Raw kinematic data**

The following raw kinematic data represents the 13 subjects that underwent barefoot fluoroscopic analyses as described in Chapter 3, and toe-only rocker fluoroscopic analyses as described in Chapter 4. Subjects 1-5 are the same subjects that underwent barefoot fluoroscopic analysis as described in Chapter 2.

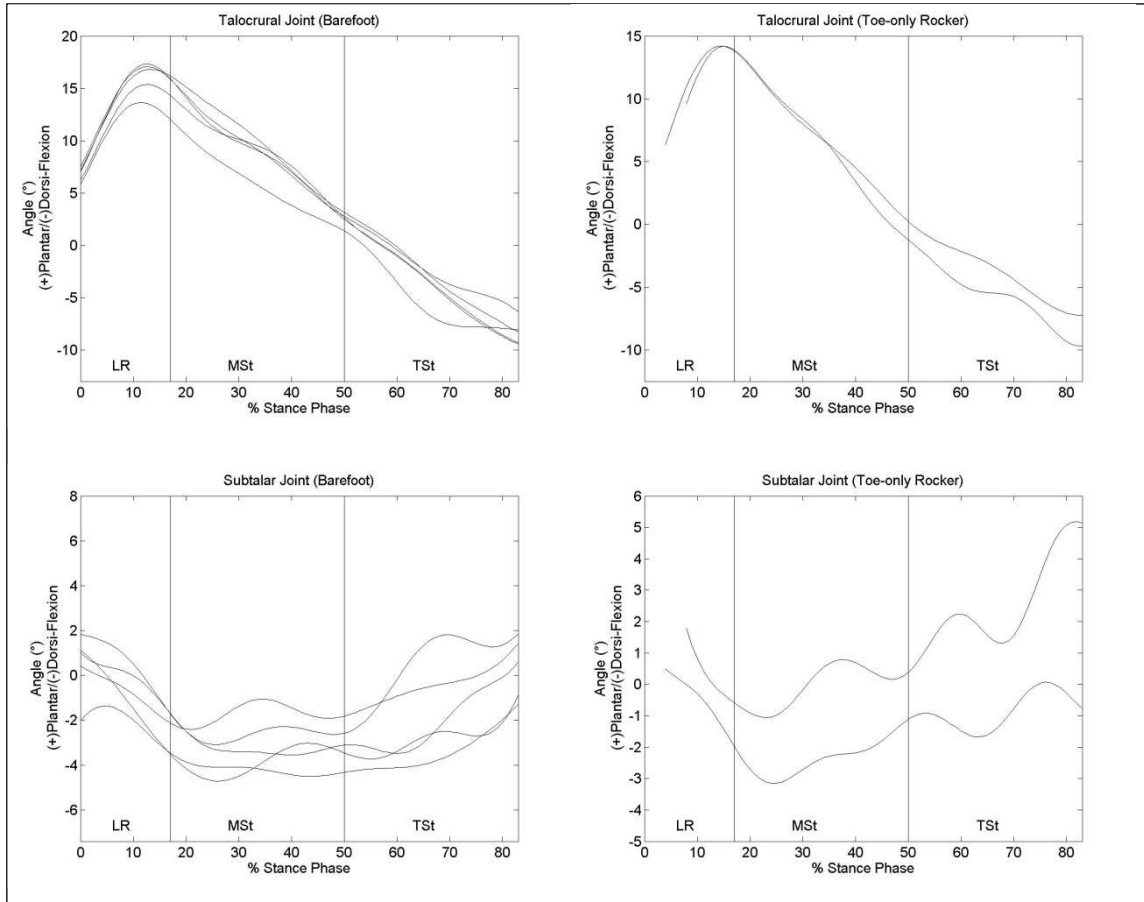


**Figure B-1** Raw kinematics: Subject 1. Subject 1 had 5 trials of barefoot motion analyzed, and 2 trials of toe-only rocker motion analyzed.

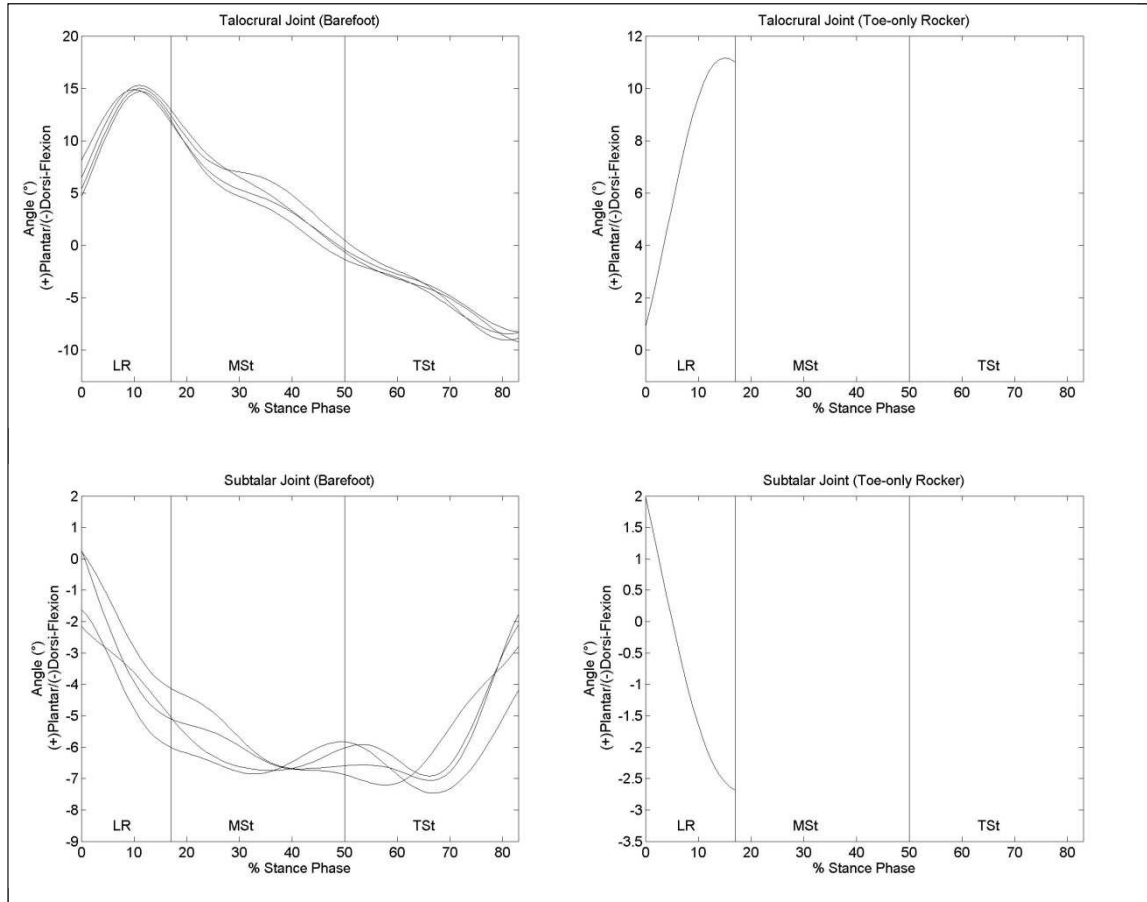


**Figure B-2** Raw kinematics: Subject 2. Subject 2 had 4 trials of barefoot motion analyzed, and 1 trial of toe-only rocker motion analyzed.

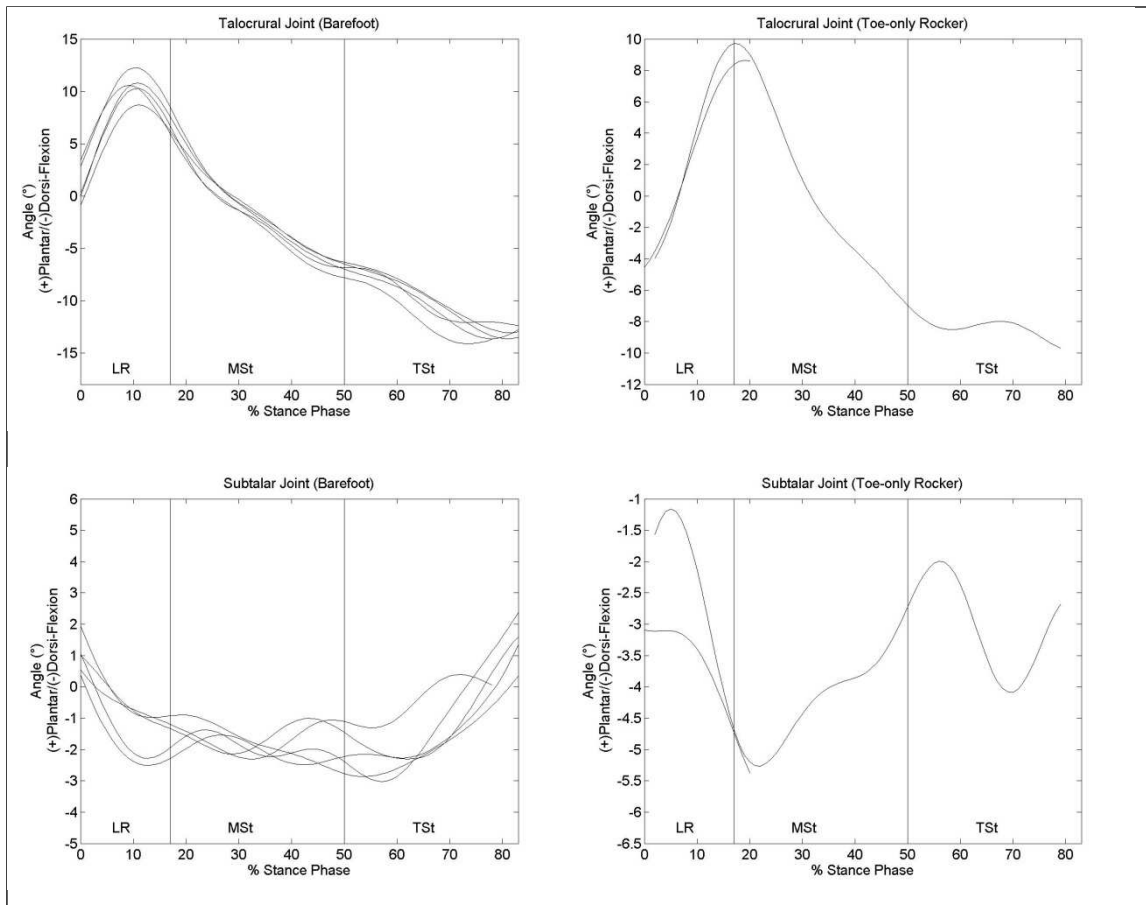


**Figure B-3** Raw kinematics: Subject 3. Subject 3 had 5 trials of barefoot motion analyzed, and 2 trials of toe-only rocker motion analyzed.

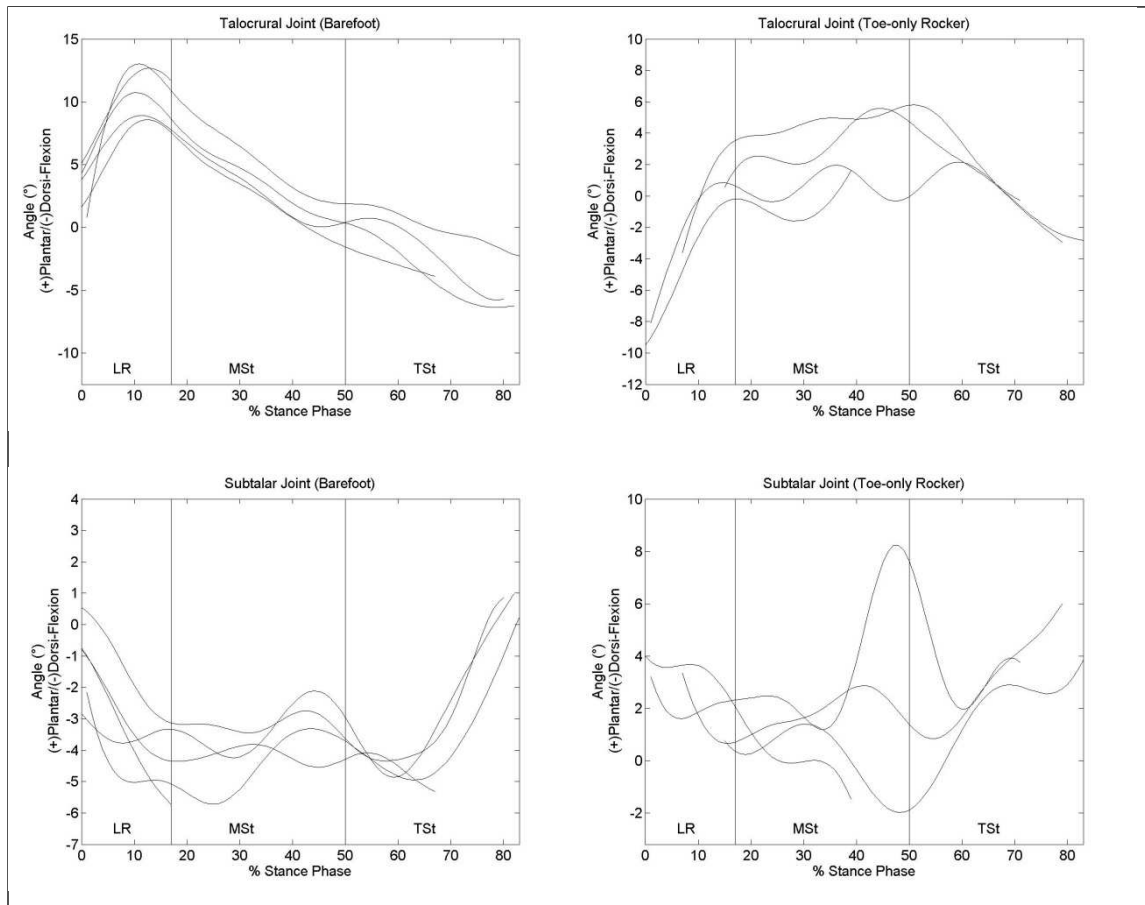


**Figure B-4** Raw kinematics: Subject 4. Subject 4 had 5 trials of barefoot motion analyzed, and 4 trials of toe-only rocker motion analyzed.

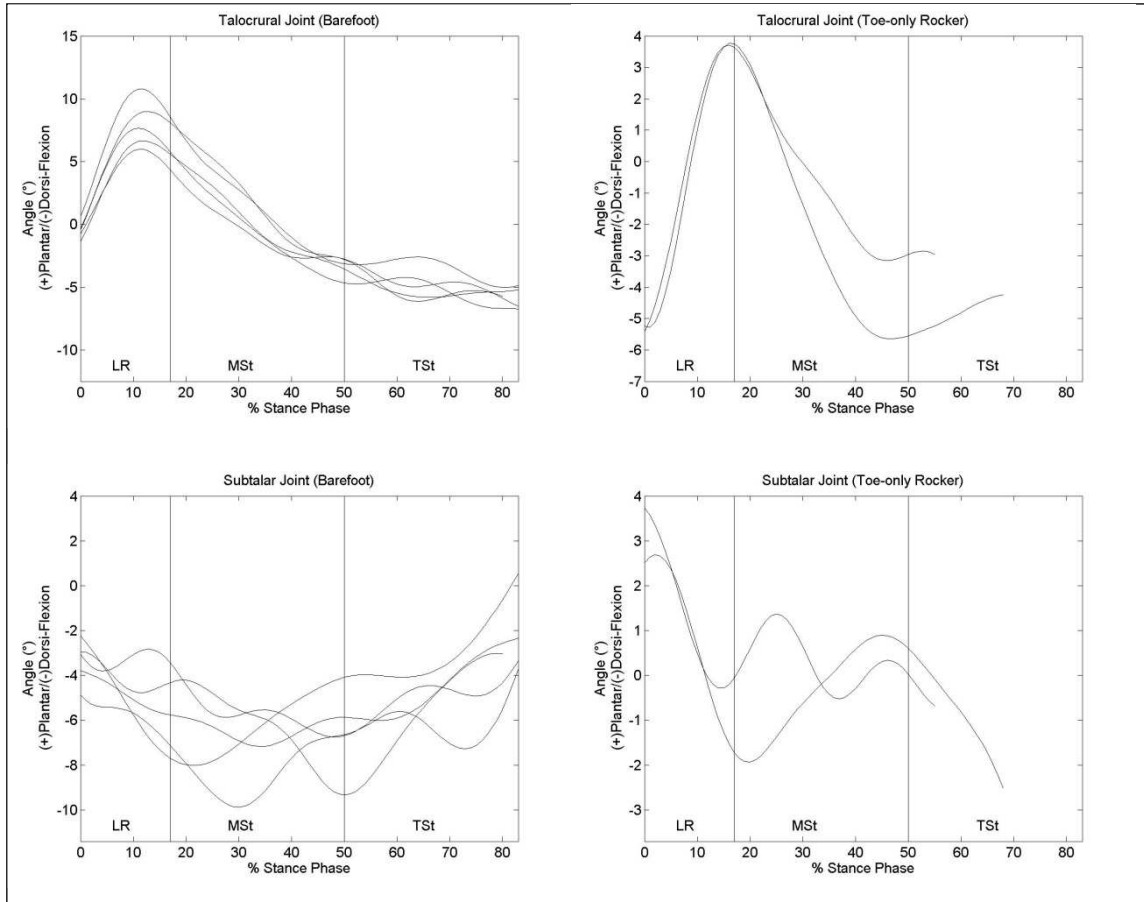


**Figure B-5** Raw kinematics: Subject 5. Subject 5 had 5 trials of barefoot motion analyzed, and 2 trials of toe-only rocker motion analyzed.

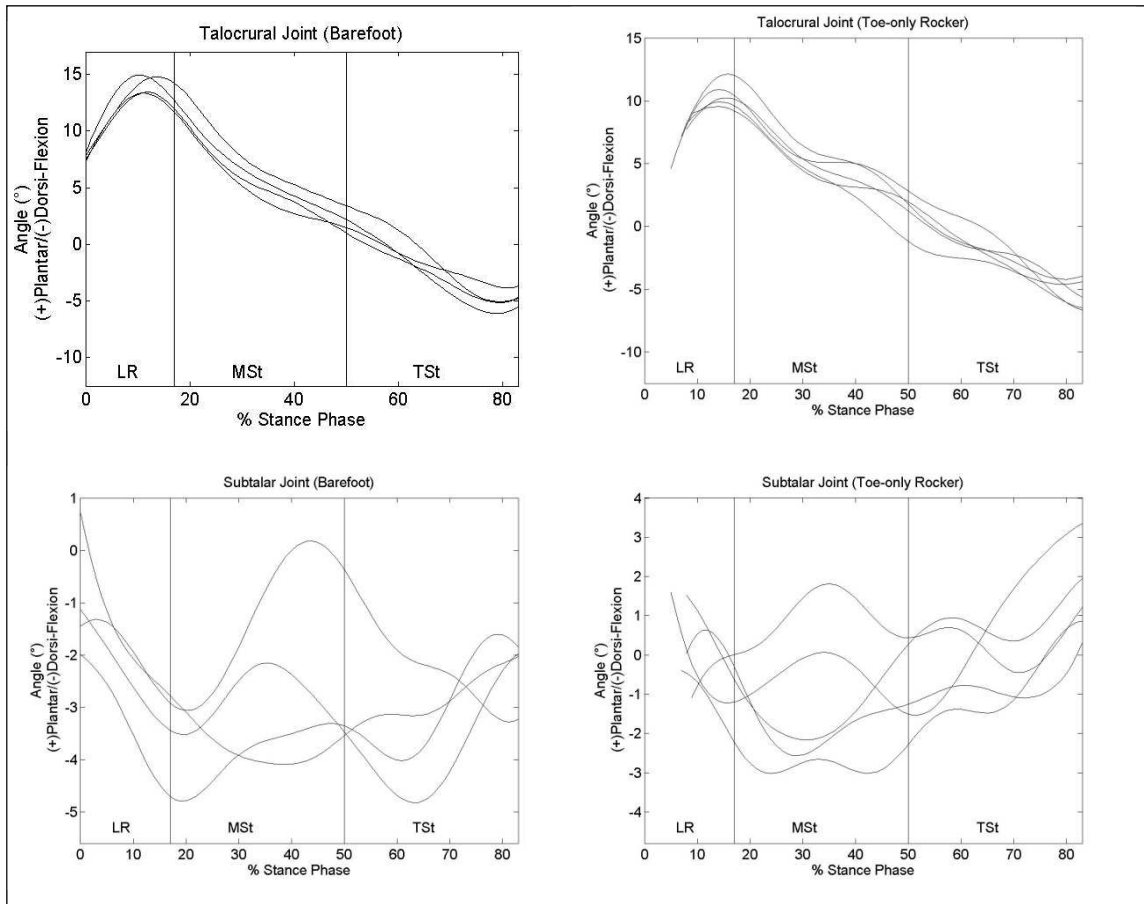


**Figure B-6** Raw kinematics: Subject 6. Subject 6 had 4 trials of barefoot motion analyzed, and 5 trials of toe-only rocker motion analyzed.

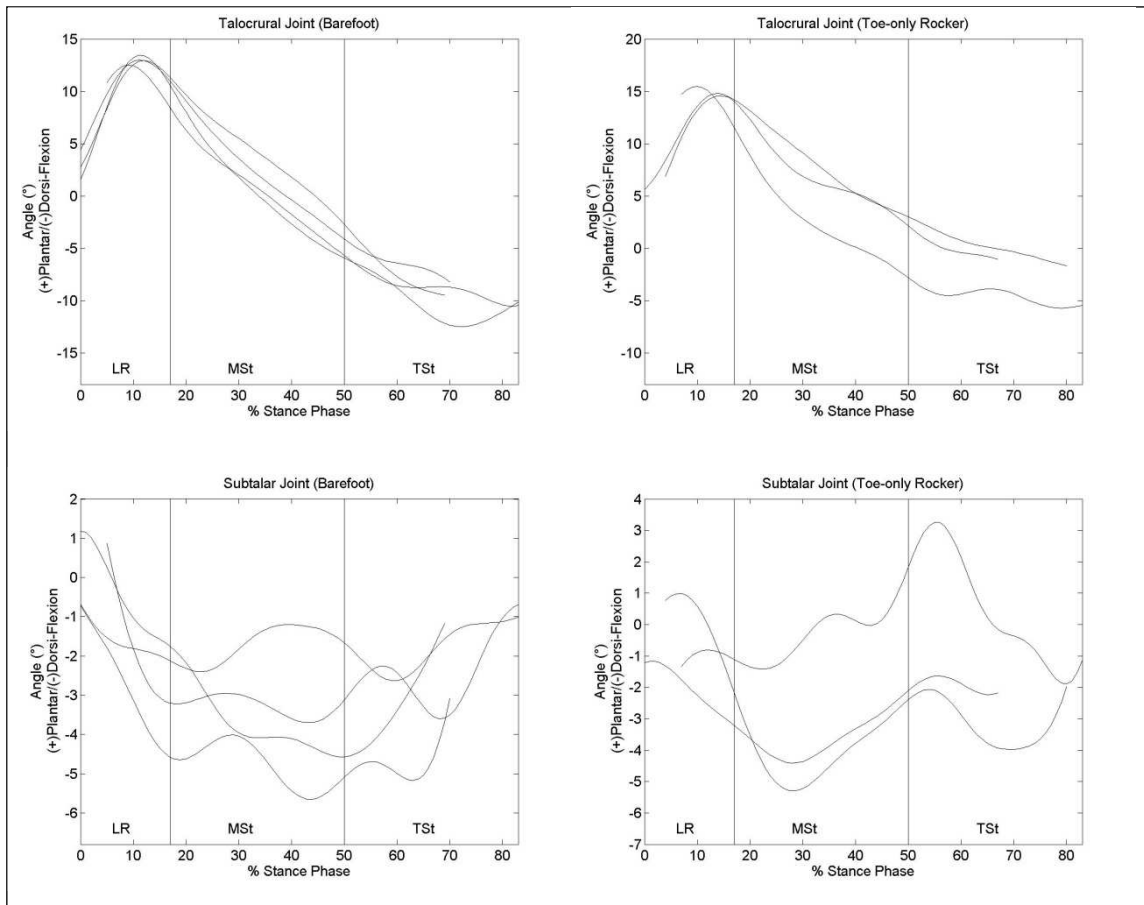


**Figure B-7** Raw kinematics: Subject 7. Subject 7 had 4 trials of barefoot motion analyzed, and 3 trials of toe-only rocker motion analyzed.

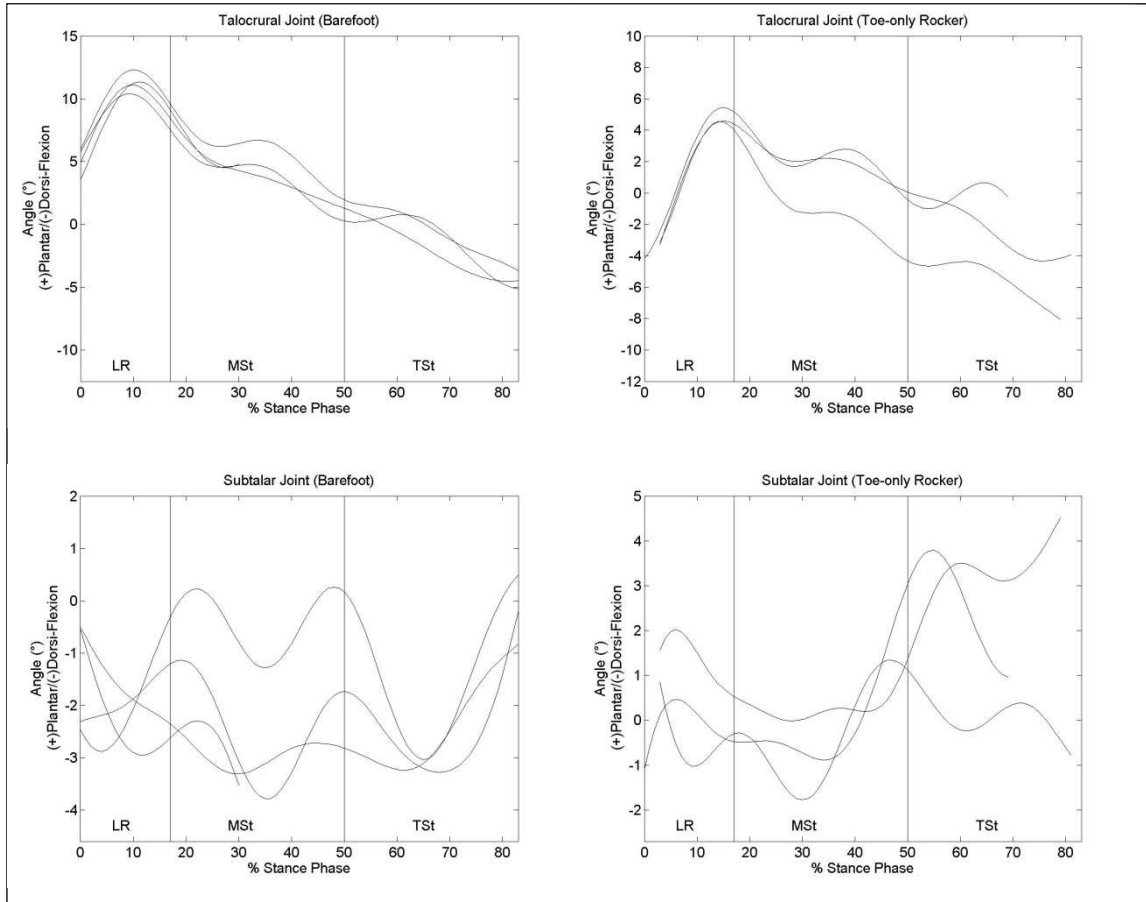


**Figure B-8** Raw kinematics: Subject 8. Subject 8 had 4 trials of barefoot motion analyzed, and 3 trials of toe-only rocker motion analyzed.

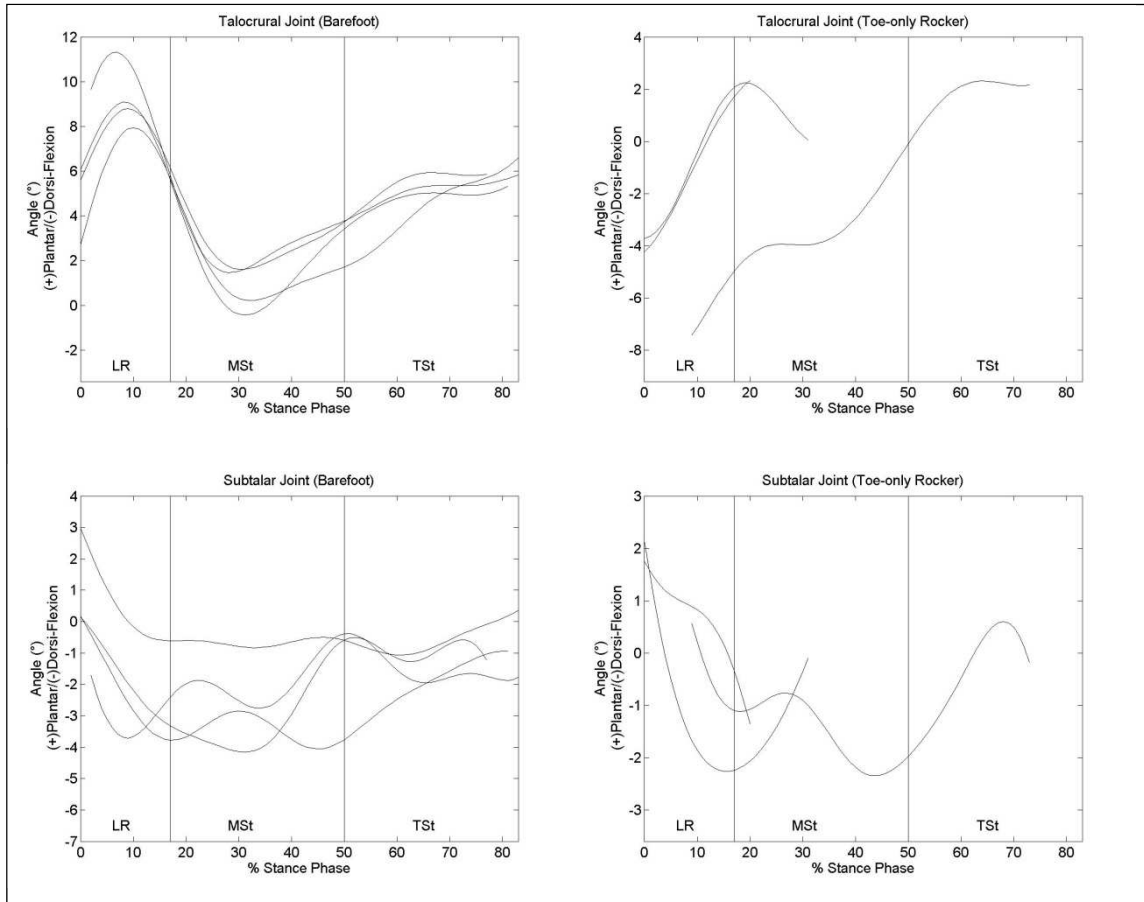


**Figure B-9** Raw kinematics: Subject 9. Subject 9 had 4 trials of barefoot motion analyzed, and 3 trials of toe-only rocker motion analyzed.

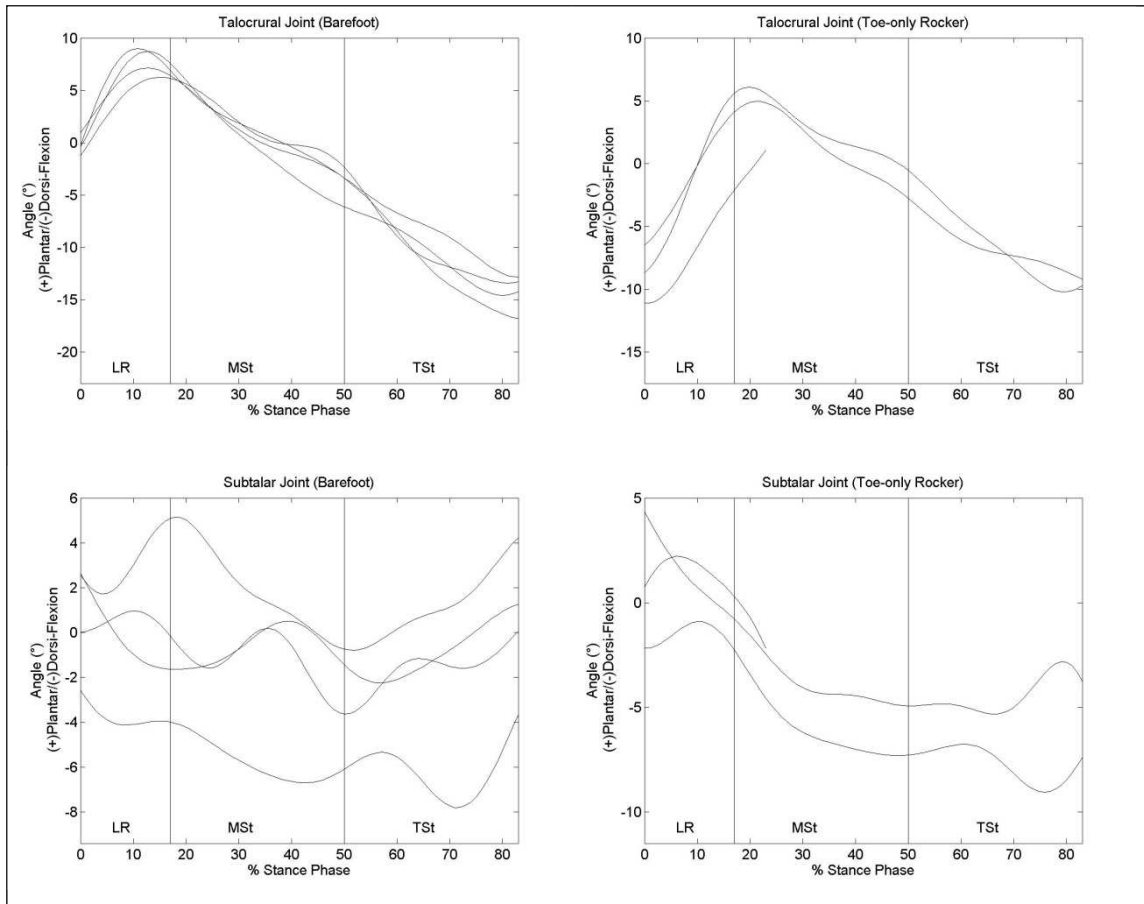


**Figure B-10** Raw kinematics: Subject 10. Subject 10 had 4 trials of barefoot motion analyzed, and 3 trials of toe-only rocker motion analyzed.

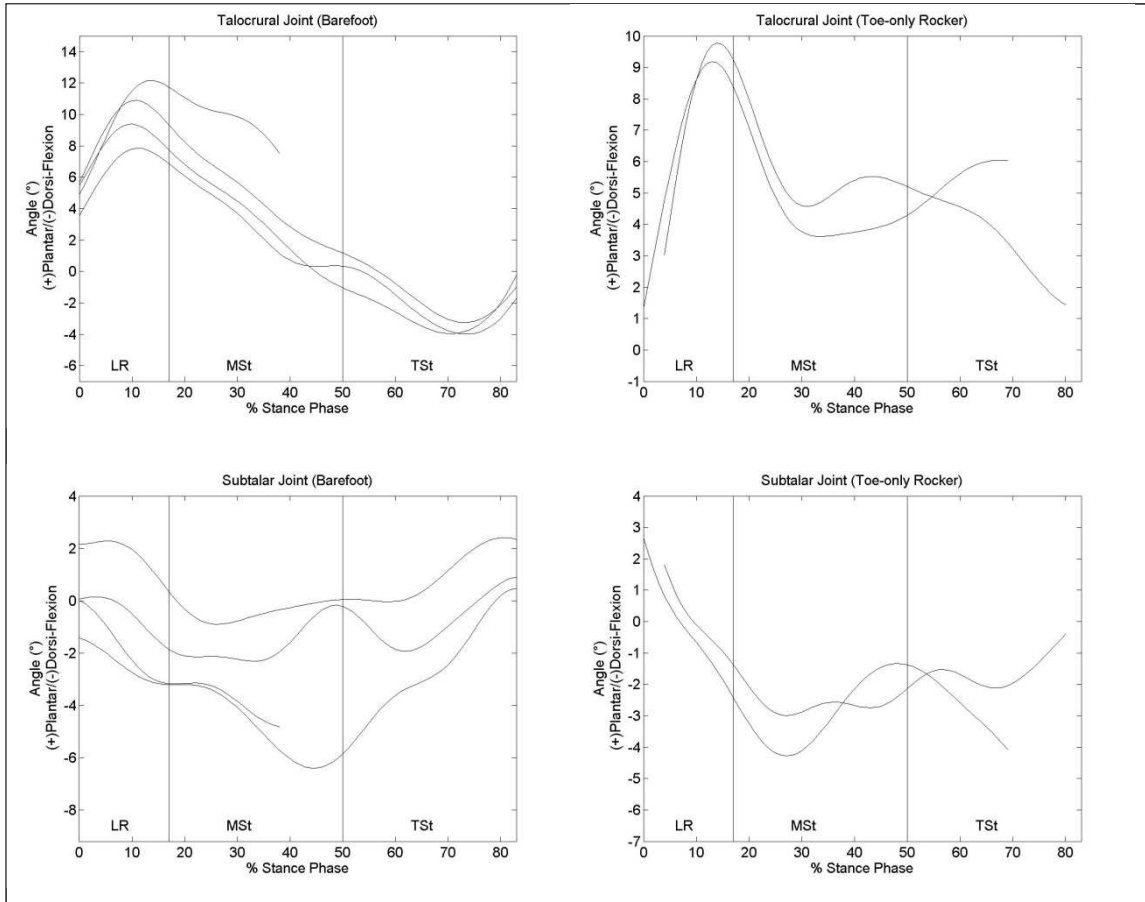


**Figure B-11** Raw kinematics: Subject 11. Subject 11 had 4 trials of barefoot motion analyzed, and 2 trials of toe-only rocker motion analyzed.

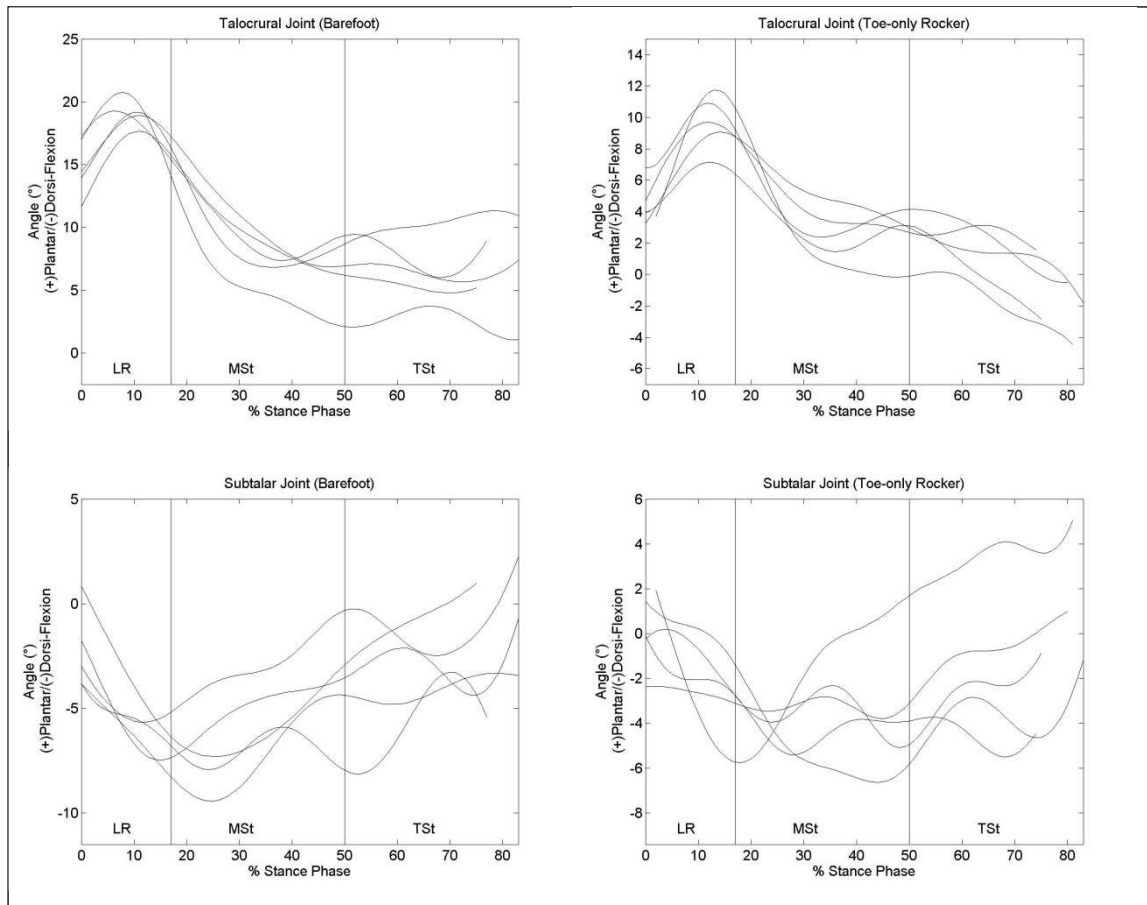


**Figure B-12** Raw kinematics: Subject 12. Subject 12 had 5 trials of barefoot motion analyzed, and 5 trials of toe-only rocker motion analyzed.

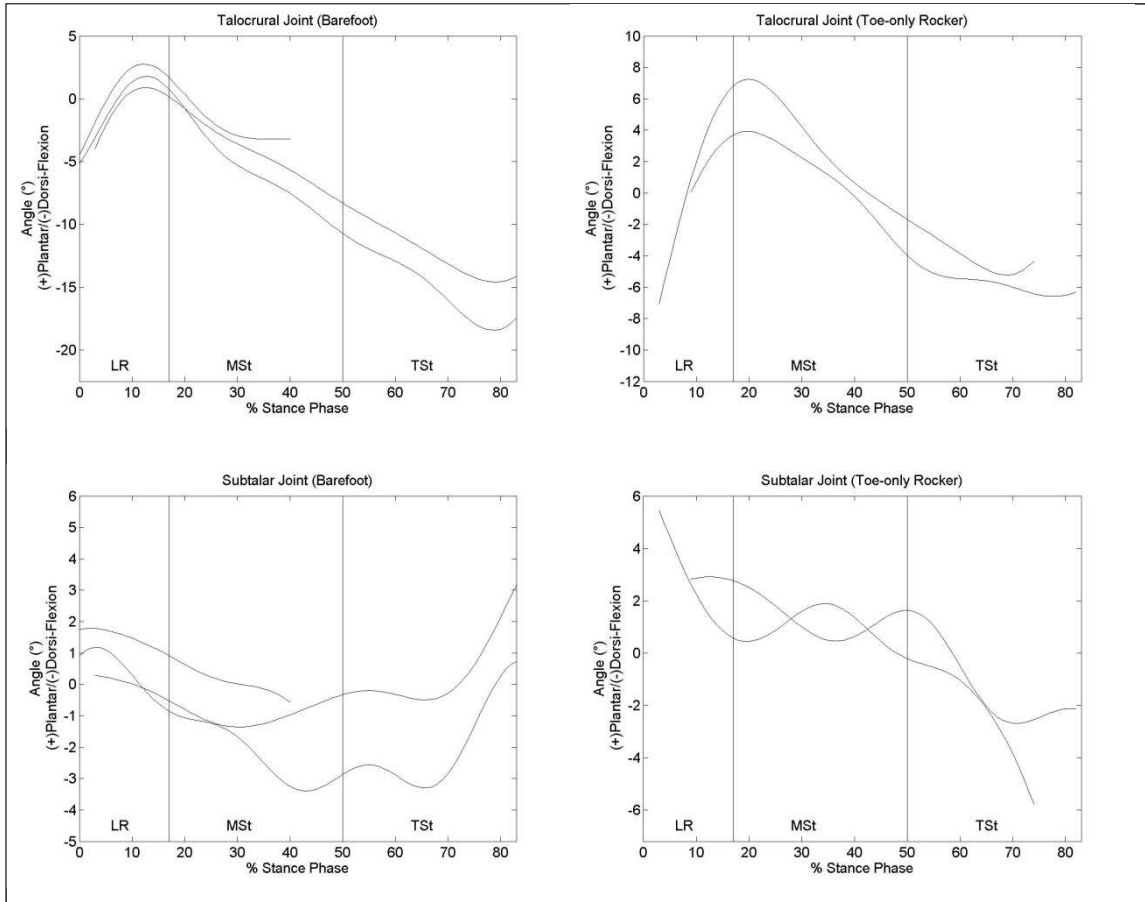


**Figure B-13** Raw kinematics: Subject 13. Subject 13 had 3 trials of barefoot motion analyzed, and 2 trials of toe-only rocker motion analyzed.